In vivo gene transfer into mobilized hematopoietic stem cells

Dissertation
Zur Erlangung des akademischen Grades

doctor rerum naturalium
(Dr. rer. nat.)

im Fach Biologie
eingereicht an der

Lebenswissenschaftlichen Fakultät
der Humboldt-Universität zu Berlin
von

Maximilian Richter, Master of Science Molekulare Biotechnologie

Präsidentin der Humboldt-Universität zu Berlin
Prof. Dr.-Ing. Dr. Sabine Kunst

Dekan der Lebenswissenschaftlichen Fakultät
Prof. Dr. rer. nat. Bernhard Grimm

Gutachter: 1. Prof. Dr. rer. nat. Wolfgang Uckert
2. André M. Lieber, M.D., Ph.D.
3. Prof. Dr. med. Hans-Dieter Volk

Tag der mündlichen Prüfung: 3.7.2017

To my parents

Summary

The gene therapy of hematopoietic stem cells holds the potential for curative treatment of several otherwise incurable inherited diseases. The majority of current gene therapy treatments relies on the collection of hematopoietic stem cells, their *ex vivo* modification with retroviral vectors and their transplantation into a myeloconditioned patient. This approach entails several disadvantages, including a reduction of stem cell engraftment potential after *ex vivo* culture and the potential danger of integrational mutagenesis. In addition, the high costs and complex logistics of this approach limit the access of patients to gene therapeutic regimens.

This work explores an alternative approach to hematopoietic stem cell (HSC) gene therapy, termed stem cell *in vivo* transduction. This approach is based on the mobilization of HSCs from the bone marrow into the peripheral blood and the transduction of the stem cells with adenoviral vectors delivering a transgene as well as a transgene integration machinery.

In the first part of this work, it was shown that first-generation adenoviral vectors could be used for the transduction of mobilized HSCs in the periphery of human CD46-transgenic mice. Further, the transduced HSCs were able to home back to the bone marrow and express the transgene. However, over the course of 14 days, a loss of transgene expression in HSCs was observed. To ameliorate these shortcomings, helper-dependent adenoviral vectors encoding a hyperactive Sleeping Beauty transposase for transgene integration were used for stable gene modification of hematopoietic stem cells following intravenous vector administration in mobilized human CD46-transgenic mice. Using this improved vector platform, gene marking of bone marrow HSCs could be observed for extended periods of time (up to 12 weeks). Further, the functionality of the modified HSCs was demonstrated both in colony-forming progenitor assays as well as through the transplantation of gene-modified HSCs into lethally irradiated recipients. Transplantation of modified HSCs led to long-term multi-lineage reconstitution showing that gene-modified stem cells were fully functional.

Subsequently the safety of systemic vector administration in mobilized hosts as well as of the Sleeping Beauty-mediated transgene integration was assessed in human CD46-transgenic mice. Lastly, the stem cell *in vivo* transduction approach was employed in NOG mice transplanted with human $CD34^+$ cells, as well as in *Macaca nemestrina* non-human primates.

Zusammenfassung

Die Gentherapie hämatopoetischer Stammzellen (HSCs) besitzt das Potenzial, verschiedene erbliche, nur symptomatisch behandelbare, Erkrankungen dauerhaft zu heilen. Die Mehrheit der aktuell angewandten Verfahren dazu, basiert auf der Isolation von hämatopoetischen Stammzellen, der *ex vivo* Modifikation dieser Zellen durch retrovirale Vektoren und der Reinfusion der modifizierten Zellen in den immunsupprimierten Patienten. Dieser Ansatz ist mit einer Reihe von Nachteilen verbunden, unter anderem einem teilweisen Verlust des Rekonstitutionsvermögens der Stammzellen nach *ex vivo* Kultur oder der Gefahr der Transformation durch Integration des retroviralen Vektorgenoms. Darüber hinaus sind aktuelle Gentherapieansätze mit hohen Kosten und großem logistischem Aufwand verbunden, was den Zugang zu diesen Behandlungen für potentielle Patienten stark einschränkt.

Die vorliegende Arbeit verfolgt einen neuen Ansatz zur Gentherapie von HSCs, der auf der Mobilisierung von Stammzellen aus dem Knochenmark in den peripheren Blutstrom und der Transduktion dieser Stammzellen mit adenoviralen Vektoren basiert. Hierbei codieren die Vektoren sowohl ein Transgen als auch eine Integrationsmaschinerie.

Der erste Teil der Arbeit belegt in einem humanen CD46-transgenen Mausmodell, dass adenovirale Vektoren der ersten Generation in der Lage sind, mobilisierte HSCs im Blut zu transduzieren und dass es den so transduzierten Stammzellen möglich ist, zurück ins Knochenmark zu migrieren und dort das Transgen zu exprimieren. Allerdings wurde im Verlauf von zwei Wochen ein Rückgang der Transgenexpression beobachtet. Um dies zu umgehen, wurde ein adenovirales Vektorsystem der dritten Generation genutzt, das eine hochaktive Sleeping Beauty Transposase, zum Zweck der Transgenintegration, codiert. Dieses System ermöglichte die stabile Genmodifikation mobilisierter hämatopoetischer Stammzellen nach intravenöser Injektion. Die Expression des Transgens konnte über

längere Zeitspannen (bis 12 Wochen) beobachtet werden. Die modifizeirten Stammzellen waren darüber hinaus in der Lage, genmodifizierte Kolonien *in vitro* zu bilden und das hämatopoetische System letal bestrahlter Mäuse nach Knochenmarkstransplantation zu rekonstituieren. Es wurde somit gezeigt, dass HSCs nach *in vivo* Modifikation weiterhin funktional waren.

Weiterhin wurde sowohl die Sicherheit der intravenös verabreichten Vektoren, als auch die Sicherheit der Transgeneintegration durch Sleeping Beauty in CD46-transgenen Mäusen bewertet. Abschließend wurde die hier beschriebene Gentherapiemethode in zwei dem Menschen ähnlicheren Modellen getestet. Zum einen wurden sogenannte humanisierte Mäuse, NOG Mäuse, die mit humanen $CD34^+$ Zellen transplantiert wurden, für diese Zwecke genutzt. Zum anderen wurde das Verfahren in Südlichen Schweinsaffen (*Macaca nemestrina*) angewandt.

Table of Contents

Abbreviations

AAV	Adeno-associated virus
Ad5	Human adenovirus serotype 5
ADA-SCID	Severe combined immunodeficiency due to adenosine deaminase deficiency
ALT	Alanine aminotransferase

ANOVA	Analysis of variance
APC	Allophycocyanin
AST	Aspartate aminotransferase
BA	Basophil
BAC	Bacterial artificial chromosome
BCNU	Bis-chloroethylnitrosourea
bp	Base pair
BSA	Bovine serum albumine
BV421	Brilliant Violet 421
BV510	Brilliant Violet 510
CAR	Coxsackie-adenovirus receptor
CAR cell	CXCL12-abundant reticular cell
CBA	Cytometric bead array
CBMCs	Cord blood mononuclear cells
CBP	CRE binding protein
CD46-tg	Transgenic for human CD46
CDS	Coding DNA sequence
CFC	Colony-forming cell
CFU	Colony-forming unit
CHMP	Committee for Medicinal Products for Human Use
CLP	Common lymphoid progenitor
CMP	Common myeloid progenitor
CMV	Cytomegalo virus
cpm	Counts per minute
CXCL12	C-X-C motif chemokine ligand 12
DAPI	4',6-diamidino-2-phenylindole
DBP	Single stranded DNA binding protein
EDTA	Ethylenediaminetetraacetic acid
Ef1α	Elongation factor 1-alpha
EMA	European Medicines Agency
EO	Eosinophil
FACS	Fluorescence activated cell sorting
FCS	Fetal calf serum
FITC	Fluorescein isothiocyanate
FLPe	Enhanced FLP recombinase
FX	Coagulation factor X
G-CSF	Granulocyte-colony stimulating factor
gDNA	Genomic DNA
GFP	Green fluorescent protein
GM-CSF	Granulocyte and macrophage-colony stimulating factor
GMP	Granulocyte and macrophage progenitor
HAdV	Human adenovirus
HCl	Hydrochloric acid
HEPES	4-(2-hydroxyethyl)-1-piperazineethanesulfonic acid

HSC	Hematopoietic stem cell
HSPC	Hematopoietic stem and progenitor cell
HSPG	Heparan sulfate proteoglycan
IFN-γ	Interferon gamma
IL-10	Interleukin 10
IL-12p70	Interleukin 12 active heterodimer
IL-2	Interleukin 2
IL-4	Interleukin 4
IL-5	Interleukin 5
IL-6	Interleukin 6
IR	Inverted repeat
ITR	Inverted terminal repeat
kb	Kilo bases
kbp	Kilo base pair
kDa	Kilo dalton
LD	Leukodystrophy
LT-HSC	Long-term repopulating HSC
LTC-IC	Long-term culture-initiating cell
LTRC	Long-term reconstituting cell
LY	Lymphocyte
MACS	Magnetism activated cell sorting
Mb	Mega bases
MCP-1	Monocyte chemoattractant protein 1
MCS	Multiple cloning site
MEP	Megakaryocyte and erythroid progenitor
MGMT	O6-alkylguanine DNA alkyltransferase
MLP	Major late promoter
MO	Monocyte
MOI	Multiplicity of infection
NaOH	Sodium hydroxyde
NE	Neutrophil
NHP	Non-human primate
NK	Natural killer cell
O6BG	O6-Benzylguanine
PB	piggyBac transpoase
PBMCs	Peripheral blood mononuclear cells
PBS	Phosphate-buffered saline
PCR	Polymerase chain reaction
PE	Phycoerythrin
PECy7	Phycoerythrin-cyanine 7
PGK	Phosphoglycerate kinase
PLT	Platelet
qPCR	Quantitative PCR
RBC	Red blood cell

s.c.	Subcutaneous
SB	Sleeping Beauty transposase
SCF	Stem cell factor
SCID	Severe combined immunodeficiency
SCID-X1	X-linked severe combined immunodeficiency
SD	Standard deviation
SDF-1	Stromal-derived factor 1, also CXCL12
SDS	Sodium dodecyl sulfate
SIN	Self-inactivating
SRC	SCID reconstituting cell
ST-HSC	Short-term repopulating HSC
TNF-α	Tumor necrosis factor alpha
TP	Terminal protein
UTR	Untranslated region
VCAM-1	Vascular cell adhesion protein 1
vg	Vector genomes
VLA-4	Integrin α4β1 (Very Late Antigen-4)
vp	Viral particle
WBC	White blood cell

1 Introduction

1.1 Hematopoiesis and hematopoietic stem cells

The cellular components of the blood are generated in a process termed hematopoiesis. In the adult, this process is based on the presence of hematopoietic stem cells (HSCs), which have the potential to give rise to every cell type of every lineage in the blood system. In addition, these HSCs possess the ability to self-renew so that a steady pool of these most primitive cells can be maintained throughout the human life span.

In order to give rise to fully differentiated, lineage-committed cells, the HSC has to undergo a cascade of differentiation steps. With each step, its multipotency is increasingly restricted, and the spectrum of cell types it can give rise to becomes narrower until the cell is fully committed and has only one path left to follow. These differentiation events are

thought to be organized in a hierarchy (**Fig. 1**). At the top of the hierarchy, the primitive HSC is found. Since these cells have the ability to long-term reconstitute the hematopoietic system of an irradiated recipient, they are also called long-term HSCs (LT-HSC). These cells hold tremendous potential, as it has been shown that a single transplanted LT-HSC is sufficient to reconstitute the whole hematopoietic system (1). The next step of differentiation are short-term HSCs (ST-HSCs). While these cells still can give rise to all hematopoietic lineages, they are not able to self-renew and are exhausted after 4 – 6 weeks after transplantation (2).

A step further down the hematopoietic hierarchy from the ST-HSCs are common progenitors. This transition marks the first lineage-restricting step, as the ST-HSC can either differentiate into a common lymphoid progenitor (CLP) or a common myeloid progenitor (CMP). CLPs are restricted to further differentiation into lymphoid cells, while CMPs are only able to give rise to myeloid cells. Further, CMPs then undergo a second lineage restricting event and split up into megakaryocyte and erythroid progenitors (MEPs) and granulocyte and macrophage progenitor (GMPs). Through various committed precursor stages of single-lineage potential, for example pro- and pre-B cells, these progenitors then differentiate into mature cells. This way, CLPs are able to give rise to B and T lymphocytes as well as natural killer (NK) cells, while MEPs can form red blood cells and megakaryocytes and GMPs form granulocytes and monocytes. The majority of these processes take place in the bone marrow, while only the fully committed and differentiated cells egress into the

Fig. 1 Hierarchy of hematopoietic cells. The hematopoietic system is organized in hierarchical form. Long-term HSCs with unlimited potential for self-renewal stand at the top and are able to differentiate into all lineages of the hematopoietic system. LT-HSC: long-term reconstituting HSC, ST-HSC: short-term reconstituting HSC, CMP: common myeloid progenitor, CLP: common lymphoid progenitor. MEP: megakaryocyte and erythroid progenitor, GMP: granulocyte and macrophage progenitor, ERY: erythrocytes, MK: megakaryocyte, GR: granulocytes, MO: monocytes, B: B cell, T: T cell, NK: natural killer cell. Adapted from (2, 206).

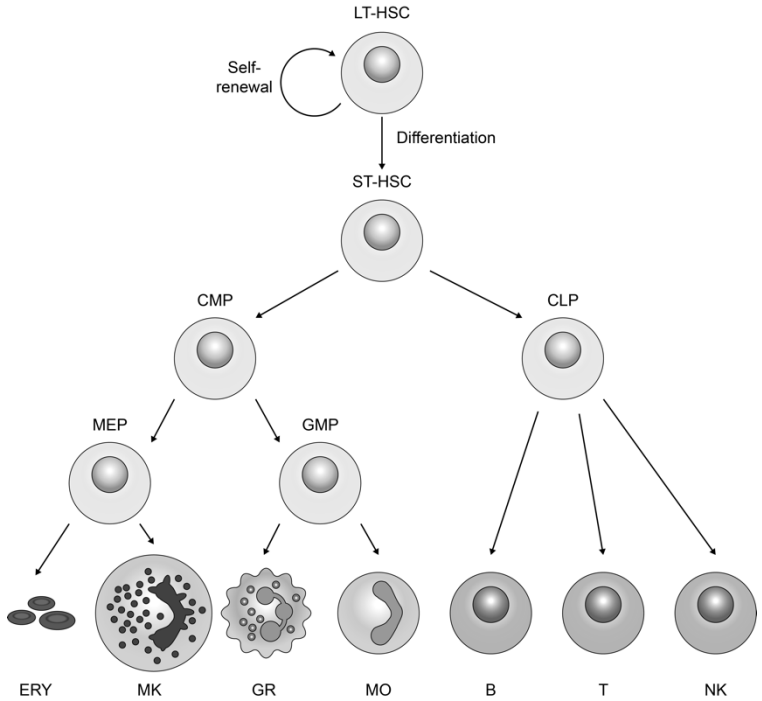

blood. The exception are lymphoid cells, which have to undergo further maturation steps once they have left the bone marrow (2).

1.1.1 The hematopoietic stem cell niche

HSCs reside in so-called stem cell niches. While the concept of the stem cell niche had been predicted by Schofield *et al.* (3), it could only be proven in recent years (4–6). The niche is conceptualized as a region of the bone marrow, where non-hematopoietic cells interact with the HSCs and regulate their dormancy and self-renewal or their differentiation and expansion (**Fig. 2**). Through interactions with the niche, HSCs are either able to remain

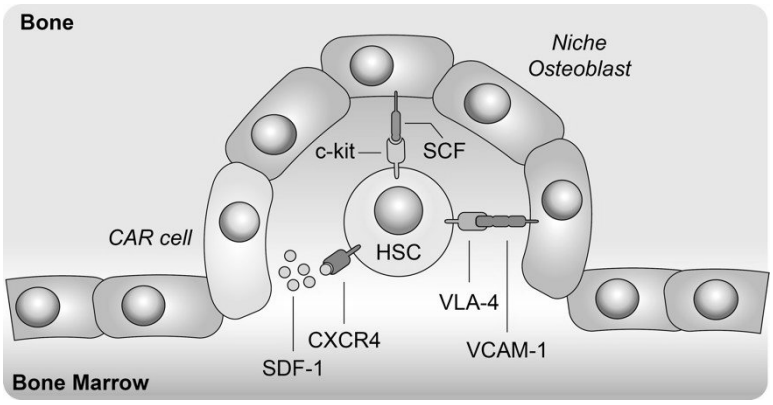

Fig. 2 The hematopoietic stem cell niche. Hematopoietic stem cells reside in a stem cell niche within the bone marrow and interact with niche osteoblasts and CXCL12-abundant reticular (CAR) cells. The niche cells interact with the HSC through different attachment and signaling molecules, actively retaining the cell in the niche and maintaining its dormancy. Adapted from (7, 47).

quiescent and occasionally undergo self-renewal, while at other times they can be pushed into a state more prone to differentiation, in which they can rapidly expand to supply vast amounts of progeny cells. To fulfill these seemingly contradictory tasks, the stem cells are capable of undergoing asymmetrical cell division. The result of this process are two daughter cells with distinct properties, functions, and cell fates. While one serves the purpose of self-renewal and will retain the primitive stem cell characteristics of its predecessor, the other can go down the path of differentiation and proliferation while slowly losing its stem cell characteristics along the way (7).

Most adult HSCs of the bone marrow are quiescent and rarely divide. To retain their dormancy, they rely on extrinsic signals from non-hematopoietic cells, for example osteoblasts and osteoclasts that create the niche environment. The retention of HSCs inside the stem cell niche is thought to be an active process involving different molecular tethers that connect the HSCs to the bone marrow stromal cells (**Fig. 2**) (8).

The most prominent of these tethers is the SDF-1-CXCR4 axis. While CXCR4 is expressed on the HSC surface, SDF-1, also known as CXCL12, is expressed by several stromal cells of the marrow and is thought to retain HSCs in the niche. In addition, it has been proposed that the SDF-1-CXCR4 axis plays a role in the maintenance of quiescence (9, 10).

Further attachment of HSCs to the bone marrow stroma is facilitated through the very late antigen 4 (VLA-4) integrin dimer on the stem cells surface. VLA-4 is able to interact with different components of the stroma, for example vascular cell adhesion molecule 1 (VCAM-

1) (11, 12) and osteopontin (13) on the surface of niche cells or fibronectin in the niche extracellular matrix (14).

In addition to the SDF1-CXCR4 axis and VLA-4, the interaction of membrane-bound stem cell factor (SCF) and c-kit plays an important role in retention of HSCs in the bone marrow niche and stem cell maintenance (15). While c-kit is highly expressed on HSCs (16), membrane bound SCF can be found in the niche (17). Binding of membrane bound SCF to c-kit can also trigger the expression of specific integrins that aid in the tethering of the HSC to the bone marrow stroma (18).

1.1.2 Hematopoietic stem cell assays

The development of the principles underlying our understanding of hematopoietic stem cells, and the formal discovery of the HSCs themselves required the development of different assays to test for stem cell properties. After initial experiments showed that irradiated hosts could be rescued through the injection of non-irradiated bone marrow cells (19), the concept of stem cells that could repopulate the hematopoietic system emerged. However, it was not clear whether these stem cells consisted of a mixed population with different stem cell types for the different lineages, or if a single stem cell could be able to give rise to multi-lineage progeny cells.

The first step in answering these questions came with the development of the colony-forming unit-spleen assay (CFU-S) (20). After injection of bone marrow cells into irradiated mice, progenitor colonies formed in the spleens of the recipients and for the first time allowed the quantification of the stem cell content in the transplanted bone marrow. Further, it was shown that these progenitor colonies contained cells of multiple lineages, proving that the same stem cell could give rise to cells of multiple lineages (21). However, it was later determined that the cells generating the splenic progenitor colonies were not able to give rise to lymphoid lineages (22, 23). Additionally, 5-fluorouracil treatment led to killing of the CFU-S but not to the death of CFU-S inducing cells in the bone marrow (24). Therefore, it was concluded that more powerful, more primitive stem cells must exist (25).

Based on work by Bradley and Metcalf (26), different *in vitro* assay systems for the detection of hematopoietic stem and progenitor cells (HSPCs) have been developed. Even

though these assays are not able to detect truly primitive, long-term repopulating HSCs, they can be used as a quick and convenient surrogate to the more complex *in vivo* assays.

The colony forming cell assay (CFC or CFU-C) is based on the growth of progenitor colonies from HSPCs in semi-solid agar or methylcellulose media. The majority of the generated colonies are lineage restricted colonies and exhibit only one or two different cell types. However, less common mixed colonies that contain erythrocytes, granulocytes, macrophages, and megakaryocytes can arise and are an indicator of more primitive colony-forming cells. The assay is usually carried out over a period of two weeks, a relatively short time that does not support the outgrowth of more primitive HSCs. Further, the generation of lymphoid colonies *in vitro* is not commonly possible in this assay system (27).

To be able to assay for more primitive cells *in vitro*, cells are cultured on layers of feeder cells for extended periods of time. The cells are then subjected to CFC assays to determine the content of long-term culture-initiating cells (LTC-IC), which can be used as a surrogate for HSC content (28).

In spite of these *in vitro* stem cell assays, repopulation assays remain the gold standard for the analysis of truly primitive LT-HSCs. The simplest of these assays is based on the detection of long-term repopulating cells (LTRCs). Irradiated mice are injected intravenously with serial dilutions of stem cells and hematopoietic reconstitution is assayed after 3 – 4 months. The content of LTRCs in the sample can be calculated based on the dilution of the sample that still allows for successful rescue of the recipient (29).

While the LTRC assays allows to test for the presence of HSCs, it does not allow any conclusions over the performance of the assayed stem cells. If the performance of a stem cell sample is to be assessed, for example after treatment with a growth factor, it needs to be compared to untreated competitor cells. To this end, competitive reconstitution assays were developed. These assays are based on the co-transplantation of untreated cells and treated cells derived from two donors that express different isotypes of CD45. After reconstitution, the ratio of CD45.1 to CD45.2 can be determined and allows conclusions over the reconstitution performance of the treated graft (27).

The study of human hematopoietic stem cells in retransplantation assays became possible with the development of NOD/SCID mouse models that allowed for the engraftment of

human HSCs and the generation of hematopoietic mouse/human chimeras. Based on this model, the SCID repopulating cells (SRCs) were accepted as a metric for human HSCs. However, one must note that this xenograft model is artificial, and the results should be regarded with a certain extent of caution (30).

The advent of flow cytometry facilitated the phenotypic characterization of hematopoietic stem cells based on the expression of surface markers. In combination with the assays outlined above, flow cytometry allowed researchers to increasingly enrich bone marrow cells for high contents of LTRCs. However, even in the most highly enriched fractions of HSCs, the long-term reconstitution potential remains at 30 – 50 %, even though the cells show homogenous surface marker expression. This shows that other characteristics of HSCs must be involved in determination of the true HSC phenotype (30).

1.1.3 Differences in HSCs between mouse and man

While hematopoietic stem cells of mice and men are similar in the vast majority of their characteristics, there are some cases in which distinct differences have been uncovered. Most important for phenotypic analysis purposes are the significant differences in surface marker expression between murine and human HSCs.

In mice, one of the phenotypic signatures of HSC-enriched cell populations is a combination of the absence of lineage markers (Lin^-) and the expression of Sca-1 and c-kit (31). These cells have been subsequently termed LSK cells (Lin^-, $Sca\text{-}1^+$, $c\text{-}kit^+$). However, cells exhibiting these markers make up a relatively heterogeneous population, and only about 10 % of the cells are true HSCs. Another set of HSC-defining markers are the so called SLAM family members, CD150, CD244, and CD48 (32). HSCs have been shown to be $CD150^+$, $CD244^-$, and $CD48^-$. The SLAM markers can be used in combination with the LSK markers to obtain a cell population that contains about 50 % of true HSCs.

In humans, CD34 was the first marker discovered to enrich for HSCs. In contrast to human HSCs, mouse HSCs have been shown to be negative for CD34. However, CD34 alone is not a stringent enough marker to sufficiently enrich cell populations for HSCs. To improve upon this, additional surface markers have been described resulting in a HSC phenotype defined by the following markers: $CD34^+$, $CD38^-$, $Thy1^+$, and $CD45RA^-$ (33–36).

In addition to these phenotypic differences, some functional differences between murine and human HSCs have been described. It is thought that these are most likely due to the differences in organism size and life span between men and mice. For example, the longer lifespan in humans increases the risk of mutations over time and increases the necessity for increased tumor suppression. As a result, human HSCs are more resistant to transformation than their murine counterparts (2).

Despite the differences mentioned above, several studies have suggested that the size of the stem cell pool for both mice and humans is roughly the same (37–39). It was estimated that both mice and humans possess roughly $1x10^4$ to $1x10^5$ HSCs.

1.2 Hematopoietic stem cell mobilization

1.2.1 Circulation of stem cells under physiological conditions

Only a small fraction of HSCs are circulating in the peripheral blood under steady state conditions, while the majority of HSCs is found in the bone marrow (8). The freely circulating HSCs are thought to be a means of exchange between different stem cell niches. For example, in case of damage to a certain niche, HSCs released from a different, distant niche can home to the damaged niche to replenish its hematopoietic potential (40). In fact, circulating HSCs appear to be able to rapidly reengraft in the marrow leading to constant egress and reengraftment of HSCs (41). In addition, it has been suggested that release of HSCs into the peripheral blood is part of bone marrow homeostasis and provides a way to dispose of superfluous stem cells (42).

In case of stress, for example following infection or chemotherapeutic treatment, the amount of circulating HSCs is increased. It is thought that HSCs closest to the site of stress are skewed towards a higher rate of differentiation at the expense of less focus on self-renewal. This leads to partial exhaustion of the hematopoietic potential of this site. HSCs released from distant niches are then able to home to the exhausted site and settle in the vacant niches in order to restore the hematopoietic potential (40).

Massive mobilization of HSCs can also be observed during development. The first hematopoietic stem cells are thought to be formed in the fetal liver, before formation of

the bones has begun. Once the bones are formed, fetal liver HSCs are released into the circulation and seed the newly created niches in the bone marrow (43–45).

1.2.2 Agents of stem cell mobilization

The enforced egress of HSCs from the bone marrow into the periphery is referred to as mobilization. The mobilization of stem cells is mainly used for the collection of HSCs, either for use in direct transplantation or for gene therapeutic modification.

Currently, the most commonly used mobilizing agent is recombinant human granulocyte-colony stimulating factor (G-CSF). It is given in form of subcutaneous injections for 5 days and leads to efficient mobilization of both HSCs as well as more differentiated cells (8). The mobilizing effect of G-CSF is achieved through different mechanisms. Firstly, G-CSF induces cell division in the bone marrow and leads to an expansion of the stem cell pool as well as overall proliferation of hematopoietic cells. Secondly, G-CSF is able to interfere indirectly with the SDF-1/CXCR4 interactions of HSCs with the bone marrow stroma. This is thought to be facilitated through two distinct pathways. Firstly, G-CSF interacts with bone marrow macrophages, which induce and then downregulate the expression of SDF-1 in osteoblasts (46–48). Secondly, G-CSF induces several proteases in the stroma, which cleave SDF-1 off of the cell surface and loosen the tethering of the HSCs to their niche (49). Furthermore, these proteases are capable of severing other connections with the stroma.

As mentioned above, hematopoietic stresses can also lead to increased levels of circulating HSCs. One example of these stressors are chemotherapy drugs, such as cyclophosphamide. Mechanistically, stress signals sent out after chemotherapeutic treatment are thought to induce the expression and release of G-CSF, which in turn triggers mobilization as described above (50).

Another class of mobilizing agents are CXCR4 antagonists, most prominently AMD3100. These agents lead to rapid mobilization of HSCs (51, 52) (compared to G-CSF) and are thought to cause mobilization solely through disruption of the SDF-1-CXCR4 axis, without the induction of HSC proliferation. AMD3100 has been shown to synergize with G-CSF mobilization (52), showing that G-CSF is only partially able to interfere with the SDF-1-

CXCR4 axis. Due to its higher mobilization power, the combination of G-CSF and AMD3100 is used as a regimen in poor mobilizers, for example chemotherapy patients (53, 54).

Along the same lines, soluble SCF is able to interrupt the connection between membrane-bound SCF and c-kit. SCF is considered a slow mobilizing agent and has to be administered for several days (55, 56).

Lastly, a relatively novel class of mobilizing agents is aiming at VLA-4. Both antibodies (57) and small molecules (58) binding to VLA-4 have been shown to be able to rapidly mobilize HSCs and are also thought to have a synergistic or at least additive effect together with G-CSF and AMD3100 (58, 59).

1.3 Gene therapy

The European Medicines Agency (EMA) uses two characteristics to describe a gene therapeutic medicinal product. Firstly, the product contains or consists of a recombinant nucleic acid that can be administered to humans with the goal of regulating, repairing, replacing, adding, or deleting a genetic sequence, and secondly, the effect achieved by this is directly related to the employed nucleic acid (60). In short, gene therapy aims at the introduction of recombinant DNA into the cell in order to cure or prevent disease.

In terms of clinical trials, the most common indication for gene therapy to date is cancer, followed by monogenic diseases, cardiovascular diseases, and infectious diseases. In these trials, adenoviral and retroviral vectors have been most commonly used for gene delivery (61)

Gene therapy regimen can alternatively be subdivided into strategies aimed at germ line cells or at somatic cells. Modifications of germ line cells would be passed on from the individual to its offspring and is ethically controversial. Therefore, thus far only gene therapy regimens aimed at somatic cells have been developed.

Even though the number of successful clinical gene therapy trials is steadily increasing, only a handful of gene therapy drugs have been approved for use in patients. The first two gene therapy drugs were approved for use in China. Gencidine, an Adenovirus serotype 5 vector that expresses p53 to combat head and neck squamous cell carcinoma, was the first (62,

63). It was followed by Oncorine, an oncolytic Adenovirus that was only able to replicate in cancer cells due to its E1B 55K viral gene deletion (64). Oncorine was approved for the treatment of late-stage refractory nasopharyngeal cancer in combination with chemotherapy (65).

In 2012, Glybera was the first gene therapeutic drug to be approved for the European market (66). Glybera is an Adeno-associated virus (AAV) type 1 carrying a hyper-functional lipoprotein lipase (LPL) gene to treat LPL deficiency (67).

The approval of these gene therapeutics made them forerunners for a new class of medicines. However, as seen in the case of Glybera, their development and approval is lengthy, and the finished product comes at a high price. The cost of one treatment of Glybera was predicted to be in the order of $1 million (68), and the treatment has only been applied once following its entry into the marketplace (69).

Another way to classify gene therapy treatments is to subdivide them into *in vivo* and *ex vivo* gene therapies. For *ex vivo* therapies, cells have to be isolated from a patient or donor and are then modified *ex vivo*, usually using retroviral vectors. This method is commonly used in the context of hematopoietic stem cell gene therapy and is described in greater detail below. Advantages of *ex vivo* gene therapy include high transduction efficiencies, the avoidance of off-target transduction events, as well as the possibility to select for modified cells or test the quality of the generated product before administration to the patient.

In contrast, for *in vivo* gene therapy, a gene therapy vector is delivered directly into the patient. The vectors in these regimens are usually non-integrating adenoviral or adeno-associated vectors. Depending on the vector platform, either transient (AdV) or long-term (AAV) gene expression can be achieved. However, due to their non-integrating nature, these vectors are usually used in post-mitotic tissues, for example cardiac (70) and skeletal (71, 72) muscle , the liver (73, 74), the retina (75–77), as well as the nervous system (78, 79)

1.3.1 Hematopoietic stem cell gene therapy

Hematopoietic stem cells, as discussed above, are at the top of the hematopoietic hierarchy. They possess the ability to generate every cellular component of the

hematopoietic system. Moreover, a single HSC is able to give rise to myriads of progeny cells. As such, they are considered promising targets for gene therapeutic treatment of hematologic disorders, since gene correction of the stem cells would also mean gene correction in all progeny cells derived from this cell. Additionally, HSCs have been the subject of extensive research for more than half a century, and the techniques to isolate, maintain and modify them have long been established.

The most common process for the gene therapy of hematopoietic stem cells involves the collection of bone marrow or mobilized peripheral blood cells. From this starting material, fractions enriched for HSCs are isolated and maintained *ex vivo.* The stem cells are then usually transduced with a retroviral vector carrying the desired transgene cassette. Since retroviral vectors possess the ability to integrate their genome into the DNA of the host, the transgene cassette can be retained throughout cell division and will be passed on to progeny cells. The modified HSCs are then transfused back into the patient, usually requiring a certain level of myeloconditioning to allow engraftment of the modified cells.

Among the most common diseases attempted to be treated with HSC gene therapy approaches are primary immunodeficiencies, such as severe combined immune deficiencies (SCIDs) (80, 81), as well as other monogenic hematologic disorders such as hemoglobinopathies (82). Since these diseases are caused by defects in single genes (monogenic), they can be treated with relatively simple gene therapy vectors encoding only one transgene.

1.3.2 Clinical successes in HSC gene therapy

The first clinical trial for gene therapy of the hematopoietic system was initiated in 1990, and it aimed at correcting adenosine deaminase deficiency severe combined immunodeficiency (ADA-SCID) in two children. T lymphocytes of the patients were *ex vivo* transduced with a gammaretroviral vector, encoding a functional copy of the ADA cDNA. Both patients responded partially to the treatment but had to remain on supplemental enzyme replacement therapy (83). This study not only showed a proof-of-principle for gene therapy, but also shifted focus towards the modification of HSCs in order to achieve higher engraftment rates and better therapeutic outcome.

In the last two decades, a host of HSC gene therapy clinical trials for several indications have been performed and not only further demonstrated the potential power of the approach, but they also uncovered complications that will have to be addressed in the future.

Several clinical trials for ADA-SCID have been carried out and more than 40 patients have been treated worldwide. All of the patients are alive and the therapeutic intervention allowed the majority of patients to be independent of enzyme replacement therapy (80, 84, 85). The gene therapeutic treatment of X-linked SCID (SCID-X1) in children was met with success in most patients (81, 86). These overwhelmingly positive outcomes in the treatment of SCIDs are at least in part thought to be due to the selective advantage that is conferred to gene-modified HSCs and their progeny. Further, vacant spaces in the hematopoietic compartments of SCID patients allowed for efficient engraftment of the transplanted cells.

Besides SCIDs, leukodystrophies (LDs), a group of monogenic diseases caused by the disability to properly form or maintain myelin sheaths in the central nervous system, have been the target of clinical HSC gene therapy trials. The treatment of both X-inked adrenoleukodystrophy (X-ALD) (87) and metachromatic leukodystrophy (MLD) (88) through gene-modified HSCs were met with success.

Another indication to be treated by HSC gene therapy is β-thalassemia caused by a lack of functional β-globin expression. In a clinical trial, a mini globin gene under the control of a minimal β-globin promoter and locus control region was transferred into HSCs using a lentiviral vector. One year after the transplantation of the gene-modified HSCs, the patient was independent of blood transfusions (82).

The most recent success in the field was the recommendation of the gene therapy product Stimvelis through the Committee for Medicinal Products for Human Use (CHMP), part of the EMA, in April 2016. CHMP recommended to grant market authorization of this treatment for ADA-SCID. Strimvelis consists of autologous $CD34^+$ cells that have been transduced with a retroviral vector encoding the ADA cDNA sequence.

The above examples demonstrate that *ex vivo* HSC gene therapy is a potent tool for the treatment of inherited diseases. However, long-term follow up of the patients treated in those trials revealed some serious complications.

1.3.3 Problems of *ex vivo* HSC gene therapy

The earliest clinical trials of HSC gene therapy employed gammaretroviral vectors to integrate the therapeutic transgene into the host genome. However, in the SCID-X1 trial mentioned above, 5 out of 20 patients developed leukemia 2.5 – 5 years after gene therapy. Sequencing of the malignant cells revealed that the viral vector had integrated into oncogene loci, most commonly into the LMO-2 locus (89–91).

In a different study, treating X-linked chronic granulomatous disease (X-CGD) with HSC gene therapy, dominant gene-modified clones were detected 5 – 15 months after treatment, which later led to the development of leukemia. Again, activation of growth-promoting genes through insertion of the vector genome was observed (92, 93).

Following these unfortunate outcomes, research of the integration behavior of retroviral vectors in human cells was intensified. This research uncovered the preferential integration of gammaretroviral vectors into gene regulatory sequences (94–97). This tendency, together with the presence of the fully intact viral long terminal repeats (LTRs), which contain promoter and enhancer elements, caused a great risk for aberrant gene regulation and clonal expansion. The usage of the intact viral LTRs was originally intended to ensure high expression levels of the encoded transgene but was later abandoned to generate a transcriptionally inactive LTR. This lead to the development of self-inactivating (SIN) retroviral vectors (98–100), not only increasing the safety of the vector but also allowing the use of customized promoter elements to drive transgene expression.

However, the use of SIN vectors alone did not alter the integration pattern of the retroviral vector. To further increase safety, researchers switched from gammaretroviral vectors to lentiviral vectors for most gene therapy applications. In contrast to gammaretroviral vectors, lentiviral vectors tend to integrate into the gene itself rather than into the regulatory elements, which lowers, but not fully eliminates, the genotoxic potential of the vector (101–103).

In addition to their lowered genotoxic potential, lentiviral vectors possess another advantage over other classes of retrovirus vectors. While gammaretroviral vectors require cell division for them to be able to integrate (104–106), the lentiviral pre-integration complex possesses the ability to enter the nucleus independently of the mitotic state of the cell (106–109). This allows lentiviral vectors to integrate into-quiescent cells and reduces the need for intensive cytokine activation of HSCs prior to transduction during *ex vivo* culture. Avoiding intense stimulation of HSCs, in turn helped to preserve their stem cell potency as much as possible as they are not forced into cycling. Even though this allows the usage of lower doses of cytokines, it cannot be completely avoided, leading to a certain loss of stemness and engraftment potential during the *ex vivo* culture of HSCs (110). This potential for loss of stem cell capabilities clearly marks one of the problems of *ex vivo* gene therapy.

In the early trials only low engraftment rates of modified cells were observed. This was later attributed to a lack of room in the marrow compartment of the patients, where the modified cells could engraft, a prerequisite for them to produce gene-corrected progeny cells. It was later suggested that chemotherapeutic myeloconditioning is able to free up the required space in the bone marrow and allows for more efficient engraftment. This was demonstrated in the X-CGD clinical trial, an example where low-dose busulfan conditioning led to satisfying engraftment rates (92), as well as in the ADA-SCID trial (80). However, it must be considered that myeloconditioning of patients that are suffering from hematological disorders, which are often connected to a compromised immune system to begin with, can pose considerable risks for the patient's health.

In summary, the genotoxic potential of the employed retroviral vectors, including the risk for the development of leukemia following gene therapy, the requirement for potentially exhausting *ex vivo* culture of the graft, and the need for myeloconditioning of the patient are among the main disadvantages of current protocols for *ex vivo* HSC gene therapy.

1.4 Adenoviruses

The family of *Adenoviridae* can be subdivided into four different genera. The Mastadenoviruses possess the ability to infect mammals. Human Adenoviruses (HAdVs) are part of this genus. Further, Aviadenoviruses infect birds, while Siadenoviruses and

Atadenoviruses can infect both mammals and birds as well as reptiles and fish (111). The group of human Adenoviruses can be further subdivided into 6 species, A to F, although a seventh species G has been proposed more recently (112). Within these groups, 70 different types can be found, although the number has been growing rapidly in recent years and can be expected to further increase. The type classification was historically based on the viruses' ability to be neutralized by specific animal antisera (serotype) but has more recently been replaced by sequence comparison of hexon, fiber and penton, or whole genome sequencing (113). An overview of the human Adenovirus types is given in **Tab. 1**.

Different Adenovirus species have been shown to utilize different cellular surface proteins as primary attachment receptors. Species B1 viruses, among others containing HAdV types 3, 7 and 14, utilize desmoglein 2 as a surface receptor (114), while species B2 viruses use CD46 to attach to target cells (115). HAdV type 37 has been shown to utilized the glycan GD1a as a receptor (116). The remaining HAdVs are thought to utilize the coxsackie-adenovirus receptor (CAR) for attachment (117). Human Adenoviruses can cause mild infections of the respiratory, gastrointestinal and urinary tract. Further, infections of the kidneys and eyes are possible. In immunocompetent individuals, these infections are usually mild, self-limiting and without complications. The adenoviral genome is organized in one single DNA molecule. For human adenovirus serotype 5 (Ad5), the length of the genome is roughly 36 kbp. As mentioned above, when packed into the capsid, the genome is associated with different core proteins. The two copies of the terminal protein interact with each other to keep the packed genome in a quasi-circular conformation.

Tab. 1: Classification of human Adenoviruses. The seven species of human Adenoviruses, their respective types, and the cellular receptor that is used for attachment to a target cell. Adapted from Knipe and Howley 2013 (118).

Species	Type	Receptor
A	12, 18, 31, 61 (119)	CAR
B1	3, 7, 14, 66 (120), 68 (121)	DSG2
B2	16, 21, 35, 50, 55 (122),	CD46
C	1, 2, 5, 6, 57 (123),	CAR
D	8, 9, 10, 13, 15, 17, 19, 20, 22–30, 32, 33, 36, 38, 39, 42–49, 51, 53, 54, 56 (124), 58 (125), 59 (126), 60 (127), 62-65 (128–131), 67 (132), 69 (133), 70 (134)	CAR
	37	GD1a

E	4	CAR
F	40, 41	CAR
G	52	CAR

Viral genes are encoded on both strands of the genome and can be subdivided into 5 transcription units (**Fig. 3A**). Four of these units (E1 – E4) are active early in the viral life cycle. They are driven by their individual promoters and supply proteins that are required for replication of the viral genome. The fifth transcription unit is active in the late stages of infection and is driven by the major late promoter (MLP), which drives several genes encoding the structural components of the virus capsid as well as two viral RNAs.

1.4.1 Adenoviral life cycle

The replication cycle of human adenoviruses can be subdivided into different phases. The cycle begins when the virus attaches to a target cell, followed by entry of the virus into the host cell and release of the viral genome into the nucleus. Once the genome reaches the nucleus, early viral gene expression ensues to provide ideal conditions for viral replication. The expression of the early genes is followed by the replication of the viral genome, which in turn is followed by expression of the late viral genes. Lastly, new viral particles are assembled, the host cell is lysed and viral progeny is released.

The attachment of the virus particle to the cell is initiated by the high affinity binding of the viral fiber knob to its respective cellular receptor on the target cell surface. Once this high affinity interaction is established, a second interaction between the viral capsid and the cell surface takes place. An Arg-Gly-Asp (RGD) peptide motif found in the penton base of many HAdV types is able to interact with integrins on the cell surface and to cause endocytotic uptake of the virus particle. At this point, the virus sheds its fibers, which initiates the organized disassembly of the viral capsid (135). The endocytotic vesicles then mature, leading to endosome escape of the virus. This step is followed by further orderly disassembly of the capsid and the transport of the subviral particle, containing the genome and viral proteins, along microtubules towards the nucleus. Once the nucleus is reached, subviral particles interact with nuclear pore complexes followed by further uncoating of the subviral particle and import of the viral genome into the nucleus (118).

Import of the virus genome into the nucleus is followed by the expression of early viral genes. There are thought to be three essential roles for early gene products: First, the host cell has to enter the S phase of the cell cycle in order to provide an optimal environment for viral DNA replication. Second, the host defense mechanisms aimed at shutting down

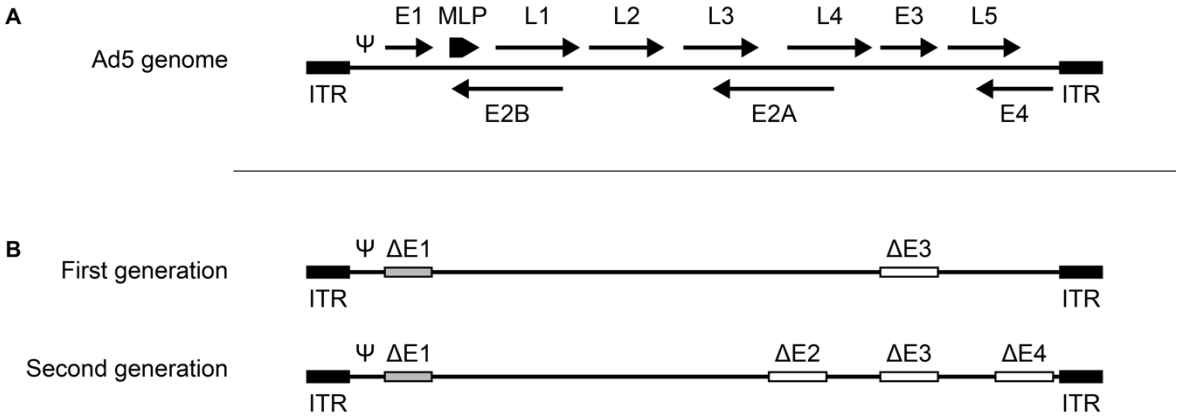

Fig. 3 Wild type Ad5 genome and adenoviral gene delivery vectors. A) The wild type genome of Ad5 is subdivided into different early transcription units (E1 – E4) controlled by individual promoters and several late transcription units (L1 – L5), which are controlled by the mayor late promoter (MLP). B) First-generation adenoviral vectors are deleted for the E1 and E3 transcription units. A transgene cassette is usually inserted into the former E1 region. Second-generation Ad vectors are additionally deleted for the E2 and E4 regions. Third-generation or helper-dependent vectors are deleted for all viral genes except for the inverted terminal repeats (ITRs) and the packaging signal (Ψ). In addition to the transgene, the genome contains stuffer DNA to ensure the correct size of the genome. Adapted from (218).

viral infection need to be blocked and thirdly, viral gene products required for viral DNA replication need to be synthesized (118).

The first viral genes to be expressed are encoded in the E1A regions of the genome. Two alternatively spliced E1A transcripts encode for the viral proteins E1A S12 and E1A S13. Both proteins are able to disrupt retinoblastoma family proteins' (pRB) repressive interaction with E2F transcription factors. This liberates E2F, which in turn is able to activate several genes required for entry into the cell cycle. In addition, E1A protein binding to regulators of chromatin structure and transcription, such as p300 and CRE-binding protein (CBP), as well as expression of the E4 gene products E4orf1 and E4orf4, are also thought to support induction of cycling in the host cell (118).

As a host defense mechanism, apoptosis can be induced following E1A and E4 gene expression through p53-mediated mechanisms and other pathways. To suppress premature cell death due to apoptosis, the early viral proteins E1B-55K and E4orf6 are able to cause degradation of p53 in the proteasome as well as repression of genes with p53

binding sites. Further, E1B-19K is able to suppress apoptosis through activation of BAX and BAK proteins. Gene products of the E3 region are furthermore responsible for suppression of externally activated apoptosis through cytotoxic T cells (118).

To set the stage for viral DNA replication, liberated E2F transcription factors come into play once more. The transcription factors are able to interact with and activate viral E2 genes, which encode essential parts of the viral DNA replication machinery. Among them are the viral DNA polymerase, the ssDNA binding protein (DBP), and terminal protein. All of these gene products are necessary for viral genome replication. The replication process takes place in two phases. The inverted terminal repeats (ITRs) of the viral genome serve as origins of replication. In the first phase of replication, DNA synthesis occurs in a semi-conservative fashion, using one of the parental DNA strands as template. This results in a parental DNA strand paired with a newly synthesized daughter strand as well as a single parental strand. Both ITRs of this single parental strand are able to anneal and form a double-stranded panhandle that can serve to initiate replication and lead to generation of a second daughter DNA strand (118).

With the onset of DNA replication, the switch from early to late viral gene expression occurs through activation of the major late promoter. The MLP drives the transcription of one 28 kbp primary transcript from which the different mRNAs for the late genes L1 - L5 can be generated. Late gene products contain structural proteins for progeny viruses as well as proteins and RNAs that facilitate the shut-off of cellular protein expression and virion assembly. The structural components of the hexon and penton capsomeres polymerize in the cytoplasm and are then imported into the nucleus. Here, pro-capsids are assembled and the viral genome is packaged. Further processing involving the viral protease results in formation of infectious viral progeny. The virus producing cells are finally lysed and progeny virions are released (118).

1.5 Adenoviral vectors for gene therapy

Early studies aimed at the possibility of transducing hematopoietic stem and progenitor cells with adenoviral vectors generated controversial results. While one group of studies employed low multiplicities of infection (MOIs) and short incubation times and concluded that vectors based on Adenovirus type 5 (Ad5) were not able to transduce these cells (136,

137), a different group of studies, using high MOIs, extended incubation periods and cytokine stimulation of HSCs found that transduction was possible (138–142). Looking at the expression of CAR and integrins required for Ad5 transduction, researchers concluded that even though HSCs were lacking the cellular receptors (143), unspecific internalization of the vector could be achieved and would be favored by high MOIs and long incubation periods. However, these infection conditions often resulted in cytotoxic effects and loss of stem cell function in the transduced cells (144, 145), and it was concluded that CAR-tropic Ad5 vectors did not fulfill the requirements of a HSC gene therapy vehicle.

1.5.1 Tropism modification of adenoviral vectors

Based on the lack of HSC transduction potential of Ad5, researchers tested other Ad serotypes for their hematopoietic cell transduction capabilities (146, 147). Several studies uncovered that Ads belonging to subgroup B were much more potent in transducing HSCs (146–149). This was due to the altered tropism of the viruses, allowing them transduction independent of CAR and integrin expression.

Fiber chimeric vectors were devised to be able to harness this improved HSPC transduction potential of subgroup B viruses and the established methods to modify the well understood Ad5 vectors. These vectors were based on Ad5, but the fiber gene was partially replaced with that of Ad11 or Ad35. Moreover, studies employing these vectors were able to show that they could transduce even primitive HSC populations, enriched for true, long-term reconstituting stem cells (138, 150).

In addition to serotype switching, several other methods of tropism modification for adenoviral vectors have been developed. These approaches can be subdivided into chemical/physical modification of the vector and genetic modification of the vector. Chemical and physical approaches are based on the modification of the vector after it has been released from the producer cell. These modifications can include the chemical attachment of targeting antibodies or adaptors to the virus capsid or the shielding of intrinsic viral targeting molecules to modify virus tropism. Genetic modifications aim at introducing targeting moieties into the fiber gene or disrupting amino acid sequences involved in natural receptor binding to achieve de-targeting.

While both approaches have been employed to allow Ad5 transduction of hematopoietic cells (151, 152), several drawbacks have to be considered. First, while genetic introduction of a polylysine motif or a cyclic RGD peptide into the fiber knob of Ad5 led to increased transduction, it is important to consider that this modification is not specific to a certain target cell and leads to a broader tropism of the modified vector. While this is acceptable for the *in vitro* transduction of purified HSCs, this approach would lead to increased off-target transduction *in vivo*. Second, while retargeting of a virus to the stem cell marker CD34 led to targeted attachment of the vector to HSPCs, the same virus was only poorly internalized, resulting in poor gene transfer potential (153). This highlights the complexity underlying the processes following attachment, i.e. internalization, endosome escape, etc. and shows that modifying the tropism requires more than just giving the virus a different target.

In light of this, a serotype swap is usually preferred over other forms of tropism modification, if it allows reasonable targeting of the desired cell type.

1.5.2 Helper-dependent adenovirus vectors

A viral gene transfer vector has to fulfill two requirements: First, it has to be able to effectively deliver its genetic payload and second, it must be safe, i.e. kept from going through its replicative program and killing the transduced cell. In early adenoviral vectors this was achieved by deleting the viral E1A and E3 genes and inserting a transgene cassette in their stead (**Fig. 3B**). Since E1A is thought to serve as the master regulator of viral gene expression and replication, the lack of E1A should lead to a virus that does not express viral genes and does not replicate. Therefore, for virus production, cell lines stably expressing E1A must be used (154–156). However, shut down of viral gene expression through E1A deletion is not complete, and leaky expression of viral genes can occur. This can trigger immune reactions against transduced cells and can diminish transgene expression (157, 158). Further, the total genome size of adenoviral vectors can only be modified within limits and deletion of the E1A and E3 region frees up relatively little space for the transgene payload. To increase the cloning capacity, second-generation Ad vectors (**Fig. 3B**) were additionally deleted for the rest of the E1 region, as well as E2 and E4 (159, 160). However, this modification did not alleviate the immunogenicity of the viral gene products.

This problem could only be solved with the development of third-generation vectors, which are also called helper-dependent, gutted or gutless adenoviral vectors (**Fig. 3B**). These vectors are devoid of all viral genes and the only viral sequences that remain are the inverted terminal repeats (ITRs) and the packaging signal (161). For the production of these viruses, coinfection with a helper virus is required. The helper virus delivers all viral proteins required for virion assembly *in trans*. To avoid competition of the helper-dependent vector genome with the helper genome for packaging into viral particles, the packaging signal of the helper virus is flanked by *loxP* sites and vector production is performed in Cre-expressing cells (162). In addition, packaging of the helper virus can be further inhibited by decreasing the size of its genome. This way, the potentially contaminating helper virus can also be removed from the helper-dependent vector in a cesium chloride density gradient ultracentrifugation.

Not only are these gutless vectors less immunogenic due to the absence of leaky viral gene expression, but they also cause less cytotoxicity when transducing hematopoietic cell lines or HSCs *in vitro*, when compared to first-generation vectors (163, 164). Moreover, gutless vectors have the potential to carry large transgene cassettes of up to 36 kb, which allows the use of endogenous promoters and other regulatory elements.

1.5.3 Adenovirus vectors for the genetic modification of HSCs

Since HSC gene therapy usually aims at integration of a therapeutic transgene into the stem cell, which then passes the modification on to progeny cells, adenoviral vectors, which lack active integration of their genome into the transduced host cells, have traditionally been deemed inadequate for gene transfer into HSCs. However, the advent of the so called designer nucleases has the potential to change this (165). The designer nucleases allow for the targeted introduction of DNA double strand breaks into virtually any region of the genome. Following the introduction of the double strand break, the cellular DNA repair machinery attempts to seal the nick, but this has a high potential for insertions or deletions, leading to frame shift mutations. These frame shifts can in turn cause the effective knock-out of the target gene. To elicit this knock-out, the nuclease only needs to be expressed transiently, while the genomic modification is stable and will be passed on to progeny cells when used in stem cells. In addition, long-term expression of these nucleases has been

associated with increased off-target effects and cytotoxicity (166), making an adenoviral vector a good choice to deliver nuclease-genes to sensitive hematopoietic stem cells.

One example for this approach was performed by Li *et al.* (167). The authors employed a first-generation adenoviral vector carrying an Ad35 fiber shaft and knob to express a pair of zinc finger nucleases (ZFNs) directed against the human CCR5 gene in HSPCs following *ex vivo* transduction. CCR5 acts as a co-receptor for HIV-1 infection in humans. In a groundbreaking study, an HIV patient developed resistance to the virus after receiving a bone marrow transplant from a CCR5-negative donor. Based on this, it had been shown that nuclease-mediated knock-out of CCR5 could artificially confer HIV resistance. In the above mentioned study, Li *et al.* showed that after transduction with a CCR5-ZFN encoding adenoviral vector, HSCs exhibited a knock-out for the CCR5 gene (167). Further, following transplantation of these modified cells into NSG mice, the HSCs were capable of long-term, multi-lineage engraftment, passing the CCR5 knock-out on to their progeny. Finally, upon HIV-1 challenge, animals showed effective protection of T cells from HIV-1 infection.

1.5.4 Integrating adenovirus vector systems

Even though the nuclease-based strategies outlined above allow for the stable modification of HSCs, they are limited to the knock-out of genes. Many of the potential HSC gene therapy applications however, require the introduction of therapeutic DNA. To be able to use adenoviral vectors in this context, so called hybrid vector systems have been developed. The methodology for these systems is to use an adenoviral vector for gene delivery that encodes an integration machinery and enables integration of a transgene.

One of these strategies can be viewed as an extension of the nuclease-based gene disruption described above. While homologous recombination can be used to introduce a transgene into the cellular genome, the recombination rates under normal conditions are very low (168). However, if nucleases are used to introduce a double strand break in the genome and a matching DNA template flanked by homology arms is delivered, the recombination efficiency can be drastically increased (169). Based on this, Ad vectors that encode both a site-specific nuclease and a transgene flanked by homology arms have been used to introduce transgenes stably into the cellular genome (168). Due to their large

cloning capacities, helper-dependent adenoviral vectors are well suited for this approach, as they allow the encoding of large transgene cassettes containing long homology arms.

Another approach is based on a hybrid vector system that combines features of adenoviral vectors with those of adeno-associated viruses (AAVs). While the Ad portion of the system is employed for efficient delivery, the AAV portion is leveraged to facilitate long term expression for the transgene. In one method, this is achieved by flanking the transgene cassette with the ITRs of AAV (170). The transgene can integrate into the host genome through the ITRs. However, this is a passive process, and only a fraction of the transgenes delivered this way will integrate into the host genome. Furthermore, this AAV Rep-independent, ITR-directed integration process has been shown to be biased towards integration into transcriptionally active regions for recombinant AAV serotype 2 vectors (171), holding the potential for genotoxic transformation. A different iteration of the Ad/AAV hybrid vector system delivers the AAV Rep proteins *in trans,* which leads to the directed integration into the AAVS1 region of the human genome (172). Even though the directed integration into the AAVS1 locus somewhat ameliorates the genotoxic potential of the system, it is important to consider that AAVS1 is a gene-rich region of the genome and holds the potential for trans-activation of neighboring genes following transgene integration. However, when looking into this problem, Lombardo *et al.* found the AAVS1 locus to be relatively resistant to upregulation of nearby genes (173), leading to acceptance of the AAVS1 locus as a safe harbor for gene integration.

A third class of integrating hybrid vectors achieves transgene integration through the use of a transposase. The most prominent transposase used for this purpose is Sleeping Beauty transposase (SB). The SB gene was reconstructed from ancient fish DNA and it was shown that, through interaction with inverted repeats (IR) of a matching transposable element – or transposon – , it could integrate the transposon into the genome of fish, mouse and human cells (174). In contrast to AAV or retroviral vectors, SB-mediated integration was found to result in close-to random distributions of integration sites across the genome (175). The transposase was later modified to give rise to several hyperactive variants of the enzyme (176, 177) resulting in the latest version, SB100x, which displays a 100-fold increased integration activity over the wild type version (178). Yant *et al.* performed the first study in which an adenoviral vector system was equipped with the Sleeping Beauty

integration machinery (179). The authors found that integration is more efficient when the transposon is delivered in a circular conformation. Since adenoviral genomes are usually linear, they included a Flp recombinase in the system that would circularize the transposon before integration. It has to be noted that the size of the transposon appears to influence the integration efficiency and that transposons with sizes upwards of 10 kbp are not considered useful at this point (180). Thus, while a helper-dependent adenoviral vector provides an efficient way to deliver a transposon, its full cloning capacity cannot be exploited with this system. Nevertheless, the Ad-SB hybrid system has been successfully employed for gene therapeutic approaches. For example, adenoviral delivery of a Sleeping Beauty transposon encoding canine factor IX led to phenotypic correction of hemophilia B in a dog model (181).

2 Aims of the study

Ex vivo HSC gene therapy holds tremendous potential for the curative treatment of a host of monogenic, hematopoietic diseases. The current treatment protocol for this therapeutic approach involves the collection of HSCs from a patient, their maintenance and transduction with a retroviral vector *ex vivo*, and retransfusion of the modified cells into the myeloconditioned patient. This process is highly complex and not without risk for the patient.

The goal of this study was to evaluate whether an alternative approach to genetically modify HSCs, termed HSC *in vivo* gene therapy, would be feasible. It is based on the mobilization of HSCs from the bone marrow into the peripheral blood, the transduction and modification of the mobilized HSCs with an adenoviral vector, and the rehoming of the modified HSCs into the bone marrow, where they persist and are able to give rise to gene-modified progeny cells.

This first part of the study aimed at determining if the mobilization of hematopoietic stem cells from the bone marrow allowed for the transduction of these cells with an intravenously injected first-generation adenoviral vector. Further, it was to be assessed whether the transduced cells were able to home back to the bone. In addition, a comparison between a first-generation vector and a helper-dependent vector for the transduction of mobilized HSCs was performed.

In order to be able to follow transduced HSCs for extended periods of time, transgene expression in transduced cells needed to occur over extended periods of time. To this end it was to be established if a switch to a helper-dependent adenoviral vector platform and the use of a transposase-based integration machinery would allow for prolonged transgene expression. In addition to being able to follow transduced cells for extended periods of time, transgene integration also enabled functional assays to reveal whether HSCs modified through *in vivo* transduction were still able to function as stem cells and to give rise to gene-modified progeny.

In addition to the efficacy of the proposed *in vivo* transduction system, its safety had to be assessed as well. For this, two questions had to be answered. First, how safe is the intravenous administration of the adenoviral vectors in a mobilized host? Second, what is the safety of the integration machinery in terms of genotoxic potential?

Lastly, to be able to better evaluate the applicability of HSC *in vivo* gene therapy in animal models closer to humans, *in vivo* transduction studies were to be performed in humanized NOG mice as well as non-human primates.

3 Results

3.1 Expression of CD46 on HSPCs

In order to be transmissible by vectors based on Ad5/35, target hematopoietic stem and progenitor cells have to express human CD46. The expression of human CD46 on human cord blood mononuclear cells (CBMCs) and mouse bone marrow cells was assayed via flow cytometry. (**Fig. 4**). In CBMCs (**Fig. 4A**), the CD46 expression level on total cells and on $CD34^+$ cells, a population enriched for HSPCs, was at comparable levels with median fluorescence intensities (MFI) of 1440 in total cells and 1283 in $CD34^+$ cells. In mice, CD46 is only expressed in the testes (182) while its role in other tissues is taken over by a different protein. To be able to study CD46-tropic measles virus in mice, Mrkic *et al.* developed a transgenic mouse model (CD46-tg) which expresses human CD46 in the same pattern and

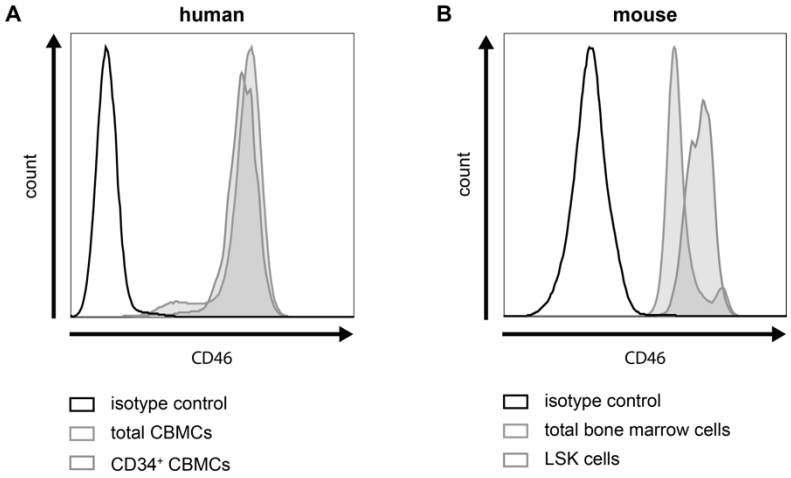

Fig. 4 Expression of human CD46 on human cord blood mononuclear cells and CD46-tg mouse bone marrow cells. The expression levels of CD46 were analyzed by flow cytometry. Shown are histograms of the recorded fluorescence signal for CD46. A) Human CD46 is expressed in human cord blood mononuclear cells (grey curve), and comparable levels of CD46 can be found in the $CD34^+$-positive fraction (blue curve), which is enriched for more primitive HSPCs. The black curve represents human cord blood mononuclear cells stained with an isotype-matched control. B) In total bone marrow cells (grey curve) of CD46-tg mice, human CD46 is expressed on all cells. A smaller fraction of these cells shows a higher CD46 expression level than the majority of cells. Bone marrow LSK cells (blue curve) show a higher level of CD46, which matches that observed for the high expression subfraction seen in total bone marrow. The black curve represents CD46-tg mouse bone marrow cells stained with an isotype matched control. Bone marrow of 3 animals was analyzed, one representative animal is shown.

at comparable expression levels that have been observed in humans (183, 184). In addition these mice possess an alpha/beta interferon receptor knock-out. In these CD46-tg mice

(**Fig. 4B**), the expression level of CD46 in total cells was lower than in cells of the HSPC-enriched LSK fraction, with an average MFI of 6335 compared to 13722 in LSK cells.

LSK cells are a subfraction of mouse bone marrow cells that are lineage-negative (lin^-), and positive for c-kit and Sca-1. This fraction is enriched for hematopoietic stem cells(185). Thus, both human HSPCs and HSPCs of CD46-tg mice express the cellular receptor CD46, as has been previously reported (186), and should be transducable with Ad5/35 vectors.

3.2 *In vitro* transduction of HSPCs with Ad5/35++ vectors

After the expression of the Ad35 cellular receptor CD46 had been confirmed on the cell surface of both human and CD46-tg mouse HSPCs, it had to be shown that these cells could be transduced with an Ad5/35-based vector *in vitro.* To this end, human $CD34^+$ cells isolated from the blood of G-CSF mobilized donors or lineage-depleted bone marrow cells of CD46-tg mice were infected with Ad5/35++-GFP at multiplicities of infection of 200 and 1000 viral particles (vp) per cell. The cells were incubated for 48 h and GFP expression was assessed via flow cytometry (**Fig. 5**). In mouse CD46-tg lin^- cells, 11.6 ± 0.4 % and 14.2 ± 0.9 % were GFP-positive after being infected with an MOI of 200 vp/cell and 1000 vp/cell, respectively. In human $CD34^+$ cells, 21.1 ± 1.0 % and 23.2 ± 0.5 % of cells were GFP-positive after being infected with 200 and 1000 vp/cell, respectively.

In conclusion, both murine and human HSPCs appear to be transducable with Ad5/35-based vectors. This is in line with the results of other studies that used adenoviral vectors carrying Ad35 fiber knobs to transduce HSPCs (148, 150, 187).

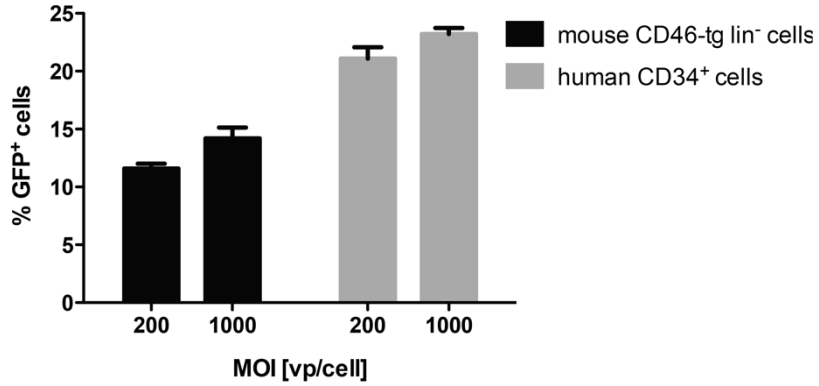

Fig. 5 *In vitro* transduction of murine and human HSPCs with Ad5/35++-GFP. Lineage-depleted (lin^-) CD46-tg mouse bone marrow cells (black) and human $CD34^+$ cells (grey) were transduced with Ad5/35++-GFP *in vitro* at the given MOIs, and GFP expression was analyzed via flow cytometry 48 h after infection. Shown are mean ± SD frequencies of GFP-positive cells of triplicate (n=3, mouse) and quadruplicate (n=4, human) infections, respectively.

3.3 Mobilization of HSPCs in CD46-tg mice

Even though the mobilization regimen of G-CSF combined with AMD3100 is well established in humans (188, 189) and has been tested in the mouse (51), its effects and dynamics had not been tested in the CD46-tg mouse model used in this study. To get a better understanding of how the mobilization would influence the CD46-tg animals, we applied a standard mobilization regimen, i.e. daily injections of G-CSF for four days followed by a subcutaneous injection of AMD3100 on the fifth day. Blood samples of animals were collected on day 5, either before the injection of AMD3100 (0 min), 40 minutes after AMD3100 or 3 hours after AMD3100. Non-mobilized CD46-tg animals were used as a reference. Red blood cells (RBCs) in the blood samples were lysed and the cells were plated out in methylcellulose medium containing a mouse cytokine cocktail. This medium promotes proliferation and differentiation of HSPCs, leading to formation of progenitor colonies that could then be enumerated (**Fig. 6A**). The baseline of HSPCs in the circulation of non-mobilized animals was at 17.6 ± 4.0 colony forming units (CFU) per 100 µl blood. Animals that had received G-CSF for four days but no AMD3100 yet (0 h) yielded 505.0 ± 113.1 CFU/100 µl. Forty minutes after addition of AMD3100, the values increased significantly ($p<0.0001$) to 1431.0 ± 251.5 CFU/100 µl. At 3 h after AMD3100, 1146 ± 159.8

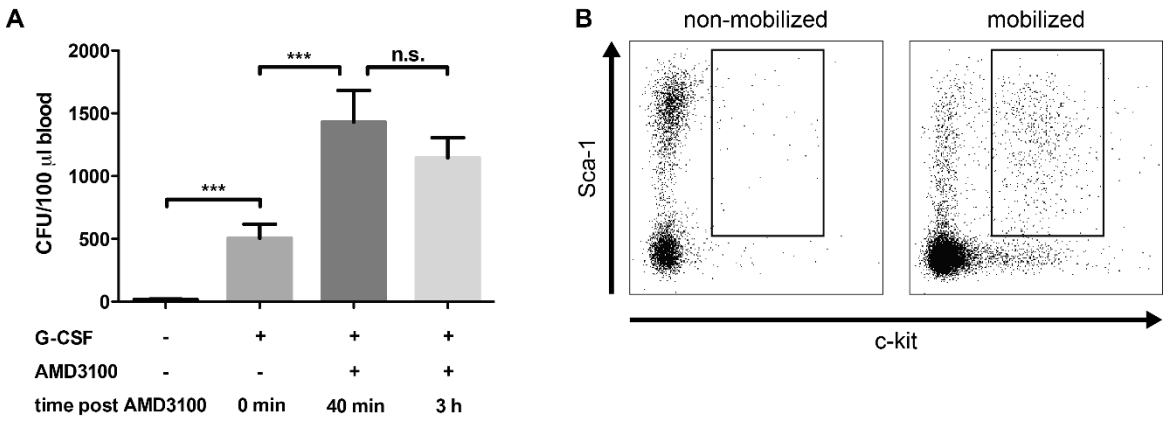

Fig. 6 HSPC mobilization in CD46-tg mice following injections of G-CSF and AMD3100. CD46-tg animals were mobilized through subcutaneous injections of G-CSF on day 1 – 4 and a subcutaneous injection of AMD3100 on day 5. A) Blood samples were collected before injection of AMD3100 as well as 40 min and 3 h after injection. Red blood cells were lysed, and the remaining cells were subjected to CFU assays. Colonies were enumerated 12 days after plating, shown are mean ± SD colonies normalized to a blood volume of 100 µl. Non-mobilized animals were used as a reference. CFU assays were performed in triplicates (n=3). Statistical significance was analyzed via one-way ANOVA with Bonferroni post testing. B) Flow cytometric analysis of non-mobilized and mobilized blood samples for the presence of HSPCs. Blood of the mobilized animals was drawn 40 min after AMD3100 injection. Shown is the c-kit and Sca-1 expression of lineage-negative PBMCs. The shown gate represents LSK cells, a fraction enriched for HSPCs. Mobilization and staining was performed in duplicates; representative animals are shown.

CFU/100 µl could still be detected in circulation. The application of G-CSF alone led to a 29-fold increase in HSPCs in the blood, while the addition of AMD3100 led to an 81-fold increase over base line at 40 min after injection.

To consolidate the findings of the CFU assays, we mobilized mice as before and 40 minutes after AMD3100 injection, sacrificed the animals and collected their blood. Red blood cells (RBCs) were lysed and the remaining peripheral blood mononuclear cells (PBMCs) were stained for LSK cells. In non-mobilized CD46-tg animals, the percentage of LSK cells in PBMCs was about 0.001 %, while 0.074 ± 0.014 % of PBMCs were LSK cells in animals that had received the mobilization treatment (**Fig. 6B**). Thus, mobilization led to an 80.9-fold increase of circulating HSPCs based on this phenotypic analysis, further corroborating the findings of the CFU assay. As a reference, the percentage of LSK cells in the bone marrow of non-mobilized animals was 0.12 % and 0.27 % in mobilized animals.

3.4 HSPC *in vivo* transduction with Ad5/35++-GFP in CD46-tg mice

After it had been determined that CD46-tg HSPCs could be transduced with Ad5/35++-GFP and that the mobilization regimen led to egress of HSPCs into the peripheral blood of animals, the next step was to show that intravenously injected Ad5/35++-GFP was able to transduce mobilized HSPCs *in vivo*. Furthermore, it had to be shown that transduced HSPCs would be able to home back to the bone marrow after mobilization and transduction.

CD46-tg animals were mobilized with G-CSF and AMD3100 as before, and Ad5/35++-GFP was injected 40 min later. Two hours after virus injection, animals were sacrificed and PBMCs as well as cells of the bone marrow and spleen were isolated and cultured for 48 h to allow GFP expression from the viral vector. Cells were then analyzed for GFP expression within the HSPC-containing LSK subpopulation (**Fig. 7A**). In the peripheral blood 14.5 $\pm$ 3.3 % of LSK cells were positive for GFP, while 0.7 $\pm$ 0.5 % and 2.7 $\pm$ 1.3 % of LSK cells were GFP-positive in the bone marrow and spleen, respectively. This shows that Ad5/35++-GFP is able to transduce HSPCs that have been mobilized from the bone marrow. While the cells are still circulating in the periphery, lower transduction rates of HSPCs in the bone marrow and spleen were observed. This could either mean that remaining HSPCs there had been transduced directly, or that HSPCs that had been transduced in the periphery were beginning to settle down in the bone marrow and spleen.

To further determine the behavior of transduced HSPCs following mobilization and transduction, animals were mobilized and injected with Ad5/35++-GFP as before. Different groups of animals were then sacrificed 3, 7, and 14 days after transduction (**Fig. 7B**). As a reference, non-mobilized animals were injected with Ad5/35++-GFP and sacrificed at 48 hours after injection. GFP expression in the bone marrow and spleen was then assessed via flow cytometry in both total cells and LSK cells. In the bone marrow of unmobilized control animals, GFP-expression was at 0.45 $\pm$ 0.33 % for total bone marrow cells and 0.31 $\pm$ 0.10 % for LSK cells. In mobilized animals, GFP levels were 0.29 $\pm$ 0.07 % and 7.55 $\pm$ 1.97 % at three days after infection, 0.14 $\pm$ 0.04 % and 3.39 $\pm$ 1.18 % at seven days after infection, and 0.08 $\pm$ 0.09 % and 2.05 $\pm$ 0.63 % at day 14 after infection for whole bone marrow cells and LSK cells, respectively.

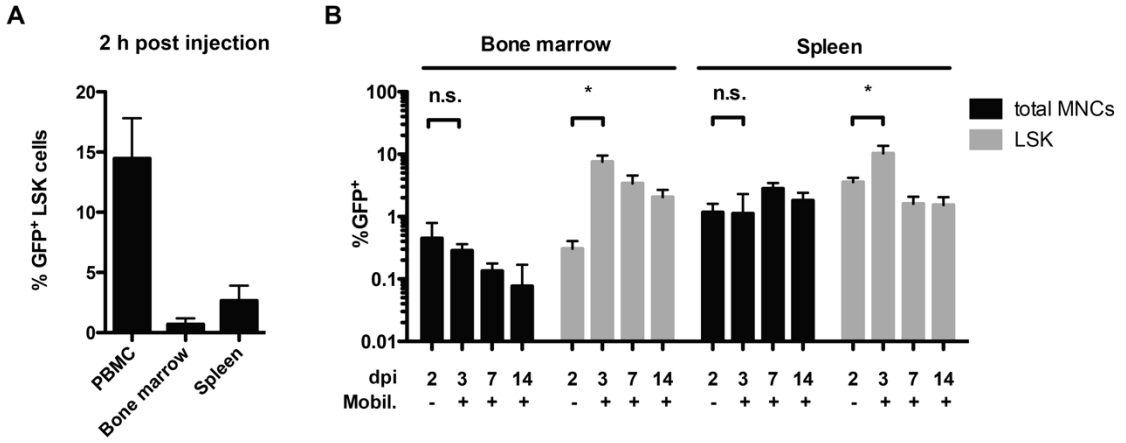

Fig. 7 HSPC *in vivo* transduction with Ad5/35++-GFP in mobilized mice. CD46-tg animals were mobilized with G-CSF and AMD3100 as before. Forty minutes after AMD3100 injection, Ad5/35++-GFP was injected intravenously. A) Animals were sacrificed 2 h after virus injection, and bone marrow and spleen cells, as well as PBMCs, were isolated. Cells were cultured for 48 h to allow for transgene expression, and GFP expression was analyzed via flow cytometry. Shown are mean percentages of GFP-positive LSK cells ± SD analyzed in triplicate animals (n=3). B) Animals were sacrificed 3, 7 and 14 days after injection (dpi). Non-mobilized control animals were sacrificed 2 days after injection. GFP expression in total cells (black) and LSK cells (grey) was analyzed via flow cytometry. Shown are mean percentages of GFP-positive cells ± SD analyzed in triplicate animals (n=3). Statistical significance was tested through unpaired T-tests.

In the spleen of unmobilized animals, 1.17 ± 0.44 % of total cells and 3.56 ± 0.62 % of LSK cells were expressing GFP. In mobilized animals sacrificed at day 3, it was 1.12 ± 1.17 % for total cells and 10.25 ± 3.39 % in LSK cells. At seven days after transduction, 2.80 ± 0.66 % of total cells and 1.61 ± 0.47 % of LSK cells were positive for GFP. At two weeks after transduction, 1.81 ± 0.60 % of total cells and 1.53 ± 0.53 % of LSK cells still showed transgene expression. It can be seen that the differences in transduction efficiencies of both bone marrow and spleen are not significantly different. Thus, mobilization did not seem to influence the transduction of the bulk of cells. Transduction levels of whole tissue cells for the spleen were roughly an order of magnitude higher than in the bone marrow. This is likely due to the spleen being thought to be in equilibrium with the peripheral blood, whereas access to the bone marrow from the peripheral blood is much harder (42). In the bone marrow, a decline in GFP-positive cells was observed over time, while GFP levels in the spleen remained almost unchanged over time.

For LSK cells, background transduction in non-mobilized animals was comparable to total cells in the bone marrow and slightly increased for the spleen. However, once the animals received the mobilization treatment , significant increases in HSPC transduction were seen in both the bone marrow and the spleen ($p<0.05$), with the effect being more pronounced

in the marrow. After the three-day time point, the percentage of GFP-positive LSK cells declined for both bone marrow and spleen. In the marrow, the decline was gradual and even after 14 days levels were still markedly increased over that seen in non-mobilized animals. While, the decline in transduced LSK cells in the spleen appeared to be much more rapid as background levels had already been reached at day seven after injection.

Even though transduction rates of spleen LSK cells upon mobilization were only three-fold increased and went back to levels seen for non-mobilized animals at later time points, the total numbers of LSK cells in the spleen have to be taken into account. While in non-mobilized animals 0.02 ± 0.01 % of cells in the spleen were HSPCs, at day 3 after mobilization 0.18 ± 0.19 % of cells in the spleen were LSK cells. Thus it can be argued that even though the percentage of GFP-positive HSPCs in the spleen with or without mobilization did not differ by values as extreme as in the bone marrow, the total numbers of transduced HSPCs in the spleen following mobilization were still much higher than in non-mobilized animals. Interestingly, at day seven after transduction the percentage in LSK cells in the spleen was 1.70 ± 0.20 %, while at day 14 it was 0.3 ± 0.06 %. Thus, between days three and seven an influx of LSK cells into the spleen could be observed.

From these experiments several conclusions could be drawn. Firstly, the mobilization regimen did force egress of bone marrow HSPCs into the periphery, where they could be transduced with an Ad5/35 vector. Secondly, following transduction, a part of HSPCs in the periphery were able to home back to the bone marrow and expressed the transgene there, while another part of the mobilized HSPCs appeared to home to the spleen. However, the percentage of transgene expressing HSPCs decreased over time. Several factors could cause this. Firstly, the vector used here is a first-generation adenoviral vector, and leaky expression of viral genes from the vector could lead to cytotoxicity or immune responses (158, 190). Furthermore, transduction with the vector could induce differentiation of some HSPCs, causing the loss of the LSK phenotype. The decline of transduction rates in LSK cells in the spleen could be caused by HSPC influx into the spleen, as seen in an increase in the percentage of LSK cells between days three and seven. Alternatively, the spleen, with its limited niches for HSPCs (191), could just not support the high number of HSPCs following mobilization, which could cause these excess cells to die off. This in turn would explain the drop in LSK cells between days 7 and 14 after transduction.

3.5 Helper-dependent adenoviral vectors for HSPC transduction *in vitro* and *in vivo*

Leaky expression of viral genes from first-generation adenoviral vectors, as mentioned above, can lead to cytotoxicity as well as immune reaction towards the infected cells (158, 190), leading to a decline of transgene expression levels over time. Switching the applied vector system from a first-generation to a third-generation or helper-dependent adenoviral vector system, which is devoid of all viral genes, should alleviate these toxicity problems (192). To assure that the transduction performance of the new helper-dependent vector HDAd5/35++-CMV-GFP was on par with the previously used Ad5/35++-GFP, the performance of both vectors for the transduction of HSPCs *in vitro* and *in vivo* was compared (**Fig. 8**).

For the comparison of transduction efficiency *in vitro*, CD46-tg HSPCs were infected as before (**Fig. 5**) and transduction levels were assessed 48 hours after infection using flow cytometric analysis. As can be seen in **Fig. 8A**, both the first-generation Ad5/35++-GFP and the helper-dependent HDAd5/35++-CMV-GFP were able to infect CD46-tg lin^- cells in very similar levels at both MOIs used.

To compare both vectors for *in vivo* transduction of HSPCs, CD46-tg animals were mobilized as before and intravenously injected with either vector at $2x10^{10}$ vp per animal. Animals were sacrificed three days later, and GFP expression in HSPCs of the bone marrow and spleen was analyzed (**Fig. 8B**). Animals transduced with Ad5/35++-GFP showed 4.6 ± 2.7 % GFP-positive LSK cells, while in the spleen, 9.0 ± 3.2 % of LSK cells were positive for GFP. In animals that were infected with the helper-dependent vector, 5.2 ± 1.3 % of bone marrow LSK cells expressed GFP and 6.6 ± 5.9 % splenic LSK cells were positive for transgene expression. The differences observed here were not of statistical significance and it can be assumed that both vectors were able to transduce HSPCs *in vivo* at similar efficiencies. Of note, the transduction levels observed for the first-generation vector Ad5/35++-GFP in this experiment were lower than those observed in the earlier *in vivo* transduction experiments (**Fig. 7B**). However, the observed differences are small enough to be attributed to animal-to-animal variations.

In order to compare the cytotoxic potential of both the first-generation and helper-dependent vector, lineage-depleted, GFP-positive bone marrow cells were collected through a combination of MACS and FACS, and the resulting cells were used to assess the colony-forming potential of transduced HSPCs in CFU assays (**Fig. 8C**). While cells that had been transduced with Ad5/35++-GFP formed 16.3 ± 12.6 colonies per 1000 lin$^-$ cells, HDAd5/35++-CMV-GFP-transduced HSPCs formed 43.8 ± 7.9 colonies. Thus, the colony-forming potential of the helper-dependent vector appeared significantly higher than that of the first-generation vector ($p<0.05$). However, when HSPCs of non-mobilized, uninfected animals were used under the same conditions, 19.2 ± 5.4 colonies formed per 1000 plated lin$^-$ cells. This shows no significant difference towards cells treated with the first-generation vector. Several scenarios could lead to this result. It has been shown above that CD46-targeting adenoviral vectors preferentially transduced LSK cells compared to whole bone

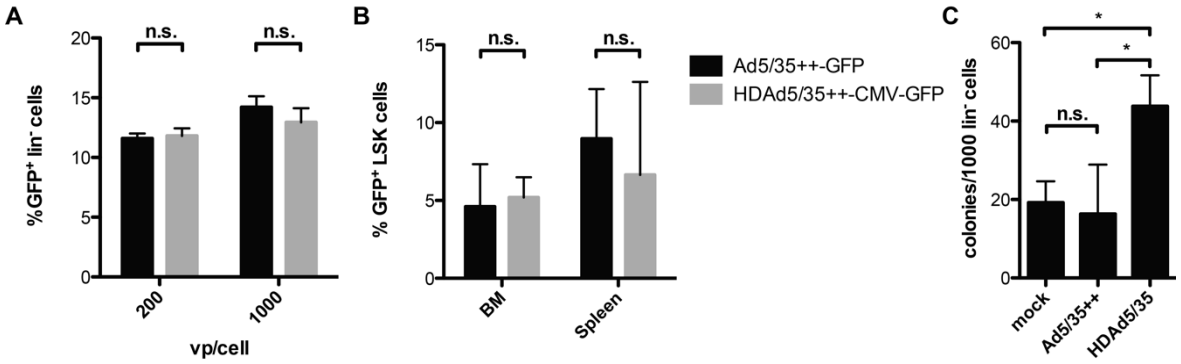

Fig. 8 Comparison of transduction with a first-generation and helper-dependent vector *in vitro* and *in vivo*. A) CD46-tg lineage-negative bone marrow cells were infected *in vitro* with either first-generation Ad5/35++-GFP (black) or helper-dependent HDAd5/35++-CMV-GFP (grey) at the given MOIs. Cells were incubated for 48 h, and GFP expression was assessed using flow cytometry. Shown are mean percentages of GFP-positive cells ± SD, infections were performed in triplicates. Testing for statistical significance was performed through unpaired T-tests. B) CD46-tg mice were mobilized as before with G-CSF and AMD3100 and were injected 40 min after AMD3100 with either first-generation Ad5/35++-GFP (black) or helper-dependent HDAd5/35++-CMV-GFP (grey). Animals were sacrificed 3 days after transduction, and GFP expression in HSPCs of the bone marrow and spleen was analyzed via flow cytometry. Shown is the mean percentage of GFP$^+$ LSK cells ± SD, n=2. Unpaired T-test were used to test for statistical significance. C) CD46-tg animals were mobilized and transduced as above. Three days after virus injection, bone marrow cells were isolated and lineage-depleted via MACS. Lin$^-$ cells were then FACS-sorted for GFP-positive cells, and these cells were plated out in CFU assays. The amount of total colonies was scored 12 days after plating. Non-infected, non-mobilized animals served as control (mock) and were also subjected to MACS and FACS sorting to provide the same level of mechanical stress. Shown are mean ± SD for colonies derived from 1000 lin$^-$ cells. Per animal, colonies were scored in triplicates, 3 animals per group. To test for statistical significance, one-way ANOVA with Bonferroni post testing was applied.

marrow cells. It could therefore be the case, that in sorting for GFP-positive cells after *in vivo* transduction, the collected fraction of cells was enriched for more primitive cells. Thus,

the non-mobilized, untreated cells might have a lower colony-forming potential just because they are not as enriched for HSPCs as the infected samples. Secondly, and along similar lines, only the treated animals received injections of G-CSF. In addition to its mobilizing properties, treatment with G-CSF also induces proliferation of HSCs in the bone marrow (193, 194), and therefore, the stem cell content as well as the colony-forming potential of non-mobilized bone marrow could be lower than that of animals that had received G-CSF.

3.6 Stable modification of cells using an integrating adenoviral vector system

Adenovirus serotype 5 (Ad5) and therefore adenoviral vectors based on Ad5 do not possess the ability to actively integrate their DNA into the host genome (195). Therefore, transgene expression from a traditional adenoviral vector will only be transient. As seen in previous experiments (see section 3.4), transgene expression in HSPCs following *in vivo* transduction decreased markedly over time. While part of this effect could be attributed to vector toxicity, the episomal presence of the vector genome was most likely also responsible. While transient expression of a transgene from an episomally retained vector can be satisfactory for some applications, it does not fulfill the requirements for HSC gene therapy. The vector genome cannot be replicated, and when a transduced cell divides, it is only passed on to one daughter cell. This is detrimental for transgene expression, especially in the modification of HSCs with a potential output of a myriad of progeny cells. Thus, a system that would allow for integration of a transgene cassette encoded in an adenoviral vector system would be preferable.

Yant *et al.* (179) described an integrating adenovirus vector system. By delivering the Sleeping Beauty transposase (SB) together with a transgene-containing donor transposon, stable integration and long-term expression of the transgene could be achieved. An adapted form of the system was used in this study. The system is comprised of two helper-dependent adenoviral vectors. The first vector, HDAd-SB, encodes the hyperactive transposase SB100x (178) as well as an enhanced version of FLP recombinase (FLPe) (196) (**Fig. 9A**). The second vector, HDAd-GFP (**Fig. 9B**), carries the transgene cassette flanked by repeats necessary for recognition by the transposase as well as FRT sites, which allow for

circularization of the transposon through FLPe prior to integration (**Fig. 9C**). The circularization of the transposon has been shown to increase the integration rate of Sleeping Beauty transposase (179). Upon co-infection of a target cell with both viruses, the first vector supplies SB100x and FLPe *in trans* which circularize and integrate the transposon into a random TA dinucleotide through a cut and paste mechanism (**Fig. 9D**) (174).

3.6.1 Integration analysis in a model cell line

To test the integration capabilities of this two vector system, experiments in M07-e cells were performed. Cells were either infected with HDAd-GFP alone or with both HDAd-GFP and HDAd-SB at a 1:1 ratio. Upon infection, GFP-positive cells were singled out and expanded for analysis of clones. After expansion, the presence of GFP-positive cells in the colonies was assessed (**Fig. 10A**). For cells infected with HDAd-GFP alone, 37 ± 12 % of analyzed colonies contained GFP-positive cells, while for the group infected with both

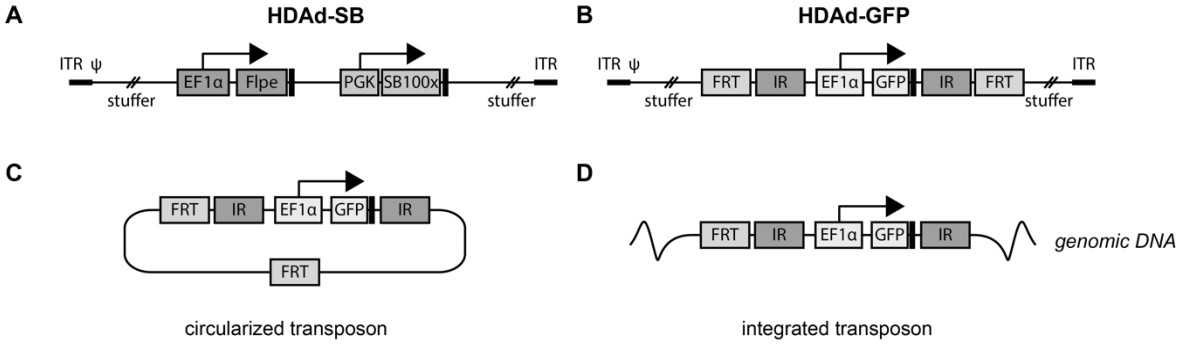

Fig. 9 Adenoviral two-vector system for stable integration of a transgene cassette. The system is comprised out of two helper-dependent adenoviral vectors. A) The first vector, HDAd-SB, provides FLPe and SB100x *in trans.* B) The second vector, HDAd-GFP, encodes the transposon containing a Ef1α-GFP cassette. The transposon is flanked by IR repeats and FRT sites. C) Upon superinfection of the same cell with both vectors, HDAd-SB supplies FLPe, which leads to circularization of the transposon through FRT sites. D) SB100x then integrates the transposon into the host genome through interaction with the IR repeats.

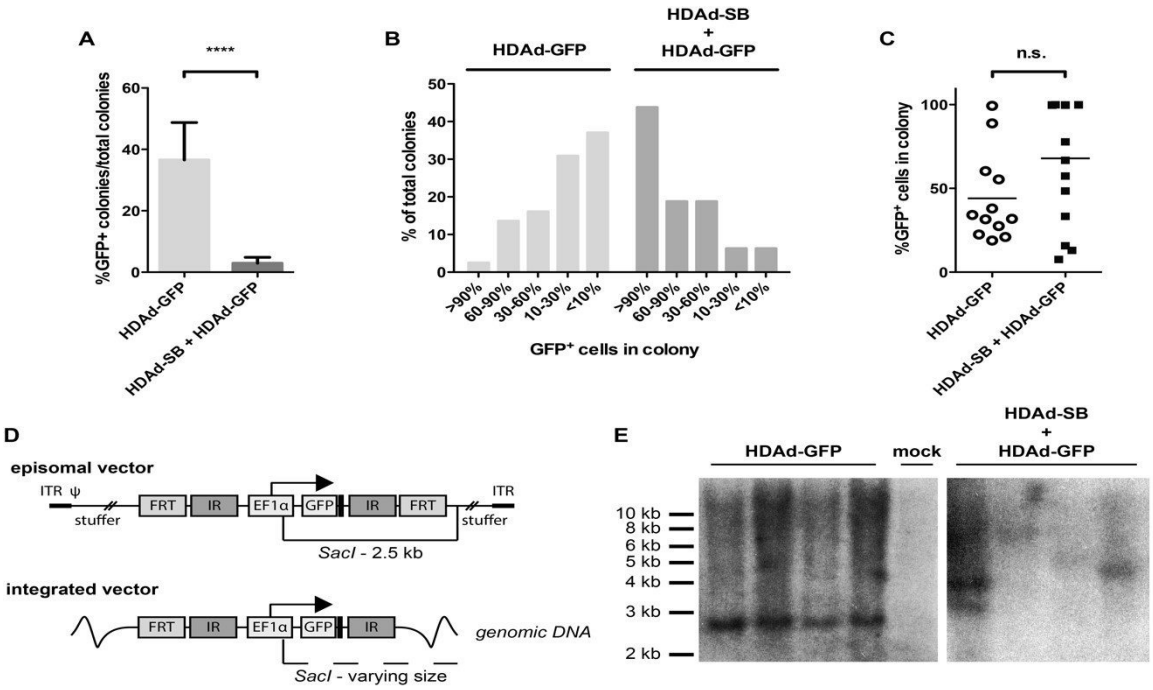

Fig. 10 Integration of a GFP transgene cassette following infection with the Sleeping Beauty two-vector system in M-07e cells. M-07e cells were infected *in vitro* either with HDAd-GFP alone or with both HDAd-GFP and HDAd-SB. Cells were incubated for 48 h, and single GFP-positive cells were isolated using FACS and expanded into colonies. A) After expansion in 96-well plates, wells were scored for the presence of GFP-positive cells. Shown is the mean percentage of GFP-positive colonies ± SD for eight 96-well plates per group. Test for statistical significance was performed using an unpaired T-test. B) Distribution of GFP expression within GFP-positive colonies. The colonies were visually inspected, and the percentage of GFP-positive cells per colony was estimated. Shown is the distribution of GFP expression for all GFP-positive colonies. C) Colonies exhibiting the highest expression levels of GFP were further expanded. After expansion, the level of GFP expression was analyzed via flow cytometry. Shown are the percentages of GFP-positive cells for single colonies as well as the mean. An unpaired T-test was performed to test for statistical significance. D) Digestion of the non-integrated, episomal donor vector HDAd-GFP with *SacI* leads to a 2500 bp restriction fragment that can be detected with a GFP-specific Southern blot probe (upper panel). If the vector had been integrated into the genomic DNA in a SB transposase-mediated fashion (lower panel), the *SacI* digest will yield a differently sized, GFP-containing fragment that can be probed. E) Southern blot analysis of selected M-07e clones that had been treated either with HDAd-GFP alone (left), HDAd-GFP and HDAd-SB (right), or that had not been transduced at all (mock). Genomic DNA was digested with *SacI* and hybridized with a radioactive, GFP-specific probe. Per group, 4 clones were analyzed.

HDAd-GFP and HDAd-SB, only 3 ± 2 % of colonies contained GFP-positive cells at all. Next, the percentage of GFP-expressing cells in each colony was assessed (**Fig. 10B**), and GFP-positive colonies formed by cells infected with HDAd-GFP alone contained relatively few GFP-positive cells. In contrast, in most of the GFP-positive colonies formed by cells infected with both viruses more than 90 % of the colonies' cells expressed GFP. These results were further corroborated by flow cytometry, where the same trends could be observed (**Fig. 10C**). Even though the observed differences were not statistically significant, it has to be

considered that only colonies with at least 10 % GFP-positive cells (based on **Fig. 10B**) were included in the flow analysis.

Most cells infected with HDAd-GFP alone likely only retained the HDAd-GFP genome episomally, and it was lost during cell division. Given the non-integrating nature of adenoviruses this was not unexpected, and it explains why the majority of colonies only showed GFP in very few cells. However, in rare cases, stable integration of the viral genome can occur through breakage of the ITRs (197). This could explain the occurrence of a few colonies that showed high percentages of GFP-positive cells. For cells infected with both viruses, only relatively few colonies expressed GFP, but they did so in the majority of their cells, suggesting successful integration. The low number of GFP-positive colonies can be explained by cells in which the FLPe was able to circularize the transposon, thereby destroying the episomal vector, which then did not get integrated by SB100x, leading to loss of GFP expression.

To confirm that transposase-mediated integration had occurred in cells infected with both viruses, 4 clones were selected for Southern blot analysis. As a control, clones infected with HDAd-GFP alone were enriched for GFP-positive cells via FACS. Before detection with a GFP-specific probe, genomic DNA was digested with the restriction endonuclease *SacI*. Digestion of the viral genome of HDAd-GFP with *SacI* yields a 2500 bp GFP-containing band. However, if the transposon had been integrated by SB100x, a shift in fragment sizes would have been expected to appear (**Fig. 10D**). It can be seen in **Fig. 10E**, that for samples infected with both viruses, fragments of varying sizes could be detected for all analyzed clones, showing that SB100x-mediated integration had occurred. However, in cells that were infected with HDAd-GFP alone, only the 2500 bp fragment was visible. Of note, this means that integration did not occur through the sleeping beauty repeats. However, it is not possible to distinguish between an episomally retained vector and a vector that integrated randomly through breakage of the ITRs.

3.6.2 Integration of the two vector system in primary mouse cells *in vitro*

Next, the integration capabilities of the two vector system were to be tested in primary mouse cells. To this end, CD46-tg bone marrow cells were lineage-depleted and infected *in vitro.* For the infection with both HDAd-GFP and HDAd-SB, the same MOI of HDAd-GFP (2000 vp/cell) was used but different MOIs for HDAd-SB were used in order to assess the best transposon to transposase ratio. Infected cells were plated in CFU assays 24 h after infection, and leftover cells were analyzed for GFP expression 48 h after infection (**Fig. 11**). Flow cytometric analysis of the cells 48 h after infection revealed that regardless of the virus(es) and MOIs used, all cells showed similar levels of GFP expression ranging from 42 % (HDAd-GFP + HDAd-SB, ratio 1:1) to 62 % (HDAd-GFP alone). In the CFU assays, the overall colony-forming potential of the cells was compared (**Fig. 11A**) as well as the percentage of GFP-positive colonies (**Fig. 11B**). Uninfected cells had formed 119 ± 20 colonies, while cells infected with HDAd-GFP had formed 114 ± 2 colonies. Cells infected with different ratios of both viruses yielded in the range of 118 to 173 colonies. The observed differences were

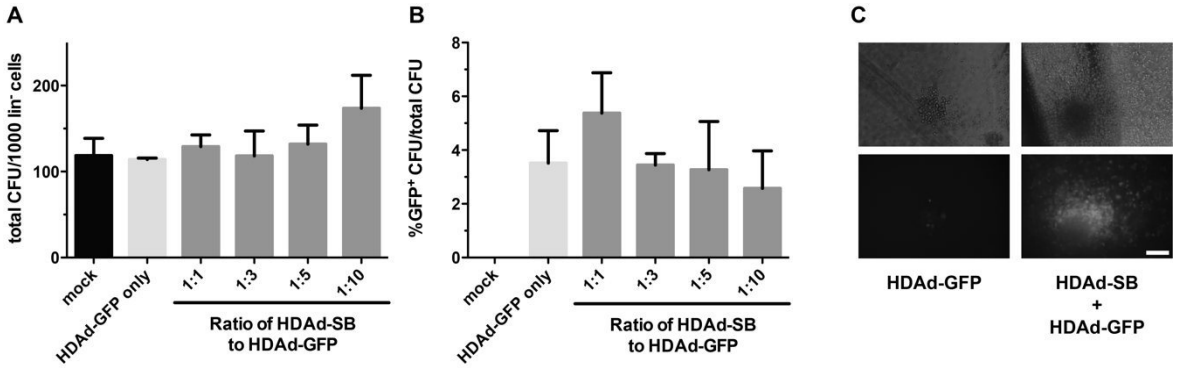

Fig. 11 *In vitro* transgene integration into bone marrow HSPCs of CD46-tg mice. Lineage-depleted CD46-tg bone marrow cells were infected *in vitro* with HDAd-GFP alone at an MOI of 2000 vp/cell or with HDAd-GFP (2000 vp/cell) in combination with HDAd-SB at the given ratios. The cells were plated out in colony forming unit assays 24 h after infection. Colonies were scored 12 days after plating. Cells were plated in triplicates (n=3). Uninfected cells were used as control (mock). A) Shown is the mean number of colonies formed per 1000 plated lin^- cells ± SD. Statistical analyses was performed using one-way ANOVA with Bonferroni post testing, no statistically significant differences were found. B) GFP expression in CFU colonies. Shown is the mean percentage ± SD of GFP-positive CFU in total CFU. No statistically significant differences between the treated groups were found upon one-way ANOVA with Bonferroni post testing. C) Bright-field (top) and UV-microscopic (bottom) images of CFU colonies derived from CD46-tg lin^- cells that had been transduced HDAd-GFP aloone or with HDAd-SB and HDAd-GFP at MOIs of 2000 vp/cell/virus. Shown are representative colonies. Scale bar is 100 µm.

not statistically significant, showing that infection with either one or two viruses did not markedly influence viability and colony-forming potential of primary mouse HSPCs.

Subsequently, GFP-expressing colonies were enumerated (**Fig. 11B**). Colonies formed by cells infected with HDAd-GFP alone showed 3.5 ± 1.5 % GFP-positive colonies. For colonies formed from cells infected with both viruses the highest percentage of GFP-positive colonies was seen for a 1:1 ratio at 5.4 ± 1.5 %, while the lowest was seen for a ratio of 1:10 at 2.6 ± 1.4 %. While the differences between cells infected with one or two viruses with regard to the percentage of GFP-positive colonies were relatively small, it can be seen in **Fig. 11C** that colonies formed by cells only infected with the transposon vector alone contained fewer GFP-positive cells per colony than CFUs from cells infected with both vectors. This is in line with the results found for M07-e cells infected *in vitro* (see section 3.6.1).

3.6.3 Integration of the two vector system in human HSPCs *in vitro*

Next, the integrating two vector system was tested on human $CD34^+$ cells *in vitro*. Cells were infected at two different MOIs either with HDAd-GFP alone or with a 1:1 mixture of HDAd-GFP and HDAd-SB. Twenty-four hours after infection, the cells were plated out in colony-forming unit assays, and the colonies were scored two weeks later. The total colony forming potential was highest for uninfected cells at 168 ± 15 CFU per 1000 plated cells, while the lowest CFU counts were observed for cells infected with the high MOIs of both

Fig. 12 *In vitro* transgene integration into human $CD34^+$ HSPCs. Human $CD34^+$ cells were infected *in vitro* at the indicated MOIs per virus per cell. Twenty-four hours after infection, cells were plated out in CFU assays in triplicates. Colonies were scored 14 days after plating. Uninfected $CD34^+$ cells were used as control (mock). A) Total colonies formed from plated cells. Shown are means ± SD of total colonies grown from 1000 $CD34^+$ cells. B) GFP expression in CFU colonies. Shown is the mean percentage of GFP-positive colonies in total colonies ± SD. Statistical analysis for significant differences was performed through unpaired T-tests between groups of the same MOI.

viruses, which formed 109 ± 15 colonies per 1000 cells (**Fig. 12A**). The data suggests that infection with viral vectors led to decreases in colony-forming potential. However, the differences were too small to be statistically significant. Subsequently, the GFP expression in the progenitor colonies was evaluated (**Fig. 12B**). For the lower MOI, cells that had been infected with HDAd-GFP alone showed 0.49 ± 0.84 % GFP-positive colonies, while 1.49 ± 0.65 % of colonies derived from cells infected with both viruses were positive for GFP. For the higher MOI, the double infection group yielded significantly more GFP-positive colonies than the donor vector-only group ($p<0.01$). For HDAd-SB + HDAd-GFP,

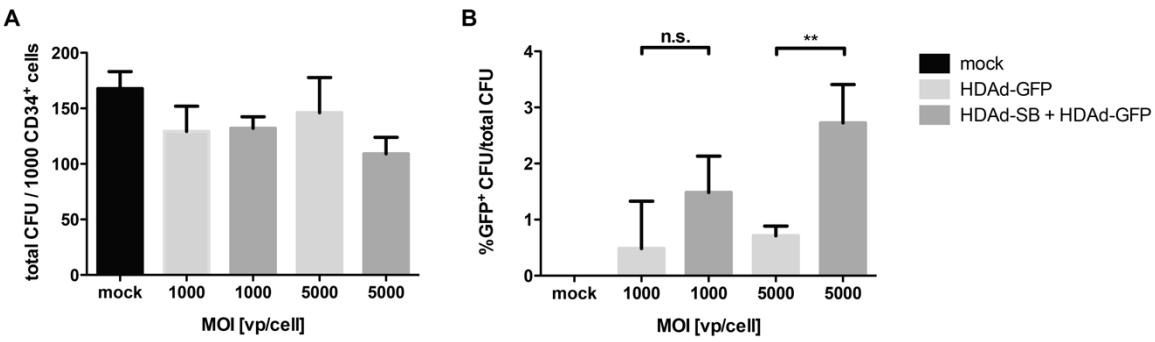

2.73 ± 0.68 % of colonies showed GFP expression, while only 0.71 ± 0.17 % of HDAd-GFP-only colonies expressed GFP.

Overall, an increase in the multiplicity of infection lead to a higher percentage of GFP-positive colonies for cells infected with both viruses. This suggests that at higher rates of superinfection, the efficiency of the integration machinery may be increased. Furthermore, it could be seen that the percentage of GFP-positive colonies for human cells infected at an MOI of 5000 vp/cell (**Fig. 12B**) was lower than that seen for mouse cells infected at MOIs of 2000 vp/cell (**Fig. 11B**). Together with the fact that the overall colony-forming potential for human and mouse cells was comparable (**Fig. 11A** ,**Fig. 12A**), this suggested that the Sleeping Beauty-mediated transgene integration could be more efficient in mouse cells than in human cells.

In conclusion, the Sleeping Beauty-mediated integration of a GFP-expressing transposon appeared to be functional in both murine and human cells following infections *in vitro*.

3.7 Multiple rounds of vector injections in mobilized animals

The most crucial step towards transgene integration using the Sleeping Beauty two vector system is the superinfection of the same cell with both vectors. While this is easily achieved *in vitro*, where the multiplicity of infection could simply be increased, the problem is more complex in an *in vivo* context, where dose-related toxicity can limit the amount of virus that can be injected at any one time. As seen in **Fig. 6A**, a significant amount of HSPCs continue circulating even three hours after administration of AMD3100. Therefore, we compared *in vivo* transduction levels of HSPCs in CD46-tg mice either after one injection of $2x10^{10}$ vp of Ad5/35++-GFP 40 min after AMD3100 or two injections of $2x10^{10}$ vp each at 30 and 60 min after AMD3100 (**Fig. 13**). In mice injected with a single dose of Ad5/35++-GFP, 14.5 $\pm$ 3.3 % of HSPCs in the peripheral blood two hours after infection had been transduced. Injecting two doses of virus significantly increased the transduction rate to 26.8 $\pm$ 2.5 % ($p<0.01$). However, three days after injection, GFP-expression was detected for 7.6 $\pm$ 2.0 % of bone marrow and 10.3 $\pm$ 3.4 % of spleen LSK cells in animals that had received one virus injection

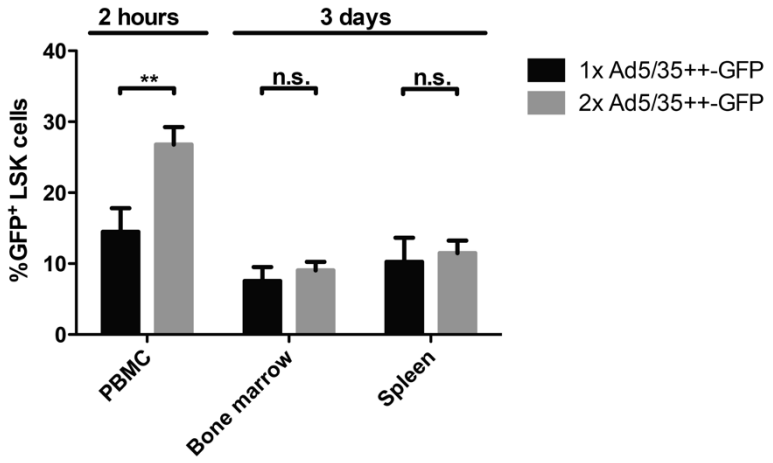

Fig. 13 Increase in *in vivo* HSPC transduction efficiency following multiple rounds of virus application. CD46-tg animals were mobilized as before and injected with one dose of $2x10^{10}$ vp Ad5/35++-GFP 40 min after application of AMD3100 or with two doses of Ad5/35++-GFP, each at $2x10^{10}$ vp, 30 min and 60 min after AMD3100 injection. To analyze GFP expression in PBMCs, blood was taken 2 h after virus application, and PBMCs were cultured for 48 h before analysis. For GFP expression in bone marrow and spleen, cells were isolated 3 days after infection. Cells were analyzed for GFP expression in LSK cells via flow cytometry. Shown is the mean percentage of GFP-positive LSK cells ± SD. Three animals per group, analysis for statistically significance was performed using unpaired T-tests.

and 9.0 $\pm$ 1.2 % and 11.5 $\pm$ 1.8 % for bone marrow and spleen of animals that had received two doses of virus. While the transduction rate in HSPCs circulating shortly after

mobilization and virus injection increased almost 2-fold, the double injection approach only translated into small increases in transduced HSPCs in bone marrow and spleen three days after injection.

One possible explanation could be the transduction of extremely short-lived cells in the peripheral blood. For example, neutrophils in the mouse are thought to have a half-life of about 6.5 hours (198). Therefore, if these are the cells that cause the increased transduction levels in the blood, they would only have a small impact after 3 days, since the majority of these cells would already have died off. Nevertheless, we decided to apply the two dose injection regimen for our experiments with the two vector system, since the higher transduction rate displayed in the periphery shortly after infection should increase the chances of superinfection of the same cell with both viruses.

3.8 HSPC *in vivo* transduction with integrating adenoviral vectors

3.8.1 *In vivo* transduction of bone marrow, spleen and PBMCs

After the functionality of the Sleeping Beauty transposase two vector system had been tested *in vitro,* it had to be shown that the system would lead to stable transduction of HSPCs *in vivo*. To this end, CD46-tg animals were mobilized with G-CSF and AMD3100 and then injected with either HDAd-GFP alone or both HDAd-GFP mixed with HDAd-SB at a 1:1 ratio. Animals were sacrificed at four, eight and twelve weeks after transduction, and GFP expression in bone marrow, PBMCs, and spleen was analyzed via flow cytometry (**Fig. 14A**). In the bone marrow of animals injected with HDAd-GFP alone, 0.39 ± 0.26 % of total cells were positive for GFP four weeks after transduction, 0.3 ± 0.25 % at eight weeks after transduction, and 0.14 ± 0.16 % at twelve weeks after transduction (**Fig. 14B**). Compared to animals that had been injected with the first-generation vector Ad5/35++-GFP (**Fig. 7**), GFP expression in bone marrow cells was retained at higher levels for markedly longer periods of time.

For animals that received both components of the two vector system, GFP transduction rates at four weeks after injection were significantly increased over the transposon vector-only group ($p<0.01$). 2.46 ± 2.57 % of bone marrow cells were GFP-positive at this time. After eight weeks, 1.11 ± 1.00 % and after twelve weeks 0.43 ± 0.43 % of cells expressed

GFP. While the animal-to-animal variation in these groups were considerable, overall, more GFP-positive cells were present at all time points compared to the HDAd-GFP-only group, and the transduced cells appeared to be retained longer. However, over time a loss of transduced cells could be observed. Of note, the observed time periods of up to twelve weeks are well over the average half-life of the majority of bone marrow cells. For example, it is thought that 10^{11} neutrophils exit the bone marrow daily under steady state conditions (198). Thus, the loss in transduced cells could in part be attributed to the natural turnover of cells.

In bone marrow LSK cells, a similar pattern to that of the whole bone marrow was observed (**Fig. 14C**). For animals transduced with HDAd-GFP alone, the transduction rates in LSK cells were 3.50 ± 0.90, 3.21 ± 1.06, and 0.65 ± 0.30 % at four, eight, and twelve weeks after transduction, respectively. For animals injected with both vectors, transduction rates of 7.76 ± 2.18 % at four weeks, 4.34 ± 0.57 % at eight weeks, and 0.89 ± 0.26 % at twelve weeks after infection were observed. Again, the group that received both vectors showed better transduction rates at all three time points, even though the same decline in transduced cells seen for total bone marrow cells was also observed here. In principle, the same explanation for the observed decline in transduced cells of total bone marrow could be applied here. However, the turnover of HSPCs is slower than that of fully committed cells (199). In addition to this effect, it is possible that less primitive progenitors that have been transduced differentiate into more committed phenotypes that do not express the LSK surface markers any longer. For example, short-term reconstituting HSCs (ST-HSCs) only have an average life span of four to six weeks, and part of the loss of transduced LSK cells could be due to them being ST-HSCs (200).

In the spleen (**Fig. 14D**), animals that had received HDAd-GFP alone showed GFP levels of 9.09 ± 7.77 % at four weeks, 5.49 ± 5.81 % at eight weeks, and 7.71 ± 9.37 % at twelve weeks after transduction, with some animals showing transduction rates around 20 % for all three time points. For animals that had been injected with both vectors, the transduction levels were 11.84 ± 10.22 % after four weeks, 17.57 ± 16.19 % after eight

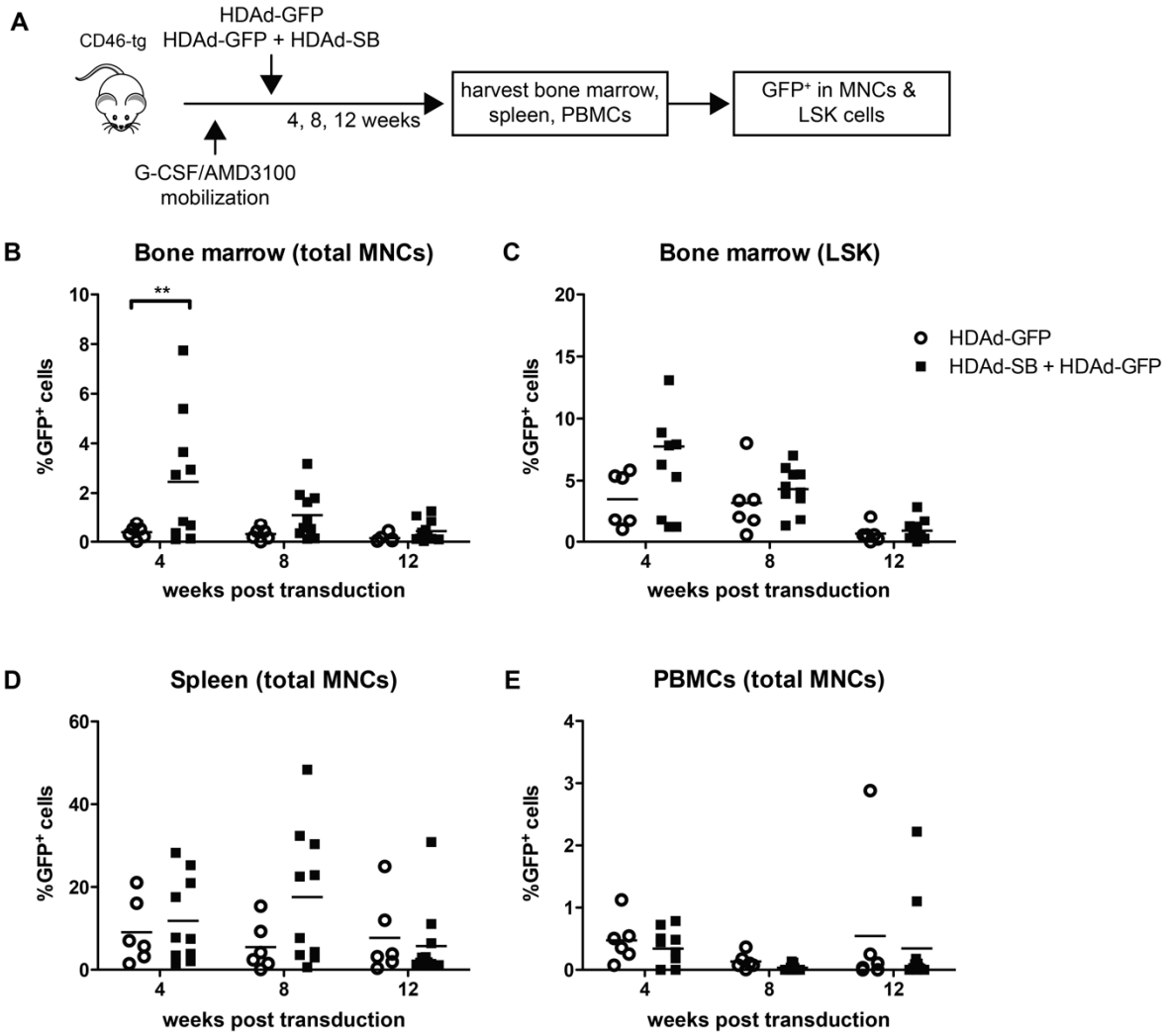

Fig. 14 *In vivo* HSPC transduction with the integrating two-vector system. CD46-tg animals were mobilized with G-CSF and AMD3100 as before and received two virus injections at 30 and 60 min post AMD application at a dose of $2x10^{10}$ vp per virus per injection. One group received the donor vector alone (HDAd-GFP), while the second group of animals received the combination of Sleeping Beauty vector and donor vector (HDAd-SB + HDAd-GFP). Animals were followed for 4, 8, and 12 weeks, respectively, and GFP expression in different tissues was analyzed via flow cytometry. Experimental group sizes were as follows: HDAd-GFP alone n=6 for 4 and 8 week time point, n=5 for 12 week time point, HDAd-GFP + HDAd-SB n=10 for 4 week time point, n=12 for 8 and 12 week time point. A) Experimental design. B – E) GFP expression following *in vivo* transduction was assessed in total bone marrow cells (B), bone marrow LSK cells (C), total cells of the spleen (D) as well as total PBMCs (E). Shown is the percentage of GFP-positive cells in single animals as well as the means per group and time point. Treatment groups were compared for each tissue and time point using two-way ANOVA with Bonferroni post testing. Differences were not statistically significant unless indicated otherwise.

weeks, and 5.70 ± 8.89 % after twelve weeks. Maximum transduction rates observed in this group were 28.3 %, 48.4 %, and 30.9 % at four, eight, and twelve weeks after transduction, respectively. First, it can be seen from these data that the transduction rates observed were much higher than those seen in the bone marrow. This was in accordance with the data for Ad5/35++-GFP (**Fig. 7B**) However, the values seen here for both groups were much higher

than those for animals transduced with first-generation vectors. This showed that helper-dependent vectors are better suited for transgene expression over longer periods of time. Looking at the different time points, it could be seen that the sharp decline observed in the bone marrow of the same animals (**Fig. 14A**) was not present in the spleen. Even though the transduction levels were the lowest at twelve weeks after transduction, no clear downward trend was visible, and for some animals, high GFP-levels appeared to be retained for extended periods of time. Furthermore, the differences between animals that only received the transposon vector and animals that had received both vectors were much smaller than what had been observed for the bone marrow. Even animals that had only received HDAd-GFP and that should not show stable integration into cells showed high transgene expression levels, even twelve weeks after infection. This would suggest that cells that had homed to the spleen following mobilization were able to remain there without undergoing cells division or dying off. In support of this, patients undergoing mobilizing treatment are know to sometimes undergo enlargement and even rupture of the spleen (201–203). However, since these observations were made in a setting where mobilized cells were collected through apheresis, no conclusions can be drawn for conditions under which no cells are removed from the system, as is the case in these mouse experiments.

In the peripheral blood cells of animals transduced with HDAd-GFP alone, the average percentage of GFP expressing cells was 0.48 ± 0.36 % at four weeks, 0.13 ± 0.13 % at eight weeks and 0.55 ± 1.15 % at twelve weeks after transduction. In the blood of animals that had received both HDAd-SB and HDAd-GFP, the observed transduction levels were 0.34 ± 0.29 % after four weeks, 0.04 ± 0.05 % after eight weeks and 0.34 ± 0.7 % after twelve weeks (**Fig. 14E**). Thus, transduction rates for HDAd-GFP alone were slightly higher than for the combination of both vectors. However, this is due to single animals at each time point that showed particularly high transduction rates. Over time, the transduction levels of PBMCs declined. However, twelve weeks after transduction, some animals of both groups started to show relatively high GFP percentages in PBMCs. One possible explanation could be that in these animals, GFP-positive PBMCs are supplied by stably modified HSPCs from the bone marrow. Even though this would be unlikely in the animals that only received the non-integrating HDAd-GFP, it cannot be excluded. However, one would expect these animals to present high percentages of GFP-positive cells in both the PBMCs and the spleen,

since those two compartments are thought to be in equilibrium (42). This was not the case. It should be noted that transduced cells in the spleen were able to persist for extended periods of time (**Fig. 14D**), and that the equilibrium between blood and spleen in these animals might not be functioning as it would under steady-state conditions.

In conclusion, even though a loss in transduction rates occurred over time, bone marrow HSPCs could be modified over extended periods of time of up to twelve weeks.

3.8.2 *In vivo* transduction of HSPCs with CFU potential

In **Fig. 14C** it had been shown via flow cytometry that mouse LSK cells could be transduced with the two vector system and that GFP was expressed up to twelve weeks after transduction. However, this phenotypic analysis does not allow conclusions about the functionality of the transduced HSPCs. To demonstrate this, the bone marrow of the animals treated before (see section 3.8.1) was depleted of lineage-committed cells via MACS and then enriched for GFP-positive cells via FACS. These cells were then plated out in CFU assays and evaluated for their colony-forming potential as well as the GFP expression in the formed colonies (**Fig. 15A**).

The total colony-forming potential of bone marrow cells from animals either treated with HDAd-GFP alone or from animals that received both vectors did not differ significantly (**Fig. 15B**). Per 1000 plated cells, animals treated with HDAd-GFP alone formed 66.6 ± 47.7 colonies at four weeks, 46.5 ± 24.8 colonies at week eight, and 26.2 ± 16.3 colonies at week twelve after *in vivo* transduction. In comparison, animals that received both HDAd-GFP and HDAd-SB formed 87.4 ± 37.0, 44.5 ± 13.5, and 48.2 ± 32.6 colonies per 1000 plated cells at four, eight, and twelve weeks after transduction, respectively. The differences between both groups were not statistically significant, showing that the increased viral dose in the group that received both vectors did not negatively impact the colony-forming potential of transduced HSPCs. However, over time there was a decrease in the number of colonies formed for both groups. Most likely, at the early time point, a relatively high amount of progenitors that have not committed to a lineage yet but are very close to this point are present. These cells are able to form colonies at this point in time, however, at later time points they have committed to a lineage and are therefore excluded during the lineage depletion step. These exhausted progenitors are replenished from the

HSC pool, but the majority of them will not express GFP. Thus, the total amount of cells, that have colony-forming potential and that express GFP will inevitably go down over time.

Although no differences between the two treatment groups were found in terms of total colony formation, the GFP expression levels within the formed colonies differed drastically (**Fig. 15C**). The percentages of GFP-positive colonies for animals treated with HDAd-GFP alone were 0.45 ± 1.00 % at four weeks and 0.39 ± 0.71 % at eight weeks after transduction. At twelve weeks after transduction, no GFP-positive colonies could be detected. In stark contrast, animals that had received the combination of HDAd-SB and HDAd-GFP expressed GFP in 4.15 ± 2.67 % of colonies at four weeks after transduction and in 7.01 ± 4.80 % and 16.50 ± 18.52 % of colonies at eight and twelve weeks after transduction, respectively. Not only were the GFP percentages for animals that received both vectors at least ten-fold higher than the HDAd-GFP-only group, but the percentages increased over time. In addition, the vast majority of colonies that scored as GFP-positive expressed the transgene in all cells of the colony (**Fig. 15D**). These results strongly suggest that in colony-forming HSPCs in animals that received both vectors, stable integration of the transgene had occurred and that all cells formed by those modified progenitors carried the modification themselves. The increase in GFP-positive colonies over time was most likely due to gradual differentiation or dying off of less primitive, transduced progenitors that only possessed limited clonogenic or proliferative potential. Their exclusion from the sorted cells at later time points effectively led to an enrichment of gene-modified cells that were capable of forming colonies. In HSPCs of animals that only had received HDAd-GFP alone, transgene expression in the progenitors was still detectable at the time of cell sorting. However, since their progeny cells in the colonies did not express the transgene, the viral genome must have been only present in its episomal form.

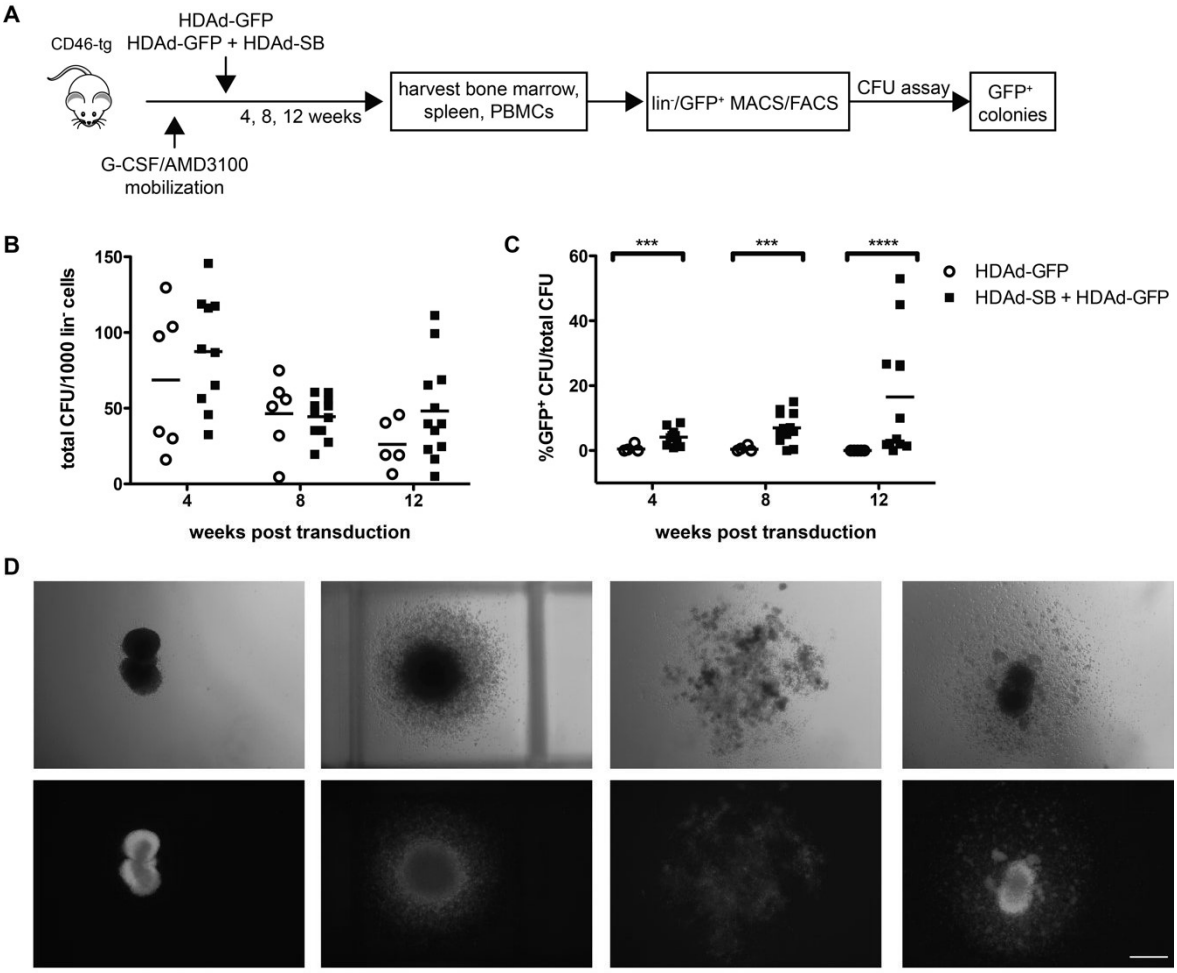

Fig. 15 Stable modification of HSPCs with colony-forming potential following *in vivo* transduction with the integrating two-vector system. CD46-tg animals were mobilized and *in vivo* transduced with HDAd-GFP alone (n=6 for 4 and 8 week time point, n=5 for 12 week time point) or a combination of HDAd-GFP and HDAd-SB (n=10 for 4 week time point, n=12 for 8 and 12 week time point). Animals were sacrificed 4, 8, or 12 weeks after transduction; bone marrow cells were isolated and lineage-depleted via MACS. GFP-positive cells were then collected via FACS. Cells were then plated in CFU assays, and colonies were scored 12 days after plating. Statistical analysis was performed using two-way ANOVA of log-transformed data. A) Experimental design. B) Formation of total colonies per 1000 lin^- cells. Shown are percentages for single animals as well as group means. C) Percentage of GFP-positive colonies among total CFUs. Shown are single animals as well as group means. D) Bright-field (top) and UV-microscopic (bottom) images of GFP-positive colonies obtained from animals transduced with both HDAd-SB and HDAd-GFP. Scale bar is 500 µm.

In conclusion, these results clearly demonstrate that *in vivo* transduction of HSPCs is feasible and that the Sleeping Beauty integration machinery allows for the stable modification of these cells.

3.8.3 Integration site analysis following in vivo transduction of HSPCs

The colony-forming unit experiments carried out previously (see section 3.8.2), suggested that the Sleeping Beauty integration machinery allowed for stable insertion of the GFP

transgene cassette into the genomic DNA of transduced HSPCs. To further substantiate this observation, a total of 20 GFP-positive colonies were collected from CFU assays, generated from the bone marrow of female animals eight weeks after *in* vivo transduction. The colonies were pooled and the genomic DNA was isolated. The DNA was then analyzed for Sleeping Beauty-mediated integrations of the GFP transgene via LAM-PCR and next-generation sequencing. Genomic DNA isolated from CFU colonies of uninfected animals was used as a reference. Both samples were treated and sequenced in two independent reactions and integration events of the transposon into TA dinucleotides were analyzed. Hits that were found in both treated and untreated samples were considered false positives and only hits that were not found in the control group but were found in both independent reactions of the treated group were considered as true integration events.

For the 20 colonies that were pooled and analyzed, a total of 155 individual integration sites had been detected. The integration sites within the mouse chromosomes are shown in **Fig. 16A**. The distribution of integration events per chromosome are shown in **Fig. 16B**. From both it can be seen, that the highest number of integration events was found on chromosome 13. Furthermore, the majority of integration events on chromosome 13 were found clustered together in the central region of the chromosome. When looking at the distribution of integration sites in relation to nearby genes, 62 % of integration events occurred in intergenic regions. Intronic regions of genes harbored 35 % of integration events, while almost 2 % were found in exonic regions (**Fig. 16C**). Looking at the mouse genome, intergenic regions make up about 60 % of the genome, while 38 % are intronic, and 3.4 % are exonic (204). Thus the distribution of integration sites matches these values relatively well, suggesting that the integration pattern observed here follows a random distribution and is not biased towards certain regions or elements.

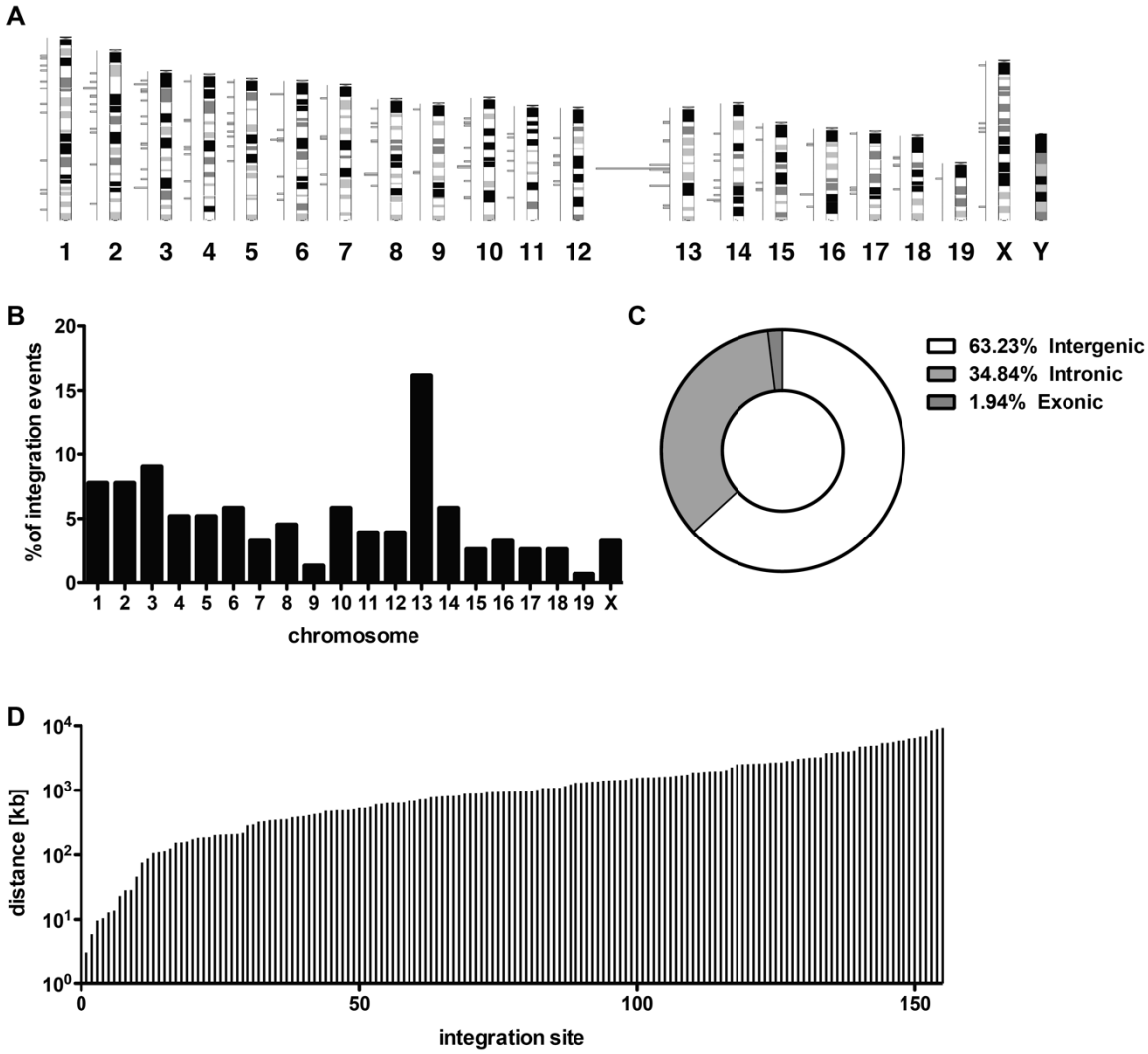

Fig. 16 Integration site analysis in CFU colonies derived from *in vivo* transduced animals. Female CD46-tg animals were mobilized and *in vivo* transduced with HDAd-GFP and HDAd-SB as before. Animals were sacrificed 8 weeks after infection, bone marrow cells were isolated and sorted for lin^-/GFP^+ using MACS and FACS. Cells were plated out in CFU assays and incubated for 12 days. A total of 20 GFP-positive colonies were collected, pooled, and genomic DNA was extracted. Sleeping Beauty-mediated integration events were detected using LAM PCR and next-generation sequencing. A) Distribution of detected integration sites within the mouse genome. Integration events are shown as red bars. B) Shown is the percentage of total integration events per chromosome. C) Integration sites were mapped to the mouse genome, and their location with respect to genes was analyzed. Shown is the percentage of integration events that occurred outside of genes, within intronic regions and within exons, respectively. D) Distance of integration sites to genes of the KEGG pathways in cancer database. The distance to the closest cancer related gene is shown for each integration site.

However, the relatively high number of independent integration events was unexpected. Assuming that each CFU colony contains clones of the original progenitor that initiated colony formation, and assuming that the probability of transducing the same mobilized progenitor with both viruses was relatively low, one would expect only one integration event per colony. However, with the observed 155 integration events, every colony-

inducing cell would have to carry eight integration events on average. Since the Sleeping Beauty-mediated integration employs a cut and paste mechanism that destroys the transposon donor vector, in order for eight integration events to occur, the same cell would have to be transduced by at least nine virus particles. Looking at the overall transduction rates observed during *in vivo* transduction, this seems very unlikely. The high number of integration events can therefore not be logically explained .

In addition, the genomic positions of the identified integration sites were compared to the genomic coordinates of the murine KEGG pathways in cancer genes (205) and the distance of each integration site to the nearest cancer related gene was calculated (**Fig. 16D**). Most importantly, none of the integration events occurred within cancer related genes. The closest distance of an integration site to a cancer related gene was 3111 bp. The median distance was 962 kbp and the majority of integration sites were at least 100 kbp up- or downstream of cancer related genes.

3.8.4 *In vivo* transduction of different lineages in the bone marrow and spleen

In addition to the GFP expression in different hematopoietic tissues over time, the transduction rates in different lineages of the bone marrow and spleen as well as the influence of mobilization and *in vivo* transduction on the cellular composition of both tissues were to be assessed. To this end, CD46-tg mice were mobilized as before and *in vivo* transduced with HDAd-GFP or both HDAd-SB and HDAd-GFP. Eight weeks after transduction, animals were sacrificed and the expression of GFP and lineage surface markers was assessed in cells isolated from the bone marrow and spleen (**Fig. 17**).

The cellular composition of the bone marrow of non-mobilized, non-infected animals and animals that had been mobilized and transduced can be seen in **Fig. 17A**. As expected, CD3-expressing T cells were rare in the bone marrow, and no significant differences between treated and non-treated animals could be observed. CD19-positive bone marrow B cells made up a significantly higher fraction of total bone marrow cells in non-treated animals than in the treated group. Conversely, the levels of myeloid cells, expressing surface markers CD11b and/or Gr-1 were higher in animals that had been mobilized and infected. In the spleen, untreated animals showed significantly higher levels of B and T cells, while

no differences in rare CD11b-positive cells were observed (**Fig. 17B**). Interestingly, animals that had received the combination of both viruses had significantly higher levels of Gr-1$^+$ cells compared to both untreated animals and animals that had been treated only with the transposon vector.

In the bone marrow of infected animals (**Fig. 17C**), significant differences in the transduction levels of the different lineages were seen. In CD3-positive T cells 2.98 $\pm$ 1.29 % expressed GFP in animals injected with HDAd-GFP alone and 4.63 $\pm$ 4.06 % were GFP-positive in animals that had received both vectors. In CD19-positive B cells, percentages of GFP-positive cells were at 5.98 $\pm$ 3.06 % for HDAd-GFP alone and 17.47 $\pm$ 10.44 for HDAd-SB + HDAd-GFP. For myeloid cells in HDAd-GFP-only animals, percentages of GFP-positive cells were at 0.255 $\pm$ 0.10 % and 0.70 $\pm$ 0.13 % for CD11b+ and Gr-1+ cells, respectively and 0.82 $\pm$ 0.44 % and 2.76 $\pm$ 0.93 for animals that received both vectors. In the spleens (**Fig. 17D**) of animals that had been injected with HDAd-GFP alone, 2.15 $\pm$ 0.45 % of CD3$^+$ cells, 4.81 $\pm$ 3.79 % of CD19$^+$ cells, 6.25 $\pm$ 2.56 % of CD11b$^+$ cells, and 3.75 $\pm$ 0.94 % of Gr-1$^+$ cells were positive for GFP. In the two vector group, the percentages were 4.67 $\pm$ 1.68 for CD3$^+$, 26.85 $\pm$ 24.46 for CD19$^+$, 29.80 $\pm$ 13.69 for CD11b$^+$, and 19.37 $\pm$ 5.54 for Gr-1$^+$ cells.

Looking at the bone marrow of *in vivo* transduced animals compared to non-mobilized, non-transduced controls, differences in the cellular composition of the marrow became apparent. In animals that had been mobilized and injected, the level of CD19-positive B cells had been reduced, while the percentage of CD11b-positve and Gr-1-positve myeloid cells had increased (**Fig. 17A**). It has been shown that G-CSF signaling is used during the induction of emergency granulopoiesis (206). While this process usually occurs during infection, systemic administration of recombinant G-CSF could have the same effect. Emergency granulopoiesis leads to rapid and massive proliferation of myeloid progenitors and leads to increases in circulating granulocytes. At the same time, it is thought that the expansion of the myeloid cell pool comes at the cost of a reduction in B cells, mainly due to space limitations in the bone marrow (207). Along the same lines, it has been shown that

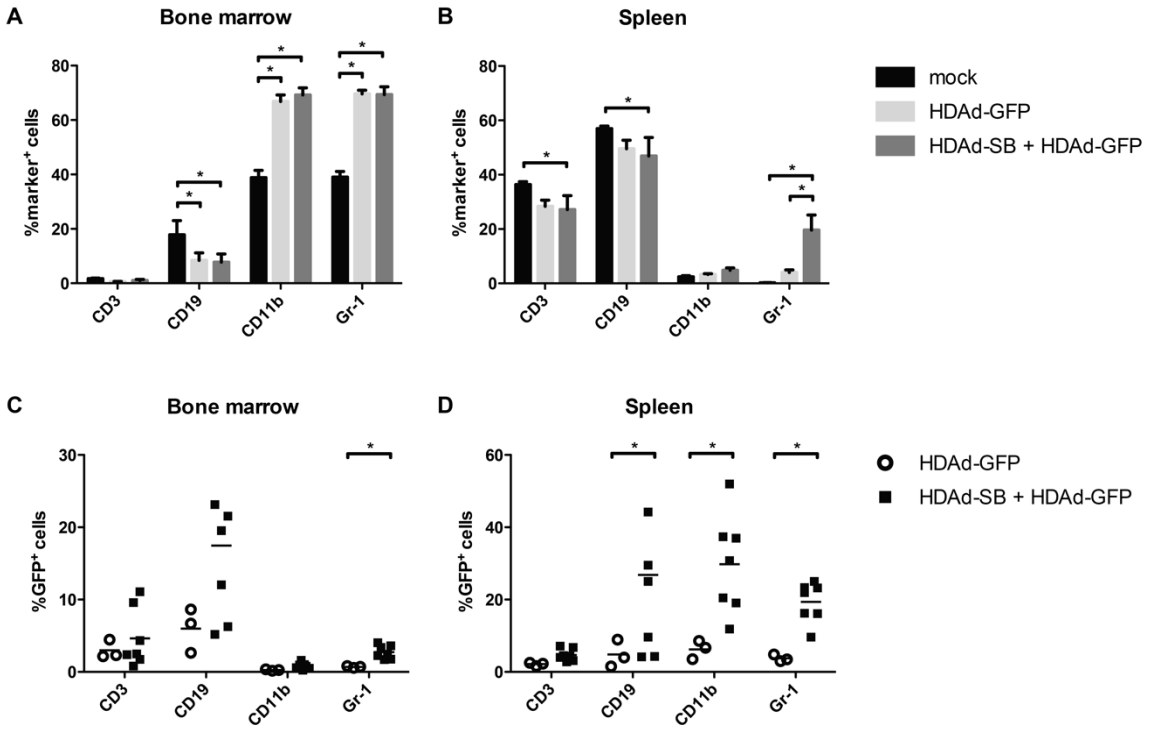

Fig. 17 Effect of *in vivo* transduction on different lineages of the bone marrow and spleen. CD46-tg animals were mobilized and *in vivo* transduced with HDAd-GFP alone (n=3) or both HDAd-SB and HDAd-GFP (n=7). Animals were sacrificed 8 weeks after transduction, and bone marrow and spleen were analyzed for transgene expression in different hematopoietic lineages via flow cytometry. Uninfected, non-mobilized CD46-tg animals were used as controls (mock, n=2). Two-way ANOVA with Bonferroni post testing was used to test for significant differences. Differences were not statistically significant unless stated otherwise. A) – B) Influence of mobilization and *in vivo* transduction on the composition of bone marrow (A) and spleen (B) in different lineages. Shown are mean ± SD percentages of cells positive for the given lineage-specific surface markers. C) – D) GFP expression in different lineages of bone marrow (C) and spleen (D). Shown is the mean ± SD percentage of GFP-positive cells in cells positive for the stated cell surface markers.

G-CSF-based HSC mobilization can interfere with B lymphopoiesis (208, 209). However, both of these processes are usually relatively short-lived and it remains questionable if the consequences of both could still be seen two months after mobilization. The rapid expansion of granulocytes and the decrease in B cell production could also explain the observed transduction levels in B cells and myeloid cells in the bone marrow (**Fig. 17C**), which showed higher transduction in B cells even though these cells are less abundant than myeloid cells. Rapid expansion and turnover of myeloid cells would lead to a relatively quick replacement of potentially transduced cells with new, untransduced cells. However, the slower turnover of mature B cells could allow relatively high amounts of cells to continually express GFP over extended periods of time. Additionally, when comparing animals that had been injected with HDAd-GFP alone to animals that had received both viruses, animals of the two vector group expressed higher levels of GFP in T cells, B cells, and in Gr-1-positive

myeloid cells. Sleeping Beauty mediated transgene integration into committed progenitors could explain these differences, while animals that only received the transposon vector would be expected to loose transgene expression in the course of progenitor proliferation and differentiation.

In the cellular composition of the spleen, untreated animals exhibited higher levels of both B and T lymphocytes compared to treated animals, even though the differences were less pronounced than in the bone marrow. While there were no significant differences in the levels of $CD11b^+$ cells, animals that had been injected with both vectors showed markedly increased levels in $Gr\text{-}1^+$ cells over both untreated control animals and animals that had received only the donor vector. The differences between the two treated groups with respect to GFP expression were more prominent in the spleen than in the bone marrow. Animals that had received both viruses showed significantly increased numbers of GFP expressing cells in both B cells and myeloid cells. The relatively low levels of transduced T cells are most likely because they are a rare population in the bone marrow and therefore not as effectively mobilized. In contrast, mobilization of B cells and myeloid cells from the bone marrow appears to be more efficient, making these cells readily available for transduction in the periphery. For myeloid cells of the spleen, GFP expression levels for animals transduced with both viruses were significantly increased over HDAd-GFP-only injected animals. At the same time, the transduction rates of myeloid cells in the bone marrow were relatively low. This suggests that these cells had been mobilized and infected, but they were either not able to home back to the bone marrow, settling in the spleen instead, or they were able to home back to both organs, but increased granulopoiesis in the marrow soon led to loss of transduced cells. In both scenarios, myeloid cells appear to be retained in the spleen and might even be able to proliferate, explaining the higher GFP marking rate of animals that had received the integrating two-vector combination. Furthermore, high transduction rates of B cells were observed for animals that had received both vectors. Even though high transduction rates could be seen for both bone marrow and spleen, animals that exhibited high levels of GFP-positive cells in the bone marrow did not show the highest levels of GFP-expression in the spleen and *vice versa*. This would argue against transduced B cell progenitors in the bone marrow being able to generate gene-modified progeny that then settles in the spleen. Alternatively, the stable modification of

mobilized B cell progenitors that then settle in the spleen and proliferate there appears much more likely.

In conclusion, *in vivo* transduction with the integrating HDAd vector system led to efficient transduction of B cells in the bone marrow and spleen and to the presence of transduced myeloid cells in the spleen. The remaining lineages of both tissues could also be transduced, albeit at lower efficiencies. Even though the cellular composition of bone marrow and spleen was influenced by the treatment, it is not clear whether this effect is due to the viral vector or due to the mobilization regimen.

3.8.5 Gene-modified HSPCs are capable of multi-lineage reconstitution

The stable integration of a transgene cassette had been shown in HSPCs that were able to induce formation of colonies of gene-modified cells (see section 3.8.2). However, the gold standard for functional assays for HSPCs is the rescue of lethally irradiated recipients after bone marrow transplantation. To this end, CD46-tg mice were mobilized and *in vivo* transduced with the two vector system (HDAd-GFP + HDAd-SB). Bone marrow cells were harvested eight weeks after transduction and pooled for several animals. C57BL/6 recipient mice were lethally irradiated and transplanted with donor bone marrow cells to rescue them. One group of recipients received unmanipulated donor bone marrow, while the second group of recipients received whole bone marrow cells that had been sorted for GFP-positive cells (**Fig. 18A**). Blood samples of recipients were drawn every other week and the expression of human CD46 and GFP in PBMCs was surveyed. In this case, human CD46 was used as a marker for graft cells.

In animals that had received unsorted bone marrow, successful engraftment, based on CD46 expression, was seen from week 4 up to week 14 (**Fig. 18B**). The majority of animals showed close to 100% CD46-expressing PBMCs, with slight variances for single animals at later time points. At four weeks after transplantation, low levels of GFP expression within

CD46⁺ PBMCs could be detected for single animals. However, the levels of GFP expression in these animal decreased further over time and stayed just barely above background levels for most of the time (**Fig. 18C**).

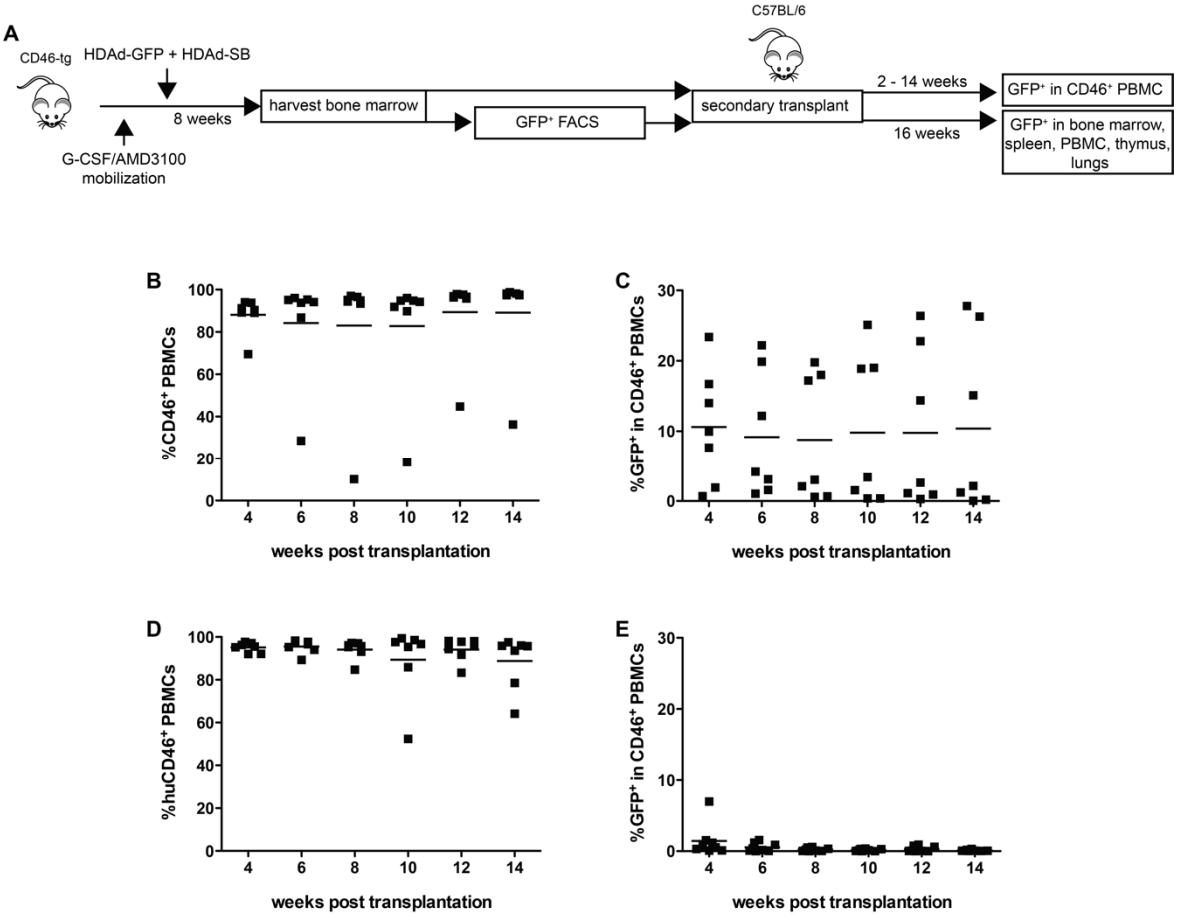

Fig. 18 Secondary transplantation of *in vivo* transduced bone marrow into lethally irradiated recipients. CD46-tg animals were mobilized and *in vivo* transduced with HDAd-GFP and HDAd-SB as before. Eight weeks after infection, animals were sacrificed, and bone marrow cells were isolated. Bone marrow from multiple animals was pooled. C57BL/6 recipients were irradiated and received 1x10⁶ donor bone marrows cells i.v. For transplantation, either whole, unsorted bone marrow (n=8), or bone marrow sorted for GFP-positive cells (n=7) was used. Blood samples of recipients were collected every other week and were analyzed for CD46 and GFP expression. Animals were followed for 16 weeks, at which time they were sacrificed, and GFP expression in different tissues was analyzed (**Fig. 19A**). A) Experimental procedure. B) Engraftment in PBMCs of recipients of GFP⁺ bone marrow. Shown is the percentage of PBMCs expressing CD46 for single animals as well as means at different time points following bone marrow transplantation. CD46 is used as a marker for engraftment since recipient C57BL/6 mice do not express CD46 on their blood cells. C) GFP expression in CD46⁺ PBMCs of mice transplanted with GFP⁺ bone marrow. Shown are percentages of GFP-positive PBMCs of single animals and group means. D) – E) Engraftment and GFP-expression in PBMCs of animals transplanted with unsorted bone marrow. Shown are single animals and group means.

In animals that had received bone marrow pre-sorted for GFP, similarly successful engraftment rates could be observed (**Fig. 18D**). However, the GFP-expression levels in the PBMCs of these animals were much higher. At four weeks after transplantation 8.1 ± 3.1 %

of $CD46^+$ PBMCs had expressed GFP. The average expression level then slightly but steadily increased to 12.5 ± 4.7 % at 14 weeks after transplantation (**Fig. 18E**). However, it can be seen that the animals could be divided into two groups based on their GFP expression. While 3 animals showed high levels of GFP expression that even increased over time, the second group showed low to moderate expression levels at four weeks after transplantation. In these animals, GFP expression levels declined within the following weeks and remained low for the rest of the observed time window.

From this data it becomes clear that the amounts of gene-modified long-term repopulating HSCs is very low. Donor bone marrow had to be sorted for GFP expressing cells in order to artificially enrich their content in the graft, as animals that received unsorted bone marrow did not show significant GFP expression following bone marrow transplantation. Even in the seven animals that had received GFP-expressing bone marrow cells, only three showed long-term expression of GFP. In these animals it has to be assumed that part of the received long-term repopulating HSCs had been stably modified. In the remaining four animals, either no stably modified HSCs had been transplanted, as indicated by low GFP expression levels from week four to week 14 after transplantation, or only short-term repopulating HSCs had been stably modified, as they expressed moderate levels of GFP in the blood four weeks after transplantation but then GFP expression levels started to decline, coinciding with the exhaustion of short-term repopulating HSCs.

A hallmark of true hematopoietic stem cells is not only their potential for long-term engraftment of irradiated recipients but also their ability to reconstitute all hematopoietic lineages in the recipient. To show that *in vivo* transduction with the Sleeping Beauty two vector system allowed for the stable modification of these cells, the GFP expression in different lineages of various hematopoietic tissues was assessed in transplanted animals.

Animals that had been transplanted with GFP-sorted bone marrow were sacrificed 16 weeks after transplantation, and GFP expression in cells of the bone marrow, spleen, blood, lungs and thymus were analyzed for GFP expression via flow cytometry. First, the cellular composition of bone marrow, spleen and peripheral blood in the transplanted animals was analyzed and compared to non-treated C57BL/6 mice (**Fig. 19A**). In the bone marrow, levels of B and T lymphocytes were comparable between transplanted and control animals. Transplanted animals showed significantly increased levels of myeloid cells. While control

bone marrow contained 42.4 ± 3.5 % CD11b-positive cells, the marrow of transplant recipients contained 55.4 ± 3.1 % of $CD11b^+$ cells. Similar results were found for the second myeloid marker, Gr-1. In the peripheral blood, control animals exhibited slightly higher amounts of B cells and myeloid cells, while transplanted animals had higher levels of T cells. However, none of these differences were statistically significant. In the spleen only marginal differences between control and transplanted animals could be detected. Thus, it can be seen that multi-lineage reconstitution from *in vivo* transduced HSC was successful in the transplant recipients.

However, to show that stably gene-modified HSCs were among those driving the multi-lineage reconstitution of the hematopoietic system in these animals, the GFP expression of different lineages in different tissues was analyzed (**Fig. 19B**). In the bone marrow, 3.4 ± 4.7 % of $CD3^+$ cells, 7.6 ± 10.5 % of $CD19^+$ cells, 7.8 ± 9.4 % of $CD11b^+$ cells, and 8.7 ± 8.8 % of $Gr\text{-}1^+$ cells expressed GFP. In the peripheral blood, GFP expression levels were at 5.1 ± 7.7 % in T cells, 6.6 ± 9.7 % in B cells and 8.7 ± 9.5 % and 21.6 ± 25.7 % in $CD11b^+$ and $Gr\text{-}1^+$ myeloid cells, respectively. In the spleen, 4.3 ± 5.9 % of T cells were GFP-positive, while 7.0 ± 9.4 % of B cells expressed GFP. In the myeloid fraction, 8.8 ± 9.9 % of $CD11b^+$ cells and 5.1 ± 6.6 % of $Gr\text{-}1^+$ cells expressed GFP.

In addition, the GFP expression in different HSPC-containing cell subsets was analyzed (**Fig. 19C**). In lineage-depleted bone marrow cells, 5.9 ± 7.2 % of cells were positive for GFP expression. In the more primitive LSK subset, 8.6 ± 11.4 % of cells expressed GFP and in the even more primitive LSK SLAM subset, 4.7 ± 5.3 % of cells were expressing GFP.

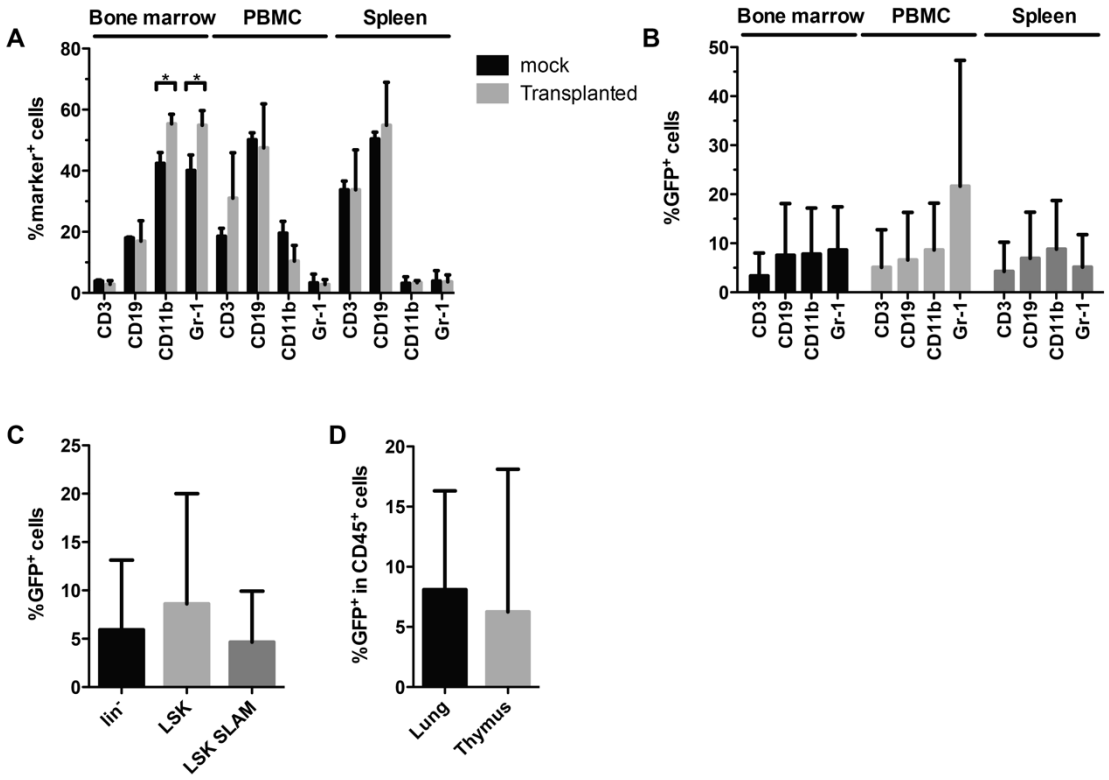

Fig. 19 Endpoint analysis of secondary recipients of Sleeping Beauty-modified bone marrow transplants The experimental procedure is described in Res. Fig. 15. C57BL/6 animals were sacrificed 16 weeks after transplantation with GFP-positive bone marrow cells from CD46-tg donors that had been *in vivo* transduced with HDAd-GFP and HDAd-SB. A) Lineage composition of bone marrow, blood, and spleen in transplanted animals (n=7). Tissues were stained for the indicated lineage markers, and expression was compared to non-transplanted C57BL/6 mice (mock, n=2). Shown are means ± SD of percentages of cells positive for the indicated lineage markers. Two-way ANOVA with Bonferroni post testing was used to test for statistically significant differences. Differences were not significant, unless indicated otherwise. B) GFP expression in different lineages of bone marrow, blood, and spleen. Shown are mean percentages of GFP-positive cells ± SD in cells gated for the indicated lineage markers. C) Expression of GFP in different cell fractions of the bone marrow enriched for HSPCs. Shown is the mean ± SD percentage of GFP-positive cells within the indicated HSPC populations. D) GFP expression in leukocytes of the lungs and thymus. Shown is the mean ± SD percentage of GFP-positive cells within the CD45-positive fraction.

This last subset, which in addition to the LSK surface markers is positive for CD150 and negative for CD48, is thought to be highly enriched for HSCs (32).

Furthermore, the expression of GFP in white blood cells isolated from the thymi and lungs of transplanted animals was assessed (**Fig. 19D**). In the lungs, 8.1 ± 8.2 % of $CD45^+$ cells expressed the transgene, while in the thymus 6.3 ± 11.9 % of $CD45^+$ cells were positive for GFP.

Substantial variations for the transgene expression levels between individual animals could be seen in all lineages and tissues. In parallel to the GFP expression levels that had been

seen in the peripheral blood over time (**Fig. 18C**), this is most likely due to one group of animals expressing GFP in many cells throughout all tissues, while a second group of animals only has low levels of transgene expressing cells. Nevertheless, the average GFP expression levels of most lineages and tissues are relatively close to 10 %, which is consistent with what was seen in the peripheral blood between weeks 4 and 14 after transplantation. Nevertheless, Gr-1-positive peripheral blood mononuclear cells expressed unusually high levels of GFP. The highest value observed was 61.8 %. No other lineage in any other tissues exhibited such a high marking rate. However, in the bone marrow and spleen, the levels of GFP-positive cells in Gr-1$^+$ cells were much more comparable to the other lineages, making this observation specific for the peripheral blood.

In addition to the flow cytometric analysis of different tissues and lineages, tissue sections of two animals (390 and 775) that showed the highest levels of GFP expression were also analyzed. In **Fig. 20**, sections of the colon, lungs, and spleen of transplant recipient animals 390 and 775 are shown in comparison to sections from a non-transplanted C57BL/6 mouse. For both transplanted animals, expression of GFP could be detected in all three analyzed organs, further corroborating the findings of the flow cytometric analysis.

Furthermore, blood samples from transplanted animals collected at the time of sacrifice were submitted to blood cell count analysis (**Fig. 21**). It can be seen that the average blood cell counts of the transplanted animals are well within the normal range for all blood cell types except for eosinophils. Eosinophil counts were slightly higher than the expected range. However, a C57Bl/6 animal used as a control also showed slightly increased counts for eosinophils, which could hint towards a systematic error or a strain specific observation.

In conclusion, judging from the presence of GFP-positive cells within all of the analyzed lineages and tissues, it can be concluded that stably modified HSCs that had been transduced *in vivo* drove multi-lineage reconstitution of the recipient animals. Since animals were analyzed at 16 weeks after transplantation, it can be assumed that this reconstitution would remain stable over time, as historically, long-term repopulation is defined as occurring after twelve weeks post bone marrow transplantation (2). This shows that the *in vivo* transduction approach presented in this work allows for the transduction of long-term repopulating hematopoietic stem cells with adenoviral vectors. Furthermore, the transgene integration driven by the Sleeping Beauty transposase allows stable genetic

modification of the cells. Moreover, the modified HSCs are still able to function in their role as stem cells and pass the modification on to their progeny. In addition, the blood cell count data shows that no aberrant expansion of any blood cell type in transplanted animals could be detected. Uncontrolled expansion could hint towards malignant transformation of a certain lineage and the onset of leukemia. Even though the sample size of transplanted animals was fairly small, none of the integration events seemed to have led to any kind of malignant transformation of transduced cells.

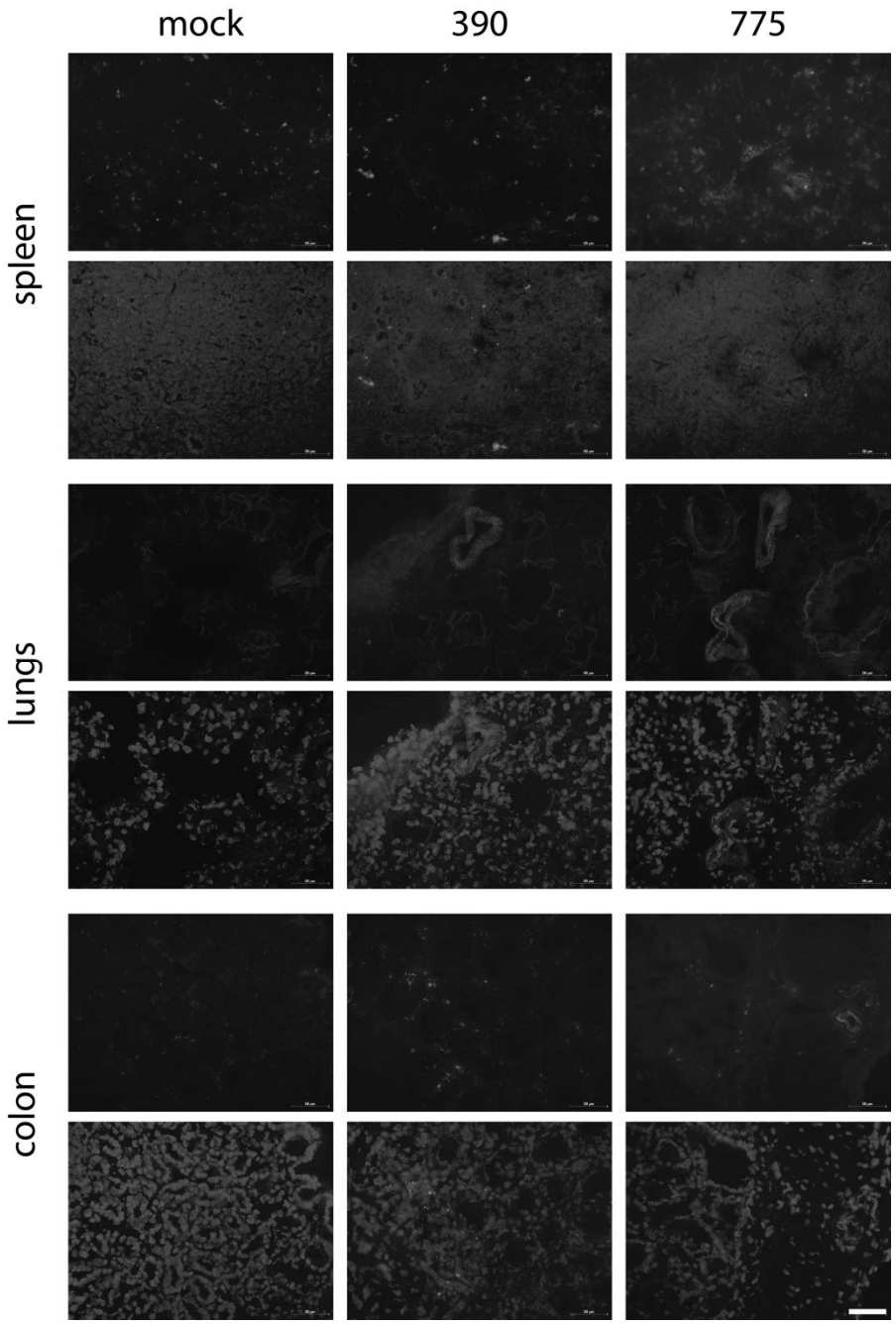

Fig. 20 GFP expression in tissue sections of transplant recipients. Experimental procedure is described in Fig. Res. 15. Two animals, 390 and 775, which both had received HDAd-SB + HDAd-GFP are shown. Tissue sections of spleen, lungs, and colon are shown together with sections of a non-transplanted C57BL/6 control animal (mock). GFP can be seen in green, while blue represents DAPI nuclear stains. Upper panels show GFP alone, lower panels show GFP and DAPI. Scale bar is 50 µm.

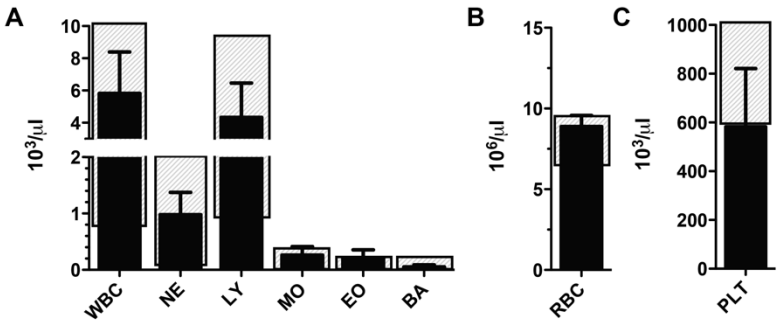

Fig. 21 Blood cells counts of secondary recipients of Sleeping Beauty-modified bone marrow transplants. The experimental procedure is described in Res. Fig. 15. Shown are the counts/µl for A) white blood cells (WBC), neutrophils (NE), lymphocytes (LY), monocytes (MO), eosinophils (EO), basophils (BA), B) red blood cells (RBCs), and C) platelets (PLT) for animals that had received bone marrow of *in vivo* transduced bone marrow cells. n=7.

3.9 Safety of HDAd *in vivo* transduction in CD46-transgenic mice

3.9.1 Biodistribution of HDAd5/35 vectors in mobilized animals

During the process of mobilization, large amounts of white blood cells are forced into the bloodstream. Since all these cells express CD46 and represent potential target cells for Ad5/35-based vectors, the biodistribution in mobilized animals could potentially be very different from that observed in a non-mobilized animal. To further understand this impact, CD46-transgenic mice were mobilized as before and injected with either HDAd-GFP or a first-generation Ad5 vector (Ad5-GFP). The animals were sacrificed 3 days after infection and the presence of viral genomes in different tissues was assayed via quantitative real time PCR (**Fig. 22**). Of note, Ad5 is used as a reference here, since it is the vector platform that has been traditionally used and is considered the serotype that is best understood.

For animals injected with Ad5-GFP, the highest concentration of viral genomes was found in the liver. Genomes could also be detected in the bone marrow, colon, heart, kidneys, lungs, and spleen, albeit at levels almost two orders of magnitude lower than in the liver. No Ad5-GFP genomes could be detected in the intestine, the ovaries or the pancreas. For the Ad5/35-based, helper-dependent HDAd-GFP, the highest number of viral genomes was

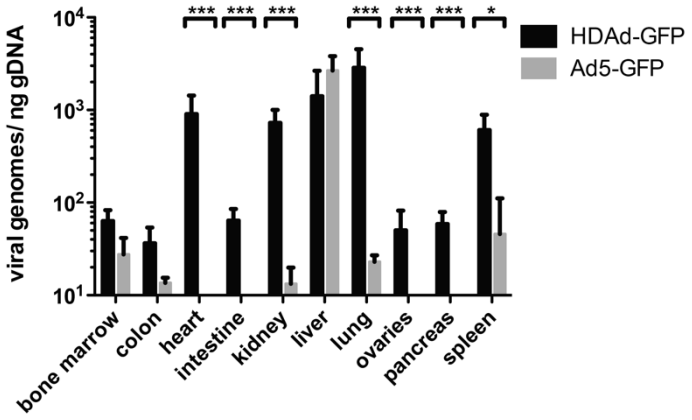

Fig. 22 Biodistribution of Ad5-GFP and HDAd-GFP vector genomes in mobilized CD46-tg animals. CD46-tg animals were mobilized as before and received intravenous injections of $4x10^{10}$ vp of either Ad5-GFP (n=2) or HDAd-GFP (n=5). Animals were sacrificed 3 days after injection, and the presence of viral genomes in different tissues was analyzed by qPCR. Shown are mean ± SD viral genomes per ng of genomic DNA. Two-way ANOVA of log transformed data with Bonferroni post testing was used to evaluate the statistical significance of differences.

found in the lungs. In addition, high viral genome copy numbers were found in the liver, heart, spleen, and kidneys. Lower amounts of viral DNA were found in the bone marrow, colon, and intestine as well as ovaries and pancreas.

The level of Ad5-GFP was higher than that of HDAd-GFP only in the liver. For the remaining organs, HDAd-GFP genomes were found in higher numbers than Ad5-GFP. Statistically significant differences were seen for the heart, kidneys, lungs, and spleen. Here, the genome copies found for HDAd-GFP were at least one order of magnitude higher than those of Ad5-GFP. Differences were also significant for the intestine, ovaries, and pancreas, although the differences were less pronounced.

The strong liver tropism of Ad5-based vectors is well known and was to be expected (210). In a biodistribution study in the same mouse model that compared wild type Ad5 to other serotypes, Ad5 showed the highest levels of uptake through the liver (211). In the same study, a wild type Ad35 virus also showed relatively high levels of liver tropism. Similar results could be expected for the serotype 5 and 35 fiber chimeric HDAd-GFP vector. Furthermore, the investigators observed that Ad5 was unable to transduce the lungs but was found in medium quantities in the spleen. In contrast, Ad35 showed high copy numbers in both spleen and lungs.

In a second study that compared the biodistribution of Ad5-based and Ad5/35-based vectors in a CD46-transgenic model (212), high levels of liver transduction and to a lesser degree transduction of the lungs was found for the Ad5 vector. The Ad5/35 vector showed high transduction levels of the lungs and heart, followed by the kidneys. In the spleen, however, relatively low levels of vector were found.

In a third study, Ad5 and Ad5/35 vectors were compared after intravenous injection into baboons (213). Here, again, the Ad5-based vector showed the highest liver uptake, while still relatively high amounts of vector were found in the spleen, lungs, kidneys, and heart. The Ad5/35 vector however, showed the highest transduction levels in the spleen, followed by liver, heart, lungs, and kidneys. Interestingly, in this study, the Ad5 vector showed higher genome copies in the bone marrow than the Ad5/35 vector.

These studies and the results presented in **Fig. 22** are in agreement in most points. Ad5 vectors show strong liver tropism, while transduction in other organs is usually much less profound. Ad35 and Ad5/35-based vectors exhibit relatively strong liver tropism and can be found in the heart, liver, and kidneys as well. Strong tropism to the spleen was found only by Stone *et al.* (214) and Ni *et al*. (213), but not by Ganesh *et al.*(212). Even though the tropism to the spleen might be arguable in non-mobilized mice, in mobilized mice even higher copy numbers of the virus in the spleen would be expected. We showed above that high amounts of mobilized bone marrow cells can be transduced in the periphery and then instead of homing back to the marrow, end up in the spleen (**Fig. 7**).

In conclusion, the mobilization regimen did not greatly influence the biodistribution of the Ad5-based Ad-GFP or the Ad5/35-based HDAd-GFP. However, tropism to hematopoietic tissues involved in the mobilization process appears to be impacted.

3.9.2 Inflammatory response and hepatotoxicity following *in vivo* transduction

To evaluate the safety of intravenous injections of helper-dependent Ad5/35 vectors into mobilized animals, cytokine responses and serum levels of liver enzymes were analyzed. Animals were mobilized as before and *in vivo* transduced with either Ad5-GFP or HDAd-GFP. For the analysis of inflammatory cytokine responses, animals received two doses of

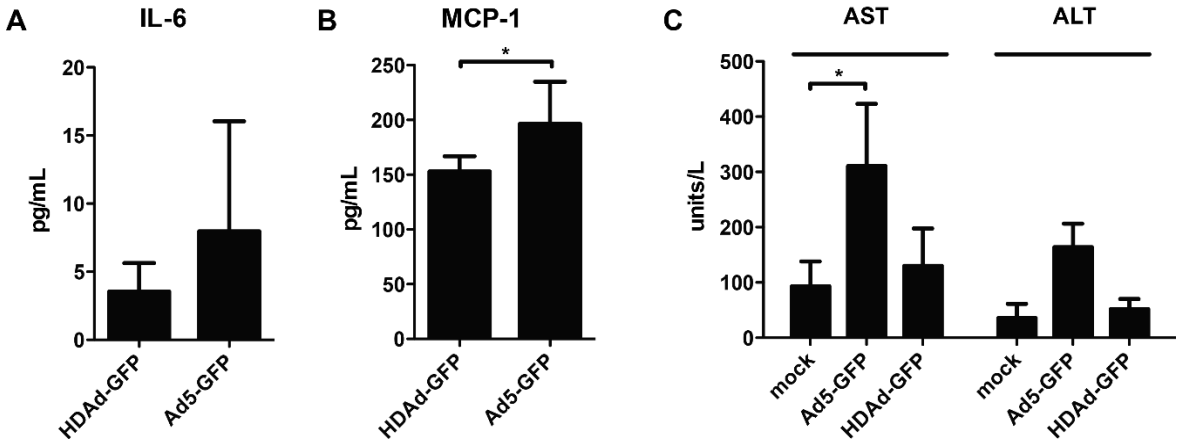

Fig. 23 Liver enzyme and cytokine levels following *in vivo* transduction in CD46-tg animals. A) – B) Animals were mobilized as before and received two doses of $4x10^{10}$ vp of Ad5-GFP or HDAd-GFP both 30 and 60 min after AMD3100 injection (n=5). Serum samples were collected 6 h after the last injection, and concentrations of IL-6 and MCP-1 were measured. Shown are mean ± SD concentrations of the indicated cytokines. It was tested for the statistical significance of differences using unpaired T tests with (IL-6) and without (MCP-1) Welch's correction. C) Animals were mobilized as before and *in vivo* transduced with $4x10^{10}$ vp of Ad5-GFP (n=2) or HDAd-GFP (n=2). Three days after transduction, animals were sacrificed, and serum samples were analyzed for presence of aspartate transaminase (AST) and alanine transaminase (ALT) as indicators of liver damage. Unmobilized, untransduced animals were used as a reference (mock, n=2). Differences were analyzed for statistical significance using one-way ANOVA with Bonferroni post testing. Differences were not significant unless stated otherwise.

each vector at $4x10^{10}$ vp per dose. Blood samples were taken six hours after the last injection and serum levels of cytokines were analyzed using a cytometric bead array (**Fig. 23A, B**). Both in animals injected with Ad5-GFP and those injected with HDAd-GFP, the levels of interleukin-10 (IL-10), interferon-γ (IFN-γ), tumor necrosis factor α (TNF-α), and IL-12p70 were below the detection limit of the assay. Interleukin-6 (IL-6) was detected at 3.5 ± 2.1 pg/ml for animals that had received HDAd-GFP and 8.0 ± 8.1 pg/ml for animals that had received Ad5-GFP (**Fig. 23A**). Animals treated with HDAd-GFP showed monocyte chemoattractant protein-1 (MCP-1) serum levels of 153.0 ± 13.9 pg/ml, while animals treated with Ad5-GFP showed serum levels of 196.4 ± 38.6 pg/ml (**Fig. 23B**).

In comparison to other studies, the levels observed here for both IL-6 and MCP-1 are extremely low. In a study that looked at cytokine responses after intravenous injections of 10^{11} vp of either Ad5 or Ad35, much higher cytokine levels were observed (211). Not only were the levels of IL-6 and MCP-1 more than 50-fold increased, but INF-γ could be observed in these animals as well. In a different study, authors found that first-generation Ad5/35 vectors induced much more severe IL-6, MCP-1, and IFN-γ responses than what was observed here for HDAd-GFP, albeit the Ad5/35 vector was being used at 10^{11} vp per

animal. In a third study comparing Ad5 and Ad5/35 vectors side by side, again more severe cytokine responses were observed for MCP-1, while IL-6 was below the detection limit in animals that received Ad5/35 (215). Of note, in this study, Ad5 caused more severe innate immune responses than Ad5/35.

The absence of a more severe cytokine response is most likely due to the use of Dexamethasone (Dex) as part of the mobilization regimen. Dex, a glucocorticoid, has been shown to be able to considerably lower the levels of inflammatory cytokines following intravenous delivery of adenoviral vectors (216). Of note, when initial *in vivo* transduction experiments were performed without the use of Dexamethasone, severe responses of mobilized animals could be observed a few minutes after virus administration. In some cases, animals did not survive the injection. To circumvent these problems, injections of Dex were included in the standard *in vivo* transduction regimen.

Adenoviral vectors, especially vectors based on serotype 5, exhibit strong liver tropism and have been shown to cause liver toxicity (210). As a marker for liver damage, the blood levels of the liver enzymes AST (aspartate transaminase) and ALT (alanine transaminase) are measured. To assess the liver damage associated with HSPC *in vivo* transduction, CD46-tg animals were mobilized as before and received an intravenous injection of either Ad5-GFP or HDAd-GFP. Three days after transduction, blood was collected and analyzed for the presence of AST and ALT (**Fig. 23C**). As a reference, unmobilized, uninjected animals were used. Animals injected with Ad5-GFP showed significantly increased AST levels in the blood, while ALT levels were elevated as well. In contrast, animals that had received HDAd-GFP only showed minimal elevations in the levels of AST and ALT.

The differences in release of liver enzymes for Ad5-GFP and HDAd-GFP were most likely due to their difference in serotype. As seen in the biodistribution study (**Fig. 22**), higher genome copy numbers of Ad5-GFP were found in the liver when compared to HDAd-GFP. Part of the adenoviral vector is taken up by resident liver macrophages (Kupffer cells) and leads to the death of these cells. The rest of the viral particles are able to transduce hepatocytes through interaction of the adenoviral capsid with coagulation factors and the uptake of virus-coagulation factor complexes into hepatocytes (217). The interaction of the virus with the coagulation factors was found to be mediated by the viral hexon protein (218–220). While Ad5-based vectors are extremely efficient in transducing the liver, it has

been shown that fiber-chimeric vectors carrying shorter fiber shaft domains exhibit less liver transduction potential (221, 222). In addition, as mentioned before, Ad5-GFP is a first-generation vector with the potential for leaky expression of viral genes and related cytotoxicity issues. HDAd-GFP does not encode any viral genes and should therefore lead to less toxicity towards transduced hepatocytes. Taken together, this explains the lower level of liver damage by HDAd-GFP, as indicated by liver enzymes in the blood. Of note, Seregin *et al.* (216) reported that dexamethasone treatment only slightly decreased the transduction of liver cells.

In conclusion, the helper-dependent HDAd-GFP vector exhibited lower inflammatory responses than Ad5-GFP, albeit low overall cytokine levels due to dexamethasone treatment. In addition, liver damage induced by HDAd-GFP was lower than that induced by the Ad5-based vector.

3.10 *In vivo* transduction in a humanized mouse model

The experiments above focused on a CD46-transgenic mouse model to study the potency of this newly developed *in vivo* transduction method. To supplement this data with a system more closely resembling the situation in humans, a humanized mouse model was employed. This model is based on the engraftment of human hematopoietic stem cells in an irradiated, immunodeficient mouse, resulting in the formation of a partly human hematopoietic system within the mouse. For this, NOD/SCID-IL-2Rγ^{null} (NOG) mice (223) were lethally irradiated and then transplanted with human CD34^{+} cells along with accessory mouse bone marrow cells from unirradiated NOG donors. Six weeks after transplantation, the engraftment rate in recipient animals was confirmed via flow cytometric analysis of human CD45 (huCD45)-positive cells in the peripheral blood (**Fig. 24A**).

To ensure that human progenitors could be mobilized out of the bone marrow, a group of humanized animals was mobilized using the same combination of G-CSF and AMD3100 as before. Following the mobilization regimen, blood samples were drawn and PBMCs were plated out in CFU assays supporting the growth of either human or murine progenitor colonies Blood from unmobilized, humanized NOG mice was used as a reference. Progenitor colonies were enumerated 14 days after plating (**Fig. 24B**). While the mobilization led to a 2.2-fold increase in mobilized, human colony-forming progenitors, an

8.2-fold increase in circulating murine progenitors could be observed. This data suggests that the effectiveness of G-CSF and AMD3100-based mobilization appeared greatly impaired in humanized NOG mice.

In comparison, in CD46-tg mice an 81-fold increase of circulating, colony-forming progenitors upon mobilization had been observed (**Fig. 6**). Studies performed in NOD/SCID mice, used for humanization experiments before the development of NOG and NSG mice, showed that G-CSF treatment of animals engrafted with human HSPCs also showed relatively low increases in the numbers of circulating human progenitors (224).

Next, humanized NOG mice were used in an *in vivo* transduction experiment. To this end, animals were mobilized as before and injected with a 1:1 mixture of HDAd-GFP and HDAd-SB. Groups of animals were sacrificed at three days and four weeks after transduction and the expression of GFP was surveyed in human and murine cells in different tissues (**Fig. 24C)** Unmobilized, uninfected, humanized NOG mice were used as a reference.

The engraftment level of human cells in the bone marrow of animals following the *in vivo* transduction regimen remained comparable to untreated animals (**Fig. 24D**). At three days after transduction 38.7 $\pm$ 23.5 % of bone marrow cells were positive for human CD45. However, animals that were analyzed four weeks after transduction showed a drastic decrease in human $CD45^+$ cells in the bone marrow down to 4.2 $\pm$ 2.3 % $huCD45^+$. In the spleen, an opposing trend could be observed. While in unmobilized, untransduced animals a splenic engraftment of 26.6 $\pm$ 15.9 % could be observed, it increased to 32.5 $\pm$ 11.7 % and 35.7 $\pm$ 17.6 % at three days and four weeks after transduction, respectively. In the peripheral blood, the engraftment rates remained comparable before and after treatment at 16.6 $\pm$ 8.3 % for untreated animals, 16.8 $\pm$ 2.9 % at three days after transduction and 12.4 $\pm$ 10.9 % at four weeks after transduction. Especially low levels of human cells in the bone marrow at four weeks after transduction could indicate the exhaustion of the human graft after extended periods of time. In support of this, when comparing the engraftment rates in the peripheral blood at six weeks after bone marrow transplantation (**Fig. 24A**) and at the time of sacrifice (up to 24 weeks after bone marrow transplantation, **Fig. 24D**) a decrease of almost 50 % of human cells could be observed.

The transduction rates for human cells in bone marrow, spleen, and PBMCs are shown in **Fig. 24E**. In human $CD45^+$ cells in the bone marrow, transduction rates were 0.21 ± 0.25 % at three days after transduction and 2.49 ± 2.25 % at four weeks after transduction. In the spleen 0.13 ± 0.15 % and 7.59 ± 4.83 % of cells were positive for GFP at three days and four weeks after transduction, respectively. In the peripheral blood, 2.24 ± 1.71 % and 0.40 ± 0.59 % of human cells were GFP-positive at three days and four weeks after transduction, respectively.

For comparison, the transduction rates in murine cells (**Fig. 24F**), which are most likely due to unspecific transduction, since these cells do not express CD46, were as follows: In the bone marrow 0.11 ± 0.12 % and 0.06 ± 0.07 % of murine cells were positive for GFP. In the spleen transduction rates were at 0.51 ± 0.63 % and 3.78 ± 2.77 %. In the peripheral blood, no GFP-positive cells could be detected three days after transduction, and at four weeks after transduction 0.25 ± 0.28 % of mouse blood cells were GFP-positive.

In addition to measuring the transduction rates, bone marrow cells from *in vivo* transduced NOG mice were sorted for $huCD45^+/GFP^+$ and plated out in CFU assays for human progenitors (**Fig. 24G**). At three days after transduction, the colony forming potential was 47.5 ± 18.1 CFU per 10^4 plated cells, while four weeks after transduction it was at 36.1 ± 7.3 CFU per 10^4 plated cells. Of note, none of the formed colonies, neither plated at three days or four weeks after transduction were expressing significant levels of GFP. The number of colonies formed in these experiments was relatively low. This, taken together with the low transduction rates observed in the bone marrow, lowers the probability to pick up a gene-modified HSPC in this colony-forming assay.

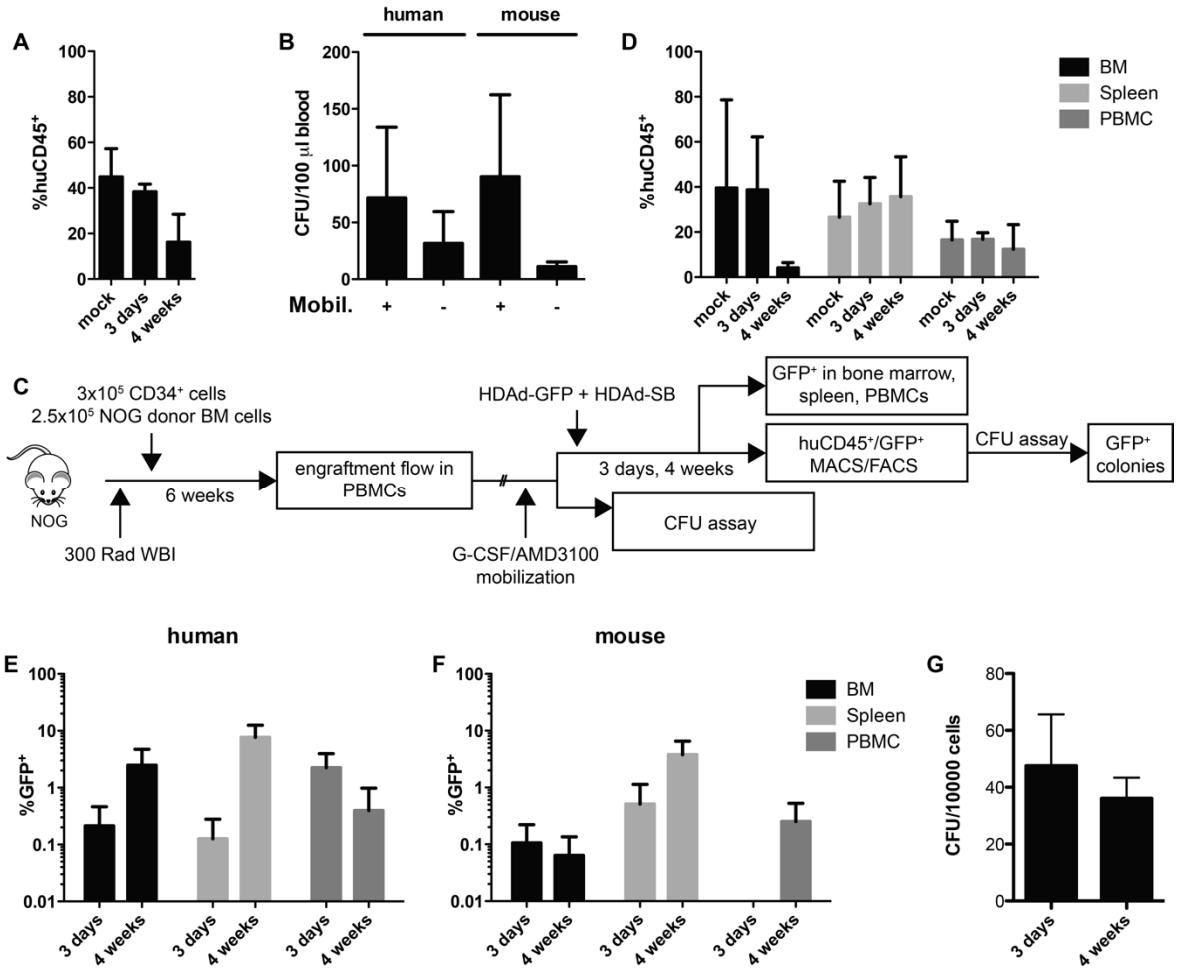

Fig. 24 *In vivo* transduction of humanized NOG mice with integrating HDAd vectors. To generate humanized NOG mice, animals were lethally irradiated and then transplanted with a mixture of human CD34$^+$ cells and unconditioned whole bone marrow of NOG donor mice. A) Successful engraftment was determined 6 weeks after transplantation through analysis of PBMCs via flow cytometry. B) Animals were mobilized with G-CSF and AMD3100, and PBMCs were isolated 90 min after AMD3100 injection. Red blood cells were lysed, and cells were plated out in CFU assays supporting the growth of either human or murine progenitor colonies. Colonies were scored 14 days after plating. Shown are mean ± SD of total colonies formed from 100 µl of whole blood (n=2). C) Animals were then mobilized as before and injected with a low dose mixture of HDAd-GFP and HDAd-SB at 30 min after AMD3100 and two high dose injections of both viruses at 60 and 90 minutes after AMD3100. Animals were sacrificed 3 days (n=4) and 4 weeks (n=7) after injection. The experimental setup is shown. D) The engraftment of human cells in the bone marrow (BM), spleen, and PBMCs was assessed via flow cytometry. Shown is the mean ± SD of human CD45$^+$ cells in the indicated tissues of unmobilized, untransduced animals (mock, n=2) and mobilized and *in vivo* transduced animals sacrificed at 3 days or 4 weeks after transduction. E) GFP expression in human cells present in bone marrow (BM), spleen and PBMCs of the same animals. Shown are mean ± SD percentages of GFP$^+$ human cells. F) GFP expression in mouse cells present in bone marrow (BM), spleen, and PBMCs. Shown are mean ± SD percentages of GFP$^+$ mouse cells. G) Bone marrow cells of *in vivo* transduced animals were sorted for human CD45$^+$/GFP$^+$ and plated out in CFU assays. Colonies were scored 14 days after plating. Shown are mean ± SD CFU normalized to 10000 plated cells for animals sacrificed 3 days and 4 weeks after *in vivo* transduction.

In conclusion, this data indicates that the mobilization and *in vivo* transduction approach in a humanized mouse model appeared to be less efficient and might also follow different kinetics than those observed in CD46-tg mice (**Fig. 14B, D**). The transduction rates observed in the bone marrow and spleen at four weeks after transduction were comparable to the values observed for CD46-tg mice. Interestingly, the values observed at three days after transduction were much lower than those at four weeks, even though the opposite trend was observed in experiments in CD46-tg mice (**Fig. 7**, **Fig. 14**). In addition, the transduction rates in the peripheral blood after three days were high compared to bone marrow and spleen, but then dropped over time. This could be indicative of the following mechanism: G-CSF and AMD3100 administration lead to mobilization of bone marrow cells into the periphery, where they were transduced by the adenoviral vectors. However, since it is not clear if the interaction between the human graft and the murine bone marrow stroma and spleen are working seamlessly, the mobilized and transduced cells might stay in circulation longer, which would explain the high transduction rates in the blood after three days. At later time points the cells were able to return to the bone marrow or settle down in the spleen, explaining the increase in transduced cells there at four weeks after transduction. An alternative explanation for the increase in transduction rates in bone marrow and spleen over time could be that Sleeping Beauty-mediated integration took place and the modified cells expanded over time. Even though no GFP-positive colonies could be detected in the CFU assays, the ability of NOG mice to maintain human primitive HSCs over extended periods of time is limited, most likely due to the missing expression of human thrombopoietin (225). Since the mice used here were transduced and analyzed at relatively late time points (up to 24 weeks after bone marrow transfer), these mice might only possess low amounts of human HSCs, which could be why their stable modification was not picked up in the CFU assay.

In addition, unspecific transduction of murine cells, which were mobilized as well, was not insignificant. In fact, at three days after transduction, GFP expression levels in murine cells in bone marrow were comparable and in the spleen were higher than those seen for human cells. However, this could in part be due to an advantage in rehoming to those tissues for the murine cells, since they are interacting with self-cells. Since the murine cells in this model did not express the viral receptor CD46, an alternative transduction mechanism had to be involved. In a study by Bradfute *et al.*, the authors transduced mouse HSPCs with Ad5-

based vectors. Even when the primary receptor for Ad5 was blocked, transductioncould be detected at low levels, most likely through interaction of the virus with cellular integrins (226). A similar mechanism could have been involved here.

3.11 HSPC *in vivo* transduction in a non-human primate model

To further demonstrate the potential of HSPC *in vivo* transduction approach, the system was applied in a non-human primate model. Two pig-tailed macaques (*macaca nemestrina*) were used for these studies. The studies were performed in cooperation with Kevin Haworth and other members of the group of Hans-Peter Kiem at the Fred Hutchinson Cancer Research Center, Seattle, WA.

The first animal, Z12406, was mobilized with G-CSF and stem cell factor (SCF), both at 50 µg/kg/day for 4 consecutive days. On the fifth day, the animal received an intravenous injection of HDAd-GFP at $2x10^{12}$ vp/kg. The second animal was mobilized with a combination of G-CSF (50 µg/kg for four days) and AMD3100 (4 mg/kg) on day four. The following day, the animal was injected with a single injection of HDAd-GFP and HDAd-SB at $2x10^{12}$ vp/kg per virus.

The effectiveness of the mobilizing regimen in both animals was assessed in blood samples drawn from the animals before, during, and after mobilization and virus injection. Both the total white blood cell (WBC) counts as well as the content of $CD34^+$ cells were analyzed (**Fig. 25A, B**). At day three before injection, an increase in WBCs over baseline for both animals could be detected. While the HDAd-GFP-only animal exhibited $4.1x10^4$ WBC/µl of blood, the HDAd-SB + HDAd-GFP animals showed $3.8x10^4$ WBC/µl. However, in blood samples drawn directly before virus injection, the HDAd-GFP animal's WBC counts had increased to $6.8x10^4$ cells/µl, while the animal that received both viruses still had WBC counts of $3.9x10^4$ cells/µl. When looking at the $CD34^+$ cell content in the peripheral blood, the differences between the two animals were even more pronounced. The HDAd-GFP-only animal showed steady increases in the percentage of $CD34^+$ cells in the peripheral blood, which peaked at the day of injection at 0.22 %. For the second animal, however, no significant increases in circulating $CD34^+$ cells could be detected over the course of mobilization, and at the day of injection 0.018 % of cells in the blood were positive for CD34.

This data clearly suggests that while mobilization in the HDAd-GFP animal was successful, the animal that received both viruses showed poor mobilization overall, as well as mobilization of HSPCs into the peripheral blood.

To assess the transduction of HSPCs in the non-human primate model, $CD34^+$ cells were isolated from peripheral blood samples before virus injection as well as two and six hours after virus injection. The cells were cultured for 72 h after virus injection to allow for transgene expression, and GFP expression was assessed via flow cytometry (**Fig. 25C**). For the HDAd-GFP-only animal, GFP expression at two hours post injection could be detected in 3.1 % of $CD34^+$ cells, while at six hours post injection 1.5 % of $CD34^+$ cells expressed GFP. The lower level of GFP expression at six hours after transduction is most likely due to transduced cells beginning to leave the peripheral blood and homing to the spleen and bone marrow. For the animal that had received both viruses, not enough $CD34^+$ cells could be isolated for meaningful analysis. This was directly connected to the poor mobilization observed in this animal.

To assess the transduction of HSPCs that had homed back to the bone marrow following mobilization, bone marrow biopsies were obtained three and seven days as well as ten weeks after virus injection. The GFP expression in $CD34^+$ HSPCs was analyzed via flow cytometry (**Fig. 25D**). For the animal that had received HDAd-GFP alone, 0.19 % of bone marrow $CD34^+$ cells expressed GFP three days after injection. At seven days after injection, the value had increased slightly to 0.23 %. At ten weeks after transduction, the majority of GFP-positive cells had been lost in the bone marrow, and only 0.01 % of $CD34^+$ cells expressed the transgene. In the second animal, which had received both HDAd-GFP and HDAd-SB, lower levels of transgene expression were detected. GFP was expressed in 0.04 % and 0.08 % of bone marrow $CD34^+$ cells after three and seven days following injection, respectively. At ten weeks after transduction, 0.01 % of bone marrow $CD34^+$ cells remained GFP-positive.

This data demonstrates that HSPC mobilization and intravenous injection of HDAd vectors allows for the transduction of mobilized HSPCs and that the mobilized HSPCs are able to home back to the bone marrow following transduction. At the same time, long-term modification of HSPCs could not be shown in the animal that had received both the transposon vector and the transposase vector. This was most likely due to the poor mobilization and low level of initial HSPC transduction.

To assess the safety of the HSPC *in vivo* transduction approach in the NHP model, plasma levels of the vector, as well as serum levels of several cytokines, were monitored over time (**Fig. 26**). The plasma clearance of the vectors was assessed via qPCR for the GFP cassette of the HDAd-GFP vector. Of note, the plasma levels of the HDAd-SB vector were not detected separately but were assumed to be similar to those observed for HDAd-GFP, since both vectors were injected at the same dose and time. For the animal that received HDAd-

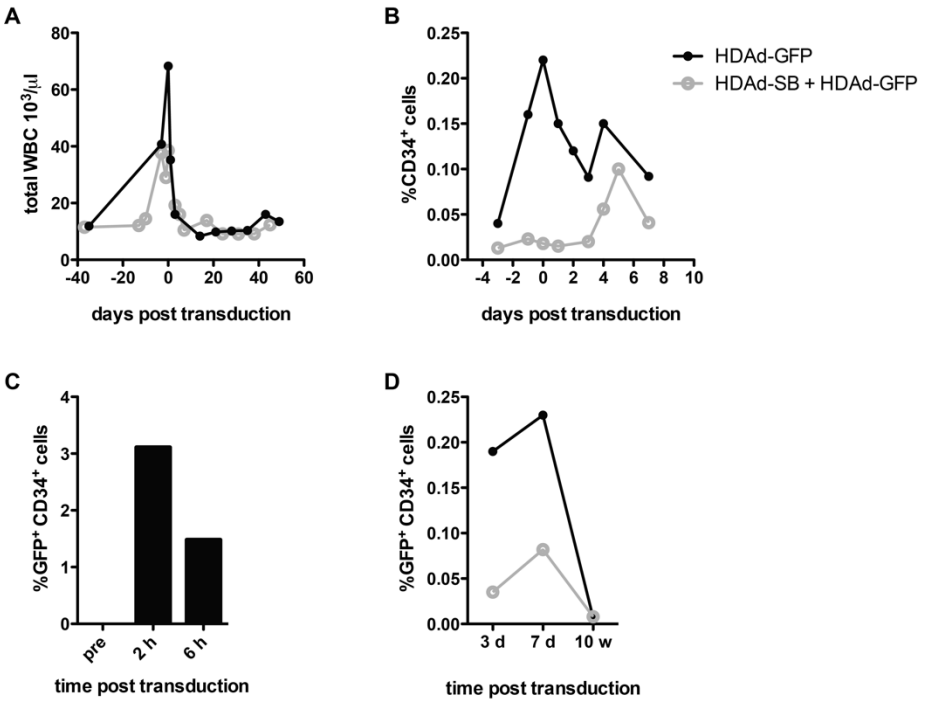

Fig. 25 Mobilization and HSPC transduction in a non-human primate model. Non-human primates were mobilized and injected intravenously with either HDAd-GFP alone or HDAd-GFP and HDAd-SB on day 0. A) Total white blood cell counts and B) $CD34^+$ cell content in the peripheral blood were measured over time. C) Peripheral blood $CD34^+$ cells were collected at the indicated time points, cultured for 72 hours, and GFP expression in the cells was assessed in the animal treated with HDAd-GFP. D) Bone marrow biopsies from both animals were collected at the indicated time points, and the GFP expression was assessed in $CD34^+$ cells.

GFP alone, the highest plasma levels of the vector were detected at two hours after injection, the earliest time point that was analyzed (**Fig. 26A**). At this time, the virus load in

the plasma was at $5.5x10^7$ vector genomes (vg) per ml of blood. The virus was then cleared from the circulation over time. One day after injection, the plasma levels were at $1.2x10^7$ vg/ml and at day four after injection, no circulating virus could be detected. For the animal that had received both viruses, the plasma level of HDAd-GFP at two hours after transduction was at $2.1x10^9$ vg/ml and decreased down to $1.1x10^7$ vg/ml at 24 h after injection. At day five after injection, the virus plasma level was at $2.3x10^5$ vg/ml. This value was slightly above the detection limit of the assay, which was at $2x10^5$ vg/ml. At seven days after transduction, no circulating virus genomes were detected.

The higher vector plasma levels in the animal that received both vectors were most likely due to both a higher amount of vector injected and the lower level of HSPC mobilization. Since this animal received twice the amount of adenoviral vector compared to the first animal, it is to be expected that the higher amount of vector will be cleared more slowly from the circulation (227). At the same time, the second animal had shown only low levels of HSPC mobilization, leading to fewer cells in the circulation with the potential to take up the vector, resulting in higher plasma levels in the second animal.

Serum samples of the injected animal were tested for the levels of IL-2, IL-4, IL-5, IL-6, IFN-γ, and TNF-α. The presence of IL-2, IL-4, and IL-5 could not be detected in the serum of both animals. The theoretical detection limits of the assay for these cytokines were as follows: IL-2 3.6 pg/ml, IL-4 0.9 pg/ml, and IL-5 0.3 pg/ml. In the animal that had received HDAd-GFP alone, only background levels of IFN-γ could be detected (**Fig. 26B**). For the second animal, which had received both viruses, levels of IFN-γ were close to the limit of detection. TNF-α could be detected on the day of injection for the animal that had received HDAd-GFP alone (**Fig. 26C**). The peak level was detected at six hours after injection at 27.7 pg/ml. For the second animal, TNF- α levels remained at background levels. Significant elevations in IL-6 serum levels were detected for both animals, with peaks at six hours after injection with 4415 pg/ml for the HDAd-GFP-only animal and 4797 pg/ml for the animal that had received both vectors (**Fig. 26D**). In both animals, the IL-6 levels returned back to normal within 24 hours after injection.

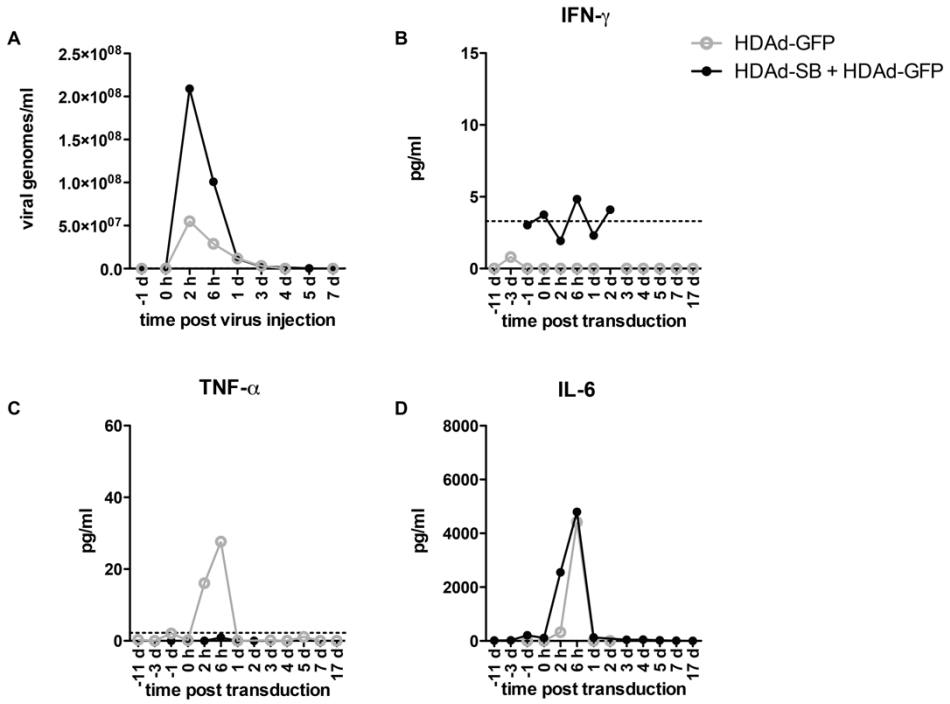

Fig. 26 Safety parameters of HSPC *in vivo* transduction in a non-human primate model. In the same animals as in **Fig. 25**, following vector injection, plasma clearance of HDAd-GFP genomes (A) and serum levels of different cytokines (B-D) were measured. Dashed lines represent the theoretical detection limit of the cytokine assays.

Elevations in IL-6 serum levels following intravenous injection of adenoviral vectors have been reported before. In a study in rhesus macaques, the intravenous delivery of a first-generation adenoviral vector at a dose of $3.8x10^{12}$ vp/kg lead to IL-6 serum levels of 240 pg/ml at six hours after injection (227). As a comparison, the animal that received $2x10^{12}$ vp of HDAd-GFP alone exhibited IL-6 levels of almost 20-fold higher, showing that the mobilization of the animal most likely had a high impact on the inflammatory response following vector administration. Another study injected different doses of first-generation adenoviral vectors into baboons (228). A dose of $5.6x10^{12}$ vp/kg lead to peak IL-6 levels of 360 pg/ml at three hours after injection. A second animal was injected with $1.1x10^{13}$ vp/kg and exhibited a severe innate immune response requiring euthanasia of the animal at nine hours after injection. While this animal showed IL-6 levels of 9850 pg/ml at six hours post injection, the levels kept increasing to 35000 pg/ml at 8.5 h after injection. While that study presented a clear vector dose dependence of the IL-6 response, similar peak levels of IL-6 were observed for both animals in this study, irrespective of whether they received only one virus or both viruses (**Fig. 26D**). As the HSPC mobilization appeared to have a major impact on the IL-6 response, this effect could have been caused by the lower level of HSPC mobilization. Even though the observed IL-6 levels were significantly higher than what had

been described for unmobilized animals, IL-6 levels returned to baseline within 24 h of vector administration, and both animals tolerated the injections well.

4 Discussion

Gene therapy of hematopoietic stem cells holds the promise of delivering curative treatments for various genetic diseases. Treatments in advanced stages of clinical development rely on the collection of patient-derived HSCs, the *ex vivo* culture of these cells followed by transduction with retroviral vectors and reinfusion of modified cells into a myelo-conditioned patient. While this approach has shown promising results in clinical trials, it entails a number of drawbacks (see section 1.3.3). Moreover, its technical complexity as well as the strict regulations imposed on facilities performing the *ex vivo* culture and transduction, severely limit the accessibility of this treatment to potential patients. To overcome these drawbacks of traditional *ex vivo* HSC gene therapy, this study outlines a new method for the genetic modification of HSCs within the patient, without the need for extraction, *ex vivo* culture or myeloablative treatment of the patient. Our system is based on the mobilization of HSPCs out of the bone marrow and into the peripheral bloodstream. Here, HSPCs can be transduced with an intravenously injected, adenoviral gene transfer vector. Following transduction, gene-modified cells home back to the bone marrow and persist as functional stem cells for extended periods of time.

4.1 Mobilization allows transduction of bone marrow HSPCs *in vivo*

The first aim of this study was to assess whether the mobilization of HSCPs from the bone marrow into the periphery would allow their transduction and if these transduced cells would be able to home back to the bone marrow afterwards.

In order for HSPCs to be transducable with a vector based on Ad5/35, the target cells are required to express the cellular receptor CD46. Both human and CD46-transgenic mouse HSPCs did express CD46 (**Fig. 4**). This is in line with reports that CD46 is expressed on human $CD34^+$ (186) cells as well as that the CD46-tg mouse model expresses CD46 in hematopoietic cells (184). The expression of CD46 allowed for the transduction of these cells *in vitro* with a first-generation Ad5/35++ vector (**Fig. 5**). While Ad5/35 had been shown to be a capable gene transfer vector for human $CD34^+$ cells, transduction of HSPCs in the CD46-transgenic mouse model had not been studied before. However, since these cells expressed even higher levels of CD46 than total bone marrow MNCs, efficient transduction with Ad5/35-based vectors was to be expected.

In addition to the vector being able to transduce HSPCs, the efficient mobilization of these cells through the treatment with G-CSF and AMD3100 had to be shown. In the CD46-tg mouse model, efficient mobilization of bone marrow HSPCs into the peripheral blood was shown both in CFU assays as well as through phenotypic analysis using flow cytometry (**Fig. 6**). In addition, a synergistic effect of mobilization of G-CSF combined with AMD3100 was observed. While this approach had not been tested in the CD46-tg mouse model before, studies in C57BL/6 mice, the founder strain of the CD46-tg mice, found similar results (51).

In conclusion, both requirements for HSPC *in vivo* transduction, the ability of Ad5/35-based vectors to transduce HSCs as well as the ability to mobilize HSCs into the peripheral blood stream, were given in the CD46-tg mouse model.

The intravenous administration of Ad5/35++-GFP into mobilized CD46-tg mice lead to transduction of HSPCs in the periphery (**Fig. 7A**). The transduced HSPCs were then able to home back to the bone marrow (**Fig. 7B**). In addition, copious amounts of transduced HSPCs were found in the spleen. The deposition of mobilized bone marrow cells in the spleen was to be expected as increases in spleen sizes following mobilization in humans have been reported (229, 230). These effects are usually transient, especially when apheresis is used to collect mobilized cells, but there is the potential for more serious side effects. In fact, in rare cases, mobilization treatment has even led to rupturing of the spleen in patients (201–203).

The mobilization status of the animals at the time of vector administration did not seem to have a pronounced effect on the transduction levels of bone marrow and spleen total MNCs, while the efficient transduction of HSPCs in both tissues was only possible following mobilization. The effect of mobilization on HSPC transduction was much more pronounced in the bone marrow (**Fig. 7B**). Over a time period of 14 days, a loss of GFP expressing cells was observed both in total MNCs of the bone marrow as well as in HSPCs of the bone marrow and spleen. For total bone marrow cells, the rapid turnover of neutrophils and their replenishment from the bone marrow most likely contributed to this observation (231). However, for HSPCs, the turnover of which is much slower, a different mechanism must be at work.

The vector that was used in these initial *in vivo* transduction experiments was a first-generation adenoviral vector deleted for the E1A and E3 region. However, all other viral genes are still encoded in the vector genome and could lead to leaky expression of viral genes, which in turn could lead to death of the transduced cells due to an immune response (158, 190). It was further shown that immune responses can also be mounted in response to an immunogenic transgene, for example GFP, leading to increased death of transduced, transgene expressing cells (232). Lastly, the vector genome of Ad5/35++-GFP can only be maintained episomally and would be lost if a transduced cell underwent multiple cell divisions. Similarly, a rapidly dividing cell in the bone marrow would also lose its HSC phenotype – and not be detected through the LSK staining used in this study – and would be lost from the pool of GFP expressing HSPCs.

Furthermore, in the spleen, in addition to a rapid loss of transgene expression, changes in the numbers of splenic HSCs were observed over time. This must be considered when evaluating the loss of transgene expressing cells in the spleen.

Summarizing the first part of this study, it was shown that the mobilization of HSCs into the peripheral blood could be achieved, that these cells could be transduced by Ad5/35-based vectors, and that transduced HSPCs were able to home back to the bone marrow. However, loss of transgene expressing cells due to an episomally maintained first-generation adenoviral vector that could induce cytotoxicity and immune reactions, showed that the vector platform would need to be modified to enable long-term transgene expression in transduced HSCs and their progeny.

4.2 Stable modification of primitive HSCs with integrating adenoviral vectors

As described above, a first-generation vector without the capability to integrate its transgene into the HSC genome is not suitable for HSC gene therapy purposes. To improve upon this system, a switch to a helper-dependent adenoviral vector platform was made. These vectors are devoid of all viral genes, and it has been extensively shown that they elicit far less severe immune responses and cytotoxicity (233). In a comparison between a first-generation Ad5/35 vector and a helper-dependent HDAd5/35 vector, both vectors were able to transduce HSPCs at comparable efficiencies both *in vitro* and *in vivo* (**Fig. 8**).

Hematopoietic stem cells giving rise to progeny cells undergo many cell divisions until the final stage of the fully differentiated progeny cell is obtained. Therefore, an episomally maintained adenoviral vector is not suitable to track gene-modified HSCs and their progeny. Instead, transgene integration is required. So called hybrid vectors have been developed; these are based on adenoviral gene transfer vectors, and they encode a transposon and a matching Sleeping Beauty transposase. These hybrids are able to stably integrate the transposon into the cellular genome, while maintaining the advantages of an adenoviral gene delivery platform. Successful gene delivery and integration into the liver of mice and dogs has been achieved using this system (181). However, the application of hybrid vectors to HSCs had not been attempted before. Nevertheless, the key components of the system were reported to function separately in HSCs: Ad5/35 vectors have been shown to efficiently transduce HSCs in this study, and the Sleeping Beauty transposase had been reported to be functional in HSCs of both mouse and human (234–236).

In this study, it was shown that the integrating adenoviral vector system could be used to integrate a GFP transgene cassette into murine and human HSPCs *in vitro* and that the modified cells were able to form gene-modified progenitor colonies (**Fig. 11**, **Fig. 12**). When the integrating vector system was employed for *in vivo* transduction experiments, higher levels of transgene expression for longer periods of time could be observed in the bone marrow when compared to a non-integrating control (**Fig. 14**). Further, the integrating vector system achieved higher transduction rates in cells of different lineages in the bone marrow and spleen when compared to a group that only received the transposon vector (**Fig. 17**). However, over time a loss of transgene-expressing cells in the bone marrow could be observed. This was most likely due to the relatively fast turnover of less primitive cells in the bone marrow, leading to a loss of transgene expressing cells. Nevertheless, gene-modified cells with colony-forming potential could be detected even after 12 weeks, the last time point analyzed (**Fig. 15**). In fact, the amount of obtained GFP-positive colonies increased over time, again arguing for a loss of transduced less primitive cells, while modified cells with colony-forming potential appeared to remain in the bone marrow.

Transduced bone marrow cells collected at 8 weeks after *in vivo* transduction with the integrating vector system were able to rescue lethally irradiated recipients, and gene marking could be observed in all hematopoietic lineages in the bone marrow, peripheral

blood, and spleen at 16 weeks after transplantation (**Fig. 18**, **Fig. 19**). This showed that long-term, multi-lineage reconstituting HSCs had been transduced upon mobilization and *in vivo* vector administration.

The efficiency of a gene therapeutic treatment will finally be determined by its ability to alleviate the underlying condition. If therapeutic levels of the transgene can be achieved, it will be efficient enough, but if those levels cannot be reached, the therapy will most likely fail. Since, in this study GFP was used as a transgene, it is difficult to judge the efficiency of the *in vivo* transduction approach presented here. Nevertheless, due to the *in vivo* administration of the vector and the resulting relatively low multiplicity of infection, the efficiency of the *in vivo* approach is most likely lower than those achieved through *ex vivo* transduction.

To improve upon the transduction efficiency of the *in vivo* transduction system, different approaches could be envisioned. One option would be to optimize the transposase used to achieve transgene integration. While the hyperactive SB100x used in this study has exhibited significantly improved activity over other generations of Sleeping Beauty transposases, there are other transposases available. The most prominent, next to Sleeping Beauty, are piggyBac (PB) and Tol2. A recent study showed that SB100x had a higher transposition efficiency than both PB and Tol2 (236, 237). However, it has been shown that the size of the transposon has a major impact on the transposition activity. While Izsvák *et al.* showed that a transposon size of over 5 kb lead to an over 75 % decrease in SB transposition activity (180), both PB and Tol2 were shown to not suffer from reduced activities for transposon sizes of up to 9.1 kb and 11 kb in size, respectively (238, 239). The potential to more efficiently integrate larger transposons is especially interesting in the context of helper-dependent adenoviral delivery. HDAds have a cloning capacity of up to 33 kb and would not be able to exhibit their full potential if the transposon size was capped at 5 kb. Furthermore, the molecular evolution of different transposases is still ongoing, and future versions with superior capabilities will eventually be available.

In summary, in this section it was shown that the HSC *in vivo* transduction approach using a Sleeping Beauty integration machinery allowed the stable gene modification of true hematopoietic stem cells after *in vivo* transduction of mobilized animals. The modified HSCs

possessed long-term, multi-lineage reconstitution potential and passed their gene modification on to their progeny.

4.3 Safety profile of HSC *in vivo* gene modification

The main concerns regarding the safety of the *in vivo* HSC gene therapy approach introduced in this study are two-fold: First, the safety of the intravenous administration of the vector in mobilized animals had to be assessed. Second, the safety of the transgene integration through the Sleeping Beauty transposase in terms of potential genotoxic events had to be evaluated.

The biodistribution of vector genomes after HDAd-GFP injection into mobilized animals was assessed through qPCR (**Fig. 22**) and compared to intravenously injected Ad5-GFP. Compared to the Ad5 vector, much higher amounts of vector genomes were found in the lungs, the heart, the kidneys and the spleen. The transduction of these organs after intravenous administration of Ad35 and Ad5/35 vectors had been reported before (211, 215). However, stronger transduction of the spleen was found in this study. This is most likely due to the uptake of mobilized cells that had been transduced in the periphery and subsequently were deposited in the spleen.

In addition, inflammatory cytokine responses following intravenous vector administration in mobilized animals was assessed. During initial experiments, injection of a first-generation Ad5/35 vector led to the death of some animals at 5 – 10 minutes after vector administration. It was concluded that this was most likely due to a severe cytokine response, as this had been reported for adenoviral vectors in mice before (216). To ameliorate these effects, the animals were pretreated with Dexamethasone, as this had been shown to limit the severity of cytokine responses following intravenous Ad vector injection (216). Using this regimen, only mild elevations of IL-6 and MCP-1 were observed (**Fig. 23A, B**). Of note, the elevation of both cytokines was lower in response to HDAd-GFP than in response to Ad5-GFP. While the need for Dexamethasone treatment could be viewed as a drawback of the HSC *in vivo* transduction approach, it has to be noted that a similar treatment has been employed before to suppress inflammatory responses when systemically administering viral vectors (240).

The hepatotoxicity of an intravenously injected vector in mobilized animals was tested for both Ad5-GFP and HDAd-GFP (**Fig. 23C**). Ad5-based vectors exhibit a strong liver tropism and are able to elicit strong hepatotoxic effects upon systemic administration (211, 241). In contrast, when HDAd-GFP was injected into mobilized animals, only slight elevations in serum levels of ALT and AST could be observed, showing that this vector exhibited reduced potential to damage the liver. This lower hepatotoxic potential is due to both the helper-dependence and the fiber chimerism of the vector. First, helper-dependent adenoviral vectors have been shown to elicit lower levels of ALT and AST in the serum of systemically injected animals compared to corresponding first-generation vectors (242). However, even for HDAd vectors this effect is dose dependent, and higher doses of HDAd vectors will still cause hepatotoxicity (228).

The fiber chimerism of HDAd-GFP is also responsible for the lower potential for liver damage of the vector compared to Ad5-GFP. When an Ad5-based vector is injected intravenously, up to 98 % of the vector is taken up by the liver within 30 minutes after injection. While the majority of vector is taken up by resident macrophages of the liver, also known as Kupffer cells, part of the injected viral particles form complexes with vitamin K-dependent coagulation factors, for example factor X (FX). These complexes are able to interact with cellular heparan sulfate proteoglycans (HSPGs), which mediate the uptake of the virus-FX complexes into hepatocytes and facilitates hepatotoxicity (241). Further, it was shown that fiber-chimeric Ad vectors that were carrying a short fiber shaft showed markedly decreased interaction with blood factors and hence, showed mitigated hepatotoxicity after systemic administration *in vivo* (221). In addition, the same study showed that short-shafted Ad vectors also induced the release of lower levels of inflammatory cytokines compared to their long-shafted counterparts (221). Since the HDAd vectors used in this study both carry the short Ad35 fiber shaft, lower serum levels of ALT and AST were to be expected.

In conclusion, the systemic administration of the integrating two-vector HDAd system in mobilized CD46-tg mice was well tolerated, and it did not cause adverse side effects that would prohibit the application of this system.

To evaluate the safety of transgene integration through the Sleeping Beauty transposase, integration site analysis of CFU progenitor colonies derived from *in vivo* transduced animals

was performed (**Fig. 16**). While a part of the integration events was mapped to the central region of chromosome 13, overall the distribution of integration sites appeared to be close-to-random. Further, the distribution of integration events over intergenic, intronic and exonic regions very closely matched the percentages of the genome that are made up by these regions, again, corroborating a random integration pattern. The random integration pattern of the Sleeping Beauty transposase has been reported before and is one of the major advantages of the system over other integration platforms (175, 237). While gammaretroviral vectors have been shown to preferentially integrate into regulatory sequences (94–97), lentiviral vectors showed tendencies to preferentially integrate into the body of genes (101–103). However, retroviral integration machineries are not the only modes of integration that exhibit integration bias. The two transposases mentioned above, piggyBac and Tol2 also have been shown that they do not integrate completely randomly (237). Therefore, the Sleeping Beauty transposases system is expected to exhibit a relatively low genotoxic potential.

In accordance with these findings, no signs of genotoxic transformation could be found in animals that had been transplanted with bone marrow cells that had been transduced with the Sleeping Beauty vector system. Even though transplanted animals showed increased numbers of myeloid cells in the bone marrow, all other lineages appeared normal when compared to non-transplanted animals. In contrast, the percentages of myeloid cells in the peripheral blood and the spleen were comparable to non-transplanted animals (**Fig. 19A**), arguing against aberrant expansion of the myeloid cells. Further, the blood cell counts for the transplanted animals were within the normal ranges for all parameters except for slightly lowered platelets (**Fig. 21**). This data suggest that gene-modified HSCs gave rise to normal cells. However, to be absolutely sure of this, a clonal tracking approach could be employed in the future to be able to analyze clonal diversity or the emergence of dominant clones (243).

Nevertheless, it was surprising to identify over 150 integration sites in the genomic DNA derived from 20 CFU progenitor colonies. Since each colony is derived from a single progenitor cell, one would expect to find a lower number of integration sites. In the presence of more than one transposon vector together with at least one particle of the Sleeping Beauty vector in the same cell, multiple integration events per cell could be

imagined. However, this process appears to be too unlikely to occur often enough to explain the large number of identified integration events. Additionally, Sleeping Beauty transposase has been shown to be able to remobilize an integrated transposon. According to the data obtained for HDAd-GFP, an episomally retained vector could still be present at the time of cell collection at 8 weeks after injection. Therefore, it cannot be excluded that the transposase was able to remobilize the transposon after the first rounds of cell division during formation of the CFU colony. However, the likelihood of this happening multiple times appears to be very low. Lastly, it is possible that the vector supplying the Sleeping Beauty gene integrated randomly into the genome of a HSC. Although it only occurs at low frequencies, unspecific integration of adenoviral genomes through breakage of the ITRs has been reported (195). If the SB100x were to be integrated and constitutively expressed in a HSC, it could lead to numerous remobilization events in the progeny of that cell. Remobilization events in model systems that constitutively expressed Sleeping Beauty transposase have shown that the reintegration of the transposon tends to appear close, i.e. 5 – 15 Mb, to the original integration site, a process termed local hopping (244, 245). Therefore, this mechanism could explain the high amount of integration events in the central region of chromosome 13. Nevertheless, the probability of this event occurring is assumed to be very low.

In conclusion, the systemic administration of the adenoviral vector system in mobilized mice did cause an inflammatory response. However, this response could be managed through the administration of glucocorticoids leading to acceptable levels of cytokine responses. Further, the gutless vectors did not elicit significant levels of hepatotoxicity due to their capsid design and their lack of viral gene expression. The observed integration pattern was random and did not show bias towards coding or regulatory regions of the genome. In addition, animals that had received gene-modified bone marrow grafts exhibited mostly normal distributions of lineage cells in hematopoietic tissues as well as normal blood cell counts. This suggests that the *in vivo* HSC gene therapy approach presented in this study is safe to use in mice.

4.4 HSC *in vivo* gene therapy is applicable in advanced pre-clinical models

The *in vivo* HSC gene therapy approach was employed in both humanized mice as well as non-human primates in order to evaluate it in models better resembling the situation in humans.

In the humanized mouse model, the *in vivo* transduction approach was shown to allow gene transfer into human bone marrow cells (**Fig. 24**). However, successful genetic long-term modification of human HSCs could not be convincingly shown in this model. Although the reasons for this are not completely understood, the interaction of human HSCs with the murine host could play a role here. It was seen that the mobilization of human bone marrow cells was very inefficient. In the same context, it is not clear if these cells were able to efficiently home back to the marrow once mobilized. Further, the mouse model used has been shown to poorly maintain human HSCs over extended periods of time (225). Therefore, to show efficient HSC *in vivo* transduction in humanized mouse, further optimization of the system is required.

Even the most sophisticated mouse model will not be able to mimic the situation in a human system quite as well as a non-human primate model. Therefore, the HSC *in vivo* transduction approach described in this study was tested in two non-human primates (**Fig. 25**, **Fig. 26**) Mobilization and HSPC transduction with a GFP vector alone was successful and transduction of bone marrow HSPCs could be demonstrated. However, due to the non-integrating nature of the vector, transgene expression was lost over time. A second animal, which instead received the combination of both components of the integrating vector system, mobilized poorly and only marginal HSPC transduction could be shown.

To assess the safety of the HSPC *in vivo* transduction approach, blood clearance of the vector as well as serum levels of different cytokines were monitored. Even though relatively high levels of IL-6 following injection were observed compared to other studies, the serum levels of IL-6 dropped back to normal levels by 24 hours after injection. The decrease in serum IL-6 had been seen in studies in which the injected vector was well tolerated (227, 228). In contrast, extended periods of high IL-6 levels were only observed in studies with fatal outcome (228, 246). Therefore, the intravenous delivery of helper-dependent

adenoviral vectors in mobilized NHPs was safe and well tolerated in the two animals that were treated in the course of this study.

4.5 Concluding remarks and future directions

In this study, it was shown that the *in vivo* HSC transduction approach with integrating adenoviral vectors allows for the stable modification of hematopoietic stem cells. As mentioned above, it is hard to judge the gene transfer efficiency of the presented system based on data generated with GFP, as different efficiencies and expression levels are expected as soon as a different transgene is used. Nevertheless, the system would most likely benefit from increases in efficiency, and different approaches to achieve this could be envisioned.

The most significant impact on efficiency of the system likely consists of the need to superinfect the same target cell with two vectors to achieve stable transgene integration. To circumvent this inherently inefficient approach, a single vector encoding both the transposon and the integration machinery would be favorable. However, in order to be able to produce these vectors, the expression of the integration machinery must be very tightly regulated, as even a single molecule of either Flpe or SB100x would be capable of destroying multiple vector genomes, leading to low yields of vector. To date, no group has achieved the development of a vector that is able to efficiently circumvent this problem.

Alternatively, the HSC *in vivo* transduction system could be employed to deliver an adenoviral vector encoding a designer nuclease against a transgene of interest (see section 1.5.3). Since this approach is based on only a single vector, it would most likely be able to stably modify HSCs at higher rates than the integration-based two vector system.

A second way to ameliorate low efficiency of the gene modification system would be the selection of a disease context that confers a selective advantage to the gene-modified cells or to apply artificial selective pressure. As mentioned above (see section 1.3.2) gene correction in ADA-SCID patients is thought to confer a survival advantage of modified cells, which has lead to sufficient gene correction rates, even when patients did not receive myeloconditioning treatment. Therefore, even a low rate of gene modification following HSC *in vivo* transduction could be sufficient to overcome the disease.

Another method of selecting for gene-modified cells is the transfer of a resistance gene cassette in addition to the therapeutic transgene, which can then be employed as a selectable marker. An example of this is the MGMT *in vivo* selection system. The gene product of the O^6-methylguanine-DNA-methyltransferase (MGMT) is able to repair the toxic chloroethyl adduct that forms on DNA after treatment with 1,3-bis(2-chloroethyl)-1-nitrosourea (BCNU) (247). BCNU alone has been shown to be a stem cell toxin due to the low expression levels of MGMT in HSCs (248). Further, O^6-benzylguanine (O6BG) has been shown to be a potent inhibitor of the native MGMT gene product. To use this system as a selectable marker, the O6BG resistant mutant P140K MGMT (249) is encoded in a gene transfer vector. After gene transfer, HSCs expressing P140K MGMT can then be selected by treatment with O6BG and BCNU (247). The feasibility of this approach has been shown in HSCs after lentiviral gene transfer and transplantation, followed by *in vivo* selection with O6BG and BCNU (250).

Lastly, two additional advantages of the HSC gene therapy approach presented here are related to the costs and logistics of gene therapeutic treatments. Firstly, the production of adenoviral vectors is cost-efficient compared to other vector platforms like lentivirus or AAV that require large scale transfections to produce the amounts of virus required for use in large animal models or humans. As an example, Sheu *et al.* compared production methods for laboratory grade lentivirus preparations and compared their cost (251). Using production in cell factories, they were able to obtain $1.75x10^9$ vector genomes (vg) for a price of $1400. When using an advanced hollow fiber bioreactor, they produced an average of $3.82x10^9$ vg at a price of $6350. The costs in these studies are only based on the price of consumables and reagents. As a comparison, the vectors used for NHP studies in this work were produced at $1x10^{13}$ vg per batch at a price of $2000 per batch, making the price per adenovirus vector genome roughly 4000-fold cheaper than the price of a lentiviral vector genome. This difference could become even greater if production was performed under clinical grade conditions. Furthermore, the adenoviral vector preparations yielded titers of $5 – 8x10^{12}$ vg/mL, while the lentiviral preparations only yielded titers of $2 – 2.5x10^8$ vg/mL. Therefore, adenoviral vector preparations could be readily used for *in vivo* applications, while the lentiviral vectors would need to be further concentrated.

In addition to the lower production cost of the adenoviral vector, the treatment logistics for HSC *in vivo* gene therapy would be much simpler than those involved in *ex vivo* HSC gene therapy. For *ex vivo* transduction, patient HSCs need to be collected, cultured and transduced according to good manufacturing practices and then reinfused into the patient. These processes require highly specialized facilities and are, in addition to the price of the vector, costly. In contrast, for the application of the *in vivo* HSC gene therapy approach described here, patients would only have to undergo a series of intravenous infusions that could be performed in most hospitals. This would likely both decrease the cost of the treatment, and also dramatically increase the access of potential patients to therapeutic treatment.

In conclusion, this work lays the groundwork for a new approach to HSC gene therapy that holds the potential to revolutionize the field in the future.

5 Materials and Methods

5.1 Adenoviral vectors

An overview of the adenoviral vectors used in this study is shown in **Tab. 2**. The first-generation vectors Ad5-GFP (148) and Ad5/35++-GFP (252) had been generated in our laboratory and have been described before. Both vectors are based on Ad serotype 5, are deleted for E1A, and carry a CMV-driven GFP cassette in the E3 region. While Ad5-GFP carries a wild type Ad5 fiber, the fiber of Ad5/35++-GFP is comprised of an Ad5 tail, a short Ad35 shaft, and an affinity enhanced Ad35 knob.

Tab. 2 Adenoviral vectors used in this study. FG – first-generation, HD – helper-dependent, Ad35++ - affinity enhanced serotype 35 knob, IR – Sleeping Beauty repeat.

Name	Type	Transgene casette	Fiber		
			Tail	Shaft	Knob
Ad5-GFP	FG	CMV-GFP	Ad5	Ad5	Ad5
Ad5/35++-GFP	FG	CMV-GFP	Ad5	Ad35	Ad35++
HDAd5/35++-CMV-	HD	CMV-GFP	Ad5	Ad35	Ad35++
HDAd-GFP	HD	FRT-IR-Ef1α-GFP	Ad5	Ad35	Ad35++
HDAd-SB	HD	Ef1α-Flpe, PGK-SB100x	Ad5	Ad35	Ad35++

5.1.1 Production of first-generation adenovirus vectors

For propagation of first-generation adenoviral vectors, virus stocks were used to infect HEK-293 cells at 90-100 % confluency in 15 cm tissue culture dishes. The next day, 5 ml fresh medium were added. When the cells began to show signs of cytopathic effect (CPE, usually 48 h post infection), the cells were harvested and freeze-thawed for four rounds. The lysate was then used to infect 4 to 5 new dishes. This process was repeated until a total of 30 plates could be infected in one step. Thirty-six hours after the final infection step, the cells were collected, pelleted and taken up in 1 ml PBS per dish. The cells were freeze-thawed for 4 rounds, pelleted, and virus particles were isolated from the supernatant through two steps of ultracentrifugation. For the first step, cesium chloride solutions of different densities were layered as follows: 0.5 ml of 1.50 g/cm^3, followed by 3.0 ml of 1.35 g/cm^3, followed by 3.5 ml of 1.25 g/cm^3. The cesium chloride solutions were then overlayed with 5 ml of virus suspension and spun for 1 h at 150000x g and 4 °C. The lowest band containing intact viral particles was collected and combined with virus bands of other

tubes. Four ml of the virus suspension were then mixed with 8 ml 1.35 g/cm^3 CsCl solution and spun overnight at 150000x g at 4 °C. The virus band was collected and dialyzed against 1000 ml of 10 mM Tris pH 7.5, 10 mM $MgCl_2$, 250 mM NaCl and 10 % glycerol overnight at 4 °C in 50 kDa cut-off dialysis tubing. The dialyzed virus was aliquoted and stored at –80 °C. To determine the optical titer of the virus, virus stock was diluted 1:20 in TE buffer (10 mM Tris pH 8.0, 1 mM EDTA pH 8.0) with 0.1 % SDS and thoroughly mixed for 5 min at room temperature. The solution was centrifuged at 16000x g for 5 min and the supernatant was transferred to a fresh tube. The absorption at 260 nm (A_{260}) was measured using a spectrophotometer and the virus titer was calculated as follows, with DF being the dilution factor (253):

$$titer\ [vp/ml] = A_{260} \times DF \times 1.1 \times 10^{12}$$

5.1.2 Production of helper-dependent adenoviral vectors

The molecular cloning of the vector genomes of HDAd-GFP and HDAd-SB was kindly performed by Liu Jing in the group of Anja Ehrhardt (University of Witten/Herdecke, Germany). The transposon vector genome of HDAd-GFP was assembled as follows: In a first cloning step, the elongation factor 1α (Ef1α)-driven GFP expression cassette was introduced into the plasmid pHM5-attB-T_{MCS}-FRT2, which has been described earlier (181), through sticky end ligation after *PacI* digest to generate pHM5-T/EF1α-GFP-FRT2. Of note, pHM5-attB-T_{MCS}-FRT2 contains a multiple cloning site (MCS), flanked by Sleeping Beauty inverted repeats (IR) and FRT sites on both ends. The bacterial artificial chromosome (BAC) containing the helper-dependent Ad5 genome (B-HCA) only contains the viral packaging signal and the inverted terminal repeats (ITRs), the remaining viral genes have been deleted and were replaced with scrambled human X-chromosomal DNA. This construct has been described earlier (254). To introduce a transgene cassette into this BAC, a recombineering approach, described earlier (254), was employed. In short, SW102 bacteria (255) that stably express a heat shock inducible recombination system were transformed with B-HCA. In a first recombination step, a negative selection marker flanked by homology arms was introduced into the Ad genome. Next, pHM5-T/EF1α-GFP-FRT2 was digested with ICeuI and PI-SceI to release the transposon flanked by IRs, FRT sites, and the same homology arms. This fragment was then introduced into the BAC, replacing the negative selection marker and resulting in a new BAC, B-HCA-FRIR-Ef1α -GFP. The sleeping beauty vector HDAd-SB

was generated along the same lines. Through recombineering, an Ef1α-driven FLPe expression cassette and a PGK-driven hyperactive Sleeping Beauty cassette (SB100x) were introduced into B-HCA.

Out of these BACs, helper-dependent Ad5/35++ vectors were generated by the group of Philip Ng (Baylor College of Medicine, Houston, TX, USA). In short, the viral genomes of HDAd-GFP or HDAd-SB were released from the respective BACs through digest with PmeI. The genomes were then transfected into 116 cells, a Cre recombinase expressing, 293-based cell line that can be grown both adherent and in suspension (256). The transfected cells were then infected with the helper virus AdNG163-5/35+. This virus encodes a chimeric fiber gene consisting of the Ad5 fiber tail, the Ad35 fiber shaft and an affinity-enhanced Ad35 fiber knob (Ad35++) (252). Lysates of infected cells were amplified by passaging them on tissue culture dishes and co-infecting the cells with the helper virus. The final production step was performed in 3 l spinner flasks. The helper-dependent viruses were then isolated through CsCl gradients. The virus preparations were tested for helper virus contamination via TaqMan quantitative real-time PCR, and the levels of helper contamination were found to be below 0.5 %. The virus titers were determined spectrophotometrically as described above.

5.2 Tissue culture

Cells were maintained in a water-jacketed incubator at 37 °C, 5 % CO_2 and maximum humidity.

HEK-293 cells (ATCC no. CRL-1573) were maintained in DMEM (Invitrogen) supplemented with 10 % fetal calf serum (FCS, HyClone Laboratories Inc.), 2 mM L-glutamine, 100 U/ml penicillin, and 100 µg/ml streptomycin (all Invitrogen).

M-07e cells (DSMZ no. ACC 104) were maintained in RPMI 1640 (Invitrogen) supplemented with 10 % FCS (HyClone Laboratories Inc.), 2 mM L-glutamine, 100 U/ml penicillin, 100 µg/ml streptomycin (all Invitrogen), and 0.1 ng/ml granulocyte-macrophage colony-stimulating factor (GM-CSF, Peprotech).

Human $CD34^+$-enriched cells from G-CSF mobilized healthy donors were obtained from the Fred Hutchinson Cancer Research Center Cell Processing Core Facility (Seattle, WA, USA).

$CD34^+$ cells were resuscitated from frozen stocks and recovered overnight in Iscove's modified Dulbecco's medium (IMDM, Invitrogen) supplemented with 10 % heat-inactivated FCS, 1 % bovine serum albumin (BSA), 0.1 mM 2-Mercaptoethanol (Sigma-Aldrich), 2 mM L-glutamine, 100 U/ml penicillin, 100 µg/ml streptomycin, 50 ng/ml Flt3 ligand, 20 ng/ml interleukin 3, 10 ng/ml thrombopoietin, and 50 ng/ml stem cell factor (all Peprotech).

For *in vitro* culture of mouse bone marrow, spleen, and peripheral blood mononuclear cells (PBMCs), cells were maintained in RPMI 1640 supplemented with 10 % heat-inactivated FCS, 10 mM HEPES (Invitrogen), 0.1 mM 2-Mercaptoethanol, 2 mM L-glutamine, 100 U/ml penicillin, 100 µg/ml streptomycin, and 0.25 µg/ml Amphotericin B (Invitrogen).

5.3 Mouse studies

All experiments involving animals were conducted in accordance with the institutional guidelines set forth by the University of Washington. Mice were housed in specific-pathogen-free facilities.

C57BL/6 mice were obtained from Charles River Laboratories. Mice transgenic for human CD46 (CD46-tg) were a generous gift from Roberto Cattaneo and have been described before (183, 184). In short, while CD46 in humans is expressed on all cells, in mice it can only be found in the testes. Therefore, a transgenic mouse model containing the whole human CD46 locus was generated, and the animals have been shown to express human CD46 in a similar pattern and at levels comparable to those found in humans. In addition, these mice are knocked out for the interferon receptor.

NOD/SCID-IL2Rγ^{null} (NOG) mice were a generous gift from Thalia Papayannopoulou and have been described before (223). These mice are based on non-obese diabetic, severe combined immunodeficiency (NOD/SCID) background. In addition, they are knocked out for the interleukin 2 receptor gamma, which effectively prevents development of mature B and T cells and allows for better engraftment of human bone marrow transplants.

5.4 HSPC *in vivo* transduction

Animals received subcutaneous (s.c.) injections of 5 µg G-CSF (Neupogen™, Amgen) diluted in 5 % (w/v) Glucose on four consecutive days. The next day, animals received an s.c. injection of AMD3100 (Sigma-Aldrich) diluted in PBS at 5 mg/kg. In addition, animals were injected with Dexamethasone (West-Ward Pharmaceuticals) at 10 mg/kg at 16 and 2 h before virus injection. In the single virus dose injection setting, the virus was injected at $4x10^{10}$ vp/animal 40 min after AMD3100 application. In the double injection setting, animals received two doses of $4x10^{10}$ vp each at 30 and 60 min after AMD3100 injection. In addition, animals received 500 µl PBS s.c. following the first virus injection.

In humanized mice, the same mobilization regimen was employed. On the day of virus injection, animals were pre-dosed with a low dose virus injection of $5x10^{8}$ vp 30 min after AMD3100 injection and two full dose injections of $4x10^{10}$ vp each at 60 and 90 min after AMD3100. Additionally, animals received 500 µl PBS s.c. following the first full dose injection of virus.

5.5 Isolation of cells from mouse tissues

Mice were anesthetized with Tribromoethanol (Sigma-Aldrich). To collect blood, an incision into the hepatic portal vein was made, blood was flushed from the circulation with PBS using the heart as a pump and the blood was transferred into heparinzed tubes. Red blood cells (RBCs) were lysed using Pharm Lyse buffer (BD Biosciences) and washed in FACS buffer (PBS supplemented with 1 % FCS).

To isolate splenocytes, the spleen was resected and ground up between frosted glass slides. The suspension was washed with FACS buffer once and RBC lysis was performed using BD Pharm lyse buffer followed by a wash in FACS buffer. The suspension was then passed through a 70 µm cell strainer.

To isolate cells of the thymus, the same procedure as for the spleen was followed, omitting the RBC lysis step.

For the isolation of cells from mouse lungs, a procedure described by Jungblut *et al.* was followed (257). In short, the lungs were resected and rinsed with PBS in a Petri dish. The

lungs were then transferred to gentleMACS C tubes (Miltenyi Biotec) containing 4.9 ml HEPES buffer (10 mM HEPES, pH 7.4, 150 mM NaCl, 5 mM KCl, 1 mM $MgCl_2$, 1.8 mM $CaCl_2$). Collagenase D (Sigma-Aldrich) and DNase I (Roche Diagnostics) were added to a final concentration of 2 mg/ml and 40 U/ml, respectively, and the lungs were homogenized using a gentleMACS Dissociator (Miltenyi Biotec). The samples were then incubated at 37 °C for 30 min on an orbital shaker. Samples were homogenized one more time and passed through a cell strainer. Finally, the cells were washed once in FACS buffer.

For the isolation of bone marrow cells, tibiae, femora, and ilia were resected. The bone marrow was flushed from the bones using a syringe. A single cell suspension was generated pipetting up and down several times. The suspension was passed through a 70 µm cell strainer and washed in FACS buffer once.

After single cell suspensions had been prepared, the cells were enumerated using a hemocytometer.

5.6 Flow cytometry and fluorescence activated cell sorting (FACS)

Cells were resuspended at $1x10^6$ cells/100 µL in FACS buffer and were incubated with FcR blocking reagent mouse and/or human (Miltenyi Biotech) for ten minutes on ice. Next, the staining antibody solution was added in 100 µL per 10^6 cells and incubated on ice for 30 minutes in the dark. After incubation, cells were washed once in FACS buffer. For secondary stainings, the staining step was repeated with a secondary staining solution. After the wash, cells were resuspended in FACS buffer and analyzed using a LSRII flow cytometer (BD Biosciences). Debris was excluded using a forward scatter-area and sideward scatter-area gate. Single cells were then gated using a forward scatter-height and forward scatter-width gate. If applicable, dead cells were stained with 4',6-Diamidin-2-phenylindol (DAPI). Flow cytometry data was then analyzed using FlowJo (version 10.0.8, FlowJo, LLC).

For fluorescence activated cells sorting (FACS), cells were washed and resuspended in FACS buffer and run on an AriaIII cell sorter (BD Biosciences) using a 70 µm nozzle. Sorted cells were collected into chilled tubes containing culturing medium or into 96-well plates using an automated cell deposition unit.

A list of the antibodies used for flow cytometry and FACS is shown in **Tab. 3**.

Tab. 3 List of antibodies used for flow cytometry. *: contains antibodies against CD5, CD45R, CD11b, Gr-1, 7/4, and Ter-119. B-S-APC: biotin-streptavidin-APC, primary antibodies are conjugated to biotin, streptavidin-APC is used as secondary detection reagent. Div.: contains multiple antibody clones. **: contains antibodies against CD2, CD3, CD14, CD16, CD19, CD56 and CD235a.

Antigen	Reactivity	Label	Clone	Manufacturer	Dilution
lineage cocktail*	mouse	B-S-APC	div.	Miltenyi Biotec	1st 1:50 2nd 1:100
c-kit (CD117)	mouse	PE	2B8	eBioscience	1:100
Sca-1 (Ly-6A/E)	mouse	PE-Cy7	D7	eBioscience	1:100
CD150	mouse	BV421	Q38-480	BD Biosciences	1:100
CD48	mouse	BV510	HM48-1	BD Biosciences	1:100
CD3	mouse	PE	17A2	BD Biosciences	1:200
CD11b	mouse	PE	M1/70	eBioscience	1:200
Gr-1 (Ly-6G)	mouse	PE	RB6-8C5	eBioscience	1:200
CD19	mouse	PE	1D3	BD Biosciences	1:200
lineage cocktail**	human	eFluor 450	div.	eBioscience	1:20
CD3	human	PE-Cy7	SK7	BD Biosciences	1:40
CD33	human	BV421	WM53	BD Biosciences	1:80
CD19	human	PE	HIB19	BD Biosciences	1:40
CD45	human	APC	5B1	Miltenyi Biotec	1:80
CD45	human	PE	HI30	BD Biosciences	1:20
CD34	human	PE	581	BD Biosciences	1:20
CD38	human	FITC	HIT2	BD Biosciences	1:10
c-kit (CD117)	human	PE-Cy7	104D2	eBioscience	1:40
CD46	human	APC	E4.3	BD Biosciences	1:80

5.7 Magnetic cell sorting (MACS)

For the depletion of lineage-committed cells, the mouse lineage cell depletion kit (Miltenyi Biotec) was used to the manufacturer's instructions. In short, cells were resuspended in MACS buffer (PBS supplemented with 0.5 % BSA, 2 mM EDTA, pH 7.2) and incubated with a biotin antibody cocktail directed against mouse lineage markers (CD5, CD45R, CD11b, Gr-1, 7/4, Ter-119), followed by magnetic anti-biotin microbeads.

The cells were washed, and non-labelled, lineage-negative cells were isolated by applying the cell suspension to a LS column mounted on a MidiMACS separator (both Miltenyi Biotec).

For the isolation of human CD45-positive cells from the bone marrow of humanized NOG mice, cells were incubated with MicroBeads directed against human CD45 (Miltenyi Biotec) according to the manufacturer's instructions. In addition, cells were incubated with a fluorescent anti-human CD45 antibody (Miltenyi Biotec). The cells were washed and positive selection in LS columns (Miltenyi Biotec) was performed following the manufacturer's instructions. The purified human cells were then subjected to FACS as described above.

5.8 Cytokine detection in serum samples

For mouse samples, blood was drawn into microcentrifuge tubes and allowed to coagulate at room temperature for 30 minutes. Samples were spun in a microcentrifuge at 2000x g for 5 minutes, and the supernatant was collected. Non-human primate (NHP) samples were drawn into serum separating tubes (SST, BD) and centrifuged at 1000x g for 10 minutes, and the upper serum phase was collected.

Cytokine analysis was performed using the BD cytometric bead array (CBA) mouse inflammation kit and the BD CBA non-human primate Th1/Th2 cytokine kit for mouse and NHP samples, respectively. The samples were processed to the manufacturer's specifications and analyzed on a LSRII flow cytometer (BD Biosciences). The resulting raw data was analyzed using FCAP array software (version 3.0.1, Soft Flow Inc.).

5.9 Quantitative real-time PCR of viral genomes

To determine the virus genome copy numbers in mouse tissues, animals were anesthetized with Tribromoethanol (Sigma-Aldrich), and blood was flushed from the circulation with PBS using the heart as a pump. Organs of interest were resected and genomic DNA (gDNA) was isolated using the DNeasy blood and tissue kit (Qiagen) to the manufacturer's specifications. The concentration of gDNA was determined spectrophotometrically and gDNA samples were subjected to quantitative polymerase chain reaction (qPCR) using 48 ng of gDNA per reaction.

To determine the viral genome copy number in plasma of non-human primates (NHPs), plasma was isolated from blood samples after Ficoll density centrifugation. Plasma samples were diluted 1:1000 in water and subjected to qPCR.

For qPCR analysis, the GFP-specific primer pair GFP_fwd and GFP_rev and the Kapa SYBR Fast qPCR master mix (Kapa Biosystems) were used, and samples were run on a StepOnePlus real time PCR system (Applied Biosystems). The total reaction volume was 10 µl per well of a 96-well plate, using both primers at 2 µM each. The parameters for the amplification consisted of 2 min at 95 °C followed by 40 cycles of 95 °C for 3 s and 60 °C for 30 s with a melting curve analysis after the final cycle. Samples were analyzed in triplicates, and viral genome copy numbers were determined using serial dilutions of purified HDAd-GFP viral DNA as a standard curve. C_T values of samples were determined using StepOne Software (version 2.1, Applied Biosystems). Wells were rejected if either the melting temperature of the amplified product did not match that observed for the standard curve or if the observed C_T value was lower than that of the highest standard curve dilution (10 genome copies per reaction).

5.10 Colony-forming unit assay

For mouse lineage-depleted cells that were infected *in vitro*, 1500 cells were plated in triplicates in ColonyGEL 1202 mouse complete medium (ReachBio) and incubated for 12 days at 37 °C in 5 % CO_2 and maximum humidity. Colonies were enumerated using a Leica MS 5 dissection microscope (Leica Microsystems). For scoring of GFP-positive colonies, an Olympus IMT-2 UV microscope was used with a DFC 300 FX camera (Leica). Images were recorded using the Leica Application Suite (version 4.1, Leica Microsystems)

In vitro infected human $CD34^+$ cells were plated at 1000 cells per dish in triplicates in ColonyGEL 1102 human complete medium (ReachBio) and incubated and scored as described above.

For colony-forming unit (CFU) assays from *in vivo* transduced animals, mouse bone marrow cells were lineage-depleted via MACS (see section 5.7) and sorted for GFP-positive cells via FACS (see section 5.6). Cells were then plated out in ColonyGEL 1202 mouse complete medium supplemented with 100 U/ml penicillin, 100 µg/ml streptomycin and 0.25 µg/ml Amphotericin B and incubated and scored as described above. As a control, bone marrow from untransduced animals was lineage-depleted and sorted for GFP-negative cells to subject them to the same level of mechanical stress.

5.11 Analysis of cryosections

For the analysis of tissue sections, animals were anaesthetized with Tribromoethanol, and blood was flushed from the circulation with PBS using the heart as a pump. Tissues were resected and embedded in cryomolds using Tissue-Tek OCT compound (Sakura Finetek) and frozen at -80 °C. For sectioning, cryomolds were pre-conditioned at -20 °C over night and sectioned at 8 µm thickness with a Leica CM 1850 cryostat (Leica Microsystems). The sections were then fixed in 4 % paraformaldehyde for 15 min at room temperature and were then washed with PBS twice for 5 min per wash. Finally, the sections were air dried and mounted with VECTASHIELD mounting medium with DAPI (Vector Laboratories). Pictures of the sections were taken using a DMLB microscope and a DFC 300 FX camera (both Leica Microsystems).

5.12 Integration analysis in M07-e cells

M07-e cells were infected *in vitro* at a multiplicity of infection (MOI) of 300 vp per virus per cell with either HDAd-GFP alone or both HDAd-GFP and HDAd-SB. The cells were incubated for 48 h and single GFP-positive cells were sorted into 96-well plates via FACS (see section 5.6). Cells were expanded for two weeks, and the number of GFP-positive wells in addition to the rough percentage of GFP-positive cells per well was determined using a UV microscope. Cell clones that showed more than 30 % GFP^+ cells were transferred to larger culture dishes and expanded further. GFP-expressing cells were sorted out via FACS, genomic DNA was isolated using the DNeasy blood and tissue kit (Qiagen), and the genomic DNA concentrations were determined spectrophotometrically.

Per clone, 10 µg of genomic DNA were digested with the restriction endonuclease *SacI* (NEB). The resulting restriction fragments were separated on a 0.7 % agarose gel and the gel was depurinated in 0.2 M HCl for 30 minutes and denatured in 0.4 M NaOH. The DNA was transferred onto a Hybond-N+ nylon membrane (Amersham) in 0.4 M NaOH overnight. The membranes were washed in 2x SSC (saline sodium citrate buffer, Sigma-Aldrich), and the DNA was cross-linked using a UV chamber.

To generate the probe, the plasmid pHM5-T/EF1α-GFP-FRT2, encoding a GFP cassette, was digested with the restriction endonucleases *NotI* and *NcoI*. The restriction fragments were

separated on an agarose gel, and the 720 bp fragment of interest was excised and cleaned up using the QIAquick gel extraction kit (Qiagen). The probe was then labelled with [α-^{32}P]dCTP (PerkinElmer) using the Rediprime II DNA labeling kit (GE Healthcare) to the manufacturer's instructions, and unicorporated radio-labelled nucleotides were removed using illustra MicroSpin G-50 columns (GE Healthcare).

Southern Blot membranes were prehybridized in Rapid-Hyb buffer (GE Healthcare), hybridized with the labelled probe at 2x10^6 cpm/ml, washed according to the manufacturer's specifications, and the membranes were autoradiographed with Biomax XAR film (Carestream Health).

5.13 Integration analysis in progenitor colonies

CFU colonies from bone marrow cells of *in vivo* transduced female CD46-tg animals were grown as described above. A total of twenty GFP-positive colonies were picked and pooled, and the genomic DNA was isolated using DNeasy blood and tissue kit (Qiagen). As a control, colonies from untransduced animals were collected and treated the same way. The integration analysis was performed by Eniko-Eva Nagy and Manvendra Singh in the group of Zsuzsanna Izsvak (Max Delbrück Center for Molecular Medicine, Berlin, Germany). Amplification of SB genomic DNA junctions was performed by linear amplification-mediated PCR as described previously (258) with some modifications. For this, the isolated genomic DNA was digested with *NlaIII* or *MluCI* restriction enzymes and ligated to adaptors having *NlaIII* (NlaIII-linker+, NlaIII-linker-) or *MluCI* (MluCI-linker+, MlucCI-linker-) compatible overhangs. Then, 2x 50 rounds of linear amplification were carried out with a biotinylated left Sleeping Beauty inverted repeat specific primer (LAM SB-50-Bio) to enrich fragments with Sleeping Beauty genomic junctions. The single-stranded biotinylated products were captured on streptavidin-coated magnetic beads using the Dynabeads kilobaseBINDER kit (Invitrogen). After washing the beads with water, the captured products were eluted in water by incubating them at 80 °C for 3 min. The products were then used as templates in a nested PCR. During amplification, barcoded primers specific for the left Sleeping Beauty inverted repeat and adapter specific primers were used, so that different libraries could be pooled in the subsequent steps. For the first PCR, the primers Linker Primer and SB-20-hmr-bio were used. For the second PCR, Nested Primer and either SB_PE_new_bc1, _bc2 or _bc3 were used. Finally, primers corresponding to Illumina

adapter sequences were used (PE_nest_ind1 and Illumina1) to yield a directional library, in which sequences complementary to the Illumina genomic DNA sequence primers were located upstream of the left Sleeping Beauty inverted repeat. The resulting libraries were pooled and sequenced on a single flow cell lane on the HiSeq Genome Analyzer platform (Illumina) with rapid 1X100 bp single end run settings.

For the bioinformatics analysis of the recovered integration sites, sample-specific barcoded sequencing reads were de-multiplexed from the multiplexed flow cell using the CASAVA software (Illumina). The quality of sequencing runs was evaluated using FastQC[1]. Reads that started with the barcode GTATGTAAACTTCCGACTTCAACTG followed by a TA dinucleotide, which is characteristic of Sleeping Beauty-mediated integration, were aligned against the latest version of the mouse reference genome (GRCm38/mm10 (Dec, 2011)), using bowtie (259). For the distribution of integration sites, annotations of untranslated regions (UTRs), exons and coding DNA sequences (CDS) were downloaded from the UCSC genome browser[2], and the percentage of integration sites overlapping with the given genomic coordinates was calculated. For the analysis of integration sites in spatial relation to genes from pathways related to cancer, pathway data from the KEGG pathways in cancer – mouse (205) database were obtained and the distance of integration sites from the closest cancer-related gene was calculated.

5.14 Blood cell counts and liver enzyme detection

Blood cell counts and the levels of the liver enzymes AST and ALT in the blood were determined in the University of Washington Medical Center Clinical Laboratories (Seattle, WA, USA). For blood cell count analysis, blood samples were collected into EDTA-coated tubes, and analysis was performed on a HemaVet 950FS (Drew Scientific). Serum samples were used for analysis of blood chemistry, including the liver enzymes aspartate aminotransferase (AST) and alanine aminotransferase (ALST). Serum was isolated as described above (see section 5.8).

[1] http://www.bioinformatics.babraham.ac.uk/projects/fastqc - last accessed on 1/30/17
[2] https://genome.ucsc.edu/cgi-bin/hgTables - last accessed on 1/30/17

5.15 Non-human primate studies

The non-human primate studies were performed at the Washington National Primate Research Center (Seattle, WA, USA). Blood cell counts and flow cytometric analysis of primate cells were performed in collaboration with Kevin Haworth in the laboratory of Hans-Peter Kiem (Fred Hutchinson Cancer Research Center, Seattle, WA, USA). Two animals (*macaca nemestrina*), Z12406 and Z13058, were used for *in vivo* HSPC transduction studies. Animal Z12406 was mobilized with a combination of G-CSF and SCF, both at 50 mg/kg for 4 consecutive days. On day 5, the animal received an intravenous injection of HDAd-GFP at $2x10^{12}$ vp/kg. The second animal, Z13058 was mobilized with G-CSF (50 mg/kg) for 4 consecutive days and with AMD3100 (4 mg/kg) 3 hours before virus injection. Additionally, both animals received Dexamethasone (0.5 mg/kg) 16 and 2 hours before vector injection. This animal received a mixture of HDAd-GFP and HDAd-SB at $2x10^{12}$ vp/kg per virus through intravenous injection. Blood samples were collected at regular intervals. Bone marrow samples were collected on day 3 and day 7 as well as 10 weeks after virus injection. The expression of GFP was analyzed in $CD34^+$ cells in blood and bone marrow samples collected on the day of virus injection. Further, vector genome copies in plasma samples were determined via qPCR as described above, and cytokine levels in serum were determined via cytometric bead arrays as described above.

5.16 Statistical analyses

All statistical analyses were performed using GraphPad Prism (version 6.00, GraphPad Software). Statistical tests were employed as indicated. To compare the means of two groups, unpaired, two-sided T-tests were employed. If testing for equal variances of the compared groups revealed statistically significant differences in the variances, Welch's correction was used. For the comparison of more than two means, one-way analysis of variance (ANOVA) with Bonferroni post testing for multiple comparisons was used. When the comparison of more than two means was influenced by two independent variables, i.e. when both the administered vector as well as the incubation time periods determined cell transduction frequencies, two-way ANOVA with Bonferroni post testing was employed. Levels of statistical significance were expressed as follows: n.s. not statistically significant, * $p<0.05$, ** $p<0.01$, *** $p<0.001$, **** $p<0.0001$.

5.17 List of oligonucleotides

Name	Sequence (5' to 3')
GFP_fwd	TCGTGACCACCCTGACCTAC
GFP_rev	GGTCTTGTAGTTGCCGTCGT
NlaIII-linker+	GTAATACGACTCACTATAGGGCTCCGCTTAAGGGACGTGACTGGAGTTCAGACT GTGCTCTTCCGATCTCATG
NlaIII-linker-	AGATCGGAAGAGCACACGTCTGAACTCCAGTCAC
MluCI-linker+	GTAATACGACTCACTATAGGGCTCCGCTTAAGGGACGTGACTGGAGTTCAGACG TGTGCTCTTCCGATCT
MluCI-linker-	AATTAGATCGGAAGAGCACACGTCTGAACTCCAGTCAC
LAM SB-50-Bio	Biotin-AGTTTTAATGACTCCAACTTAAGTG
Linker Primer	GTAATACGACTCACTATAGGGC
SB-20hmr-Bio	Biotin-AACTTAAGTGTATGTAAACTTCCGACT
Nested Primer	AGGGCTCCGCTTAAGGGAC
SB_PE_new_bc1	ACACTCTTTCCCTACACGACGCTCTTCCGATCTATCACGGTATGTAAACTTCCGAC TTCAA
SB_PE_new_bc2	ACACTCTTTCCCTACACGACGCTCTTCCGATCTACATCGGTATGTAAACTTCCGAC TTCAA
SB_PE_new_bc3	ACACTCTTTCCCTACACGACGCTCTTCCGATCTGCCTAAGTATGTAAACTTCCGAC TTCAA
PE_nest_ind1	CAAGCAGAAGACGGCATACGAGATCGTGATGTGACTGGAGTTCAGACGTGTGCT CTTCCGATCT
Illumina 1	AATGATACGGCGACCACCGAGATCTACACTCTTTCCCTACACGACGCTCTTCCGAT CT
GFP_fwd	TCGTGACCACCCTGACCTAC

5.18 List of suppliers and manufacturers

Company	Location
Amersham	Little Chalfont, UK
Amgen	Thousand Oaks, CA, USA
Applied	Foster City, CA, USA
BD Biosciences	San Diego, CA, USA
Carestream	Rochester, NY, USA
Charles River	Wilmington, MA, USA
Drew Scientific	Waterbury, CT, USA
FlowJo, LLC	Ashland, OR, USA
GE Healthcare	Little Chalfont, UK
GraphPad	La Jolla, CA, USA
HyClone	Logan, UT, USA
Illumina	San Diego, CA, USA
Invitrogen	Carlsbad, CA, USA
Kapa Biosystems	Boston, MA, USA
Leica	Heerbrugg, Switzerland
Milentyi Biotec	San Diego, CA, USA

NEB (New	Ipswich, MA, USA
Olympus	Center Valley, PA, USA
Peprotech	Rocky Hill, NJ, USA
PerkinElmer	Waltham, MA, USA
Qiagen	Valencia, CA, USA
ReachBio	Seattle, WA, USA
Roche Diagnostics	Indianapolis, IN, USA
Sakura Finetek	Torrance, CA, USA

6 References

1. **Osawa M**, **Hanada K**, **Hamada H**, **Nakauchi H**. 1996. Long-term lymphohematopoietic reconstitution by a single CD34-low/negative hematopoietic stem cell. Science **273**:242–5.

2. **Doulatov S**, **Notta F**, **Laurenti E**, **Dick JE**. 2012. Hematopoiesis: A human perspective. Cell Stem Cell **10**:120–136.

3. **Schofield R**. 1978. The relationship between the spleen colony-forming cell and the haemopoietic stem cell. Blood Cells **4**:7–25.

4. **Xie T**, **Spradling AC**. 1998. Decapentaplegic is essential for the maintenance and division of germline stem cells in the Drosophila ovary. Cell **94**:251–60.

5. **Zhang J**, **Niu C**, **Ye L**, **Huang H**, **He X**, **Tong W-G**, **Ross J**, **Haug J**, **Johnson T**, **Feng JQ**, **Harris S**, **Wiedemann LM**, **Mishina Y**, **Li L**. 2003. Identification of the haematopoietic stem cell niche and control of the niche size. Nature **425**:836–41.

6. **Calvi LM**, **Adams GB**, **Weibrecht KW**, **Weber JM**, **Olson DP**, **Knight MC**, **Martin RP**, **Schipani E**, **Divieti P**, **Bringhurst FR**, **Milner LA**, **Kronenberg HM**, **Scadden DT**. 2003. Osteoblastic cells regulate the haematopoietic stem cell niche. Nature **425**:841–6.

7. **Wilson A**, **Trumpp A**. 2006. Bone-marrow haematopoietic-stem-cell niches. Nat Rev Immunol **6**:93–106.

8. **Bonig H**, **Papayannopoulou T**. 2012. Mobilization of hematopoietic stem/progenitor cells: general principles and molecular mechanisms. Methods Mol Biol **904**:1–14.

9. **Kawabata K**, **Ujikawa M**, **Egawa T**, **Kawamoto H**, **Tachibana K**, **Iizasa H**, **Katsura Y**, **Kishimoto T**, **Nagasawa T**. 1999. A cell-autonomous requirement for CXCR4 in long-term lymphoid and myeloid reconstitution. Proc Natl Acad Sci U S A **96**:5663–7.

10. **Cashman J**, **Clark-Lewis I**, **Eaves A**, **Eaves C**. 2002. Stromal-derived factor 1 inhibits the cycling of very primitive human hematopoietic cells in vitro and in NOD/SCID mice. Blood **99**:792–9.

11. **Papayannopoulou T**, **Craddock C**, **Nakamoto B**, **Priestley G V**, **Wolf NS**. 1995. The VLA4/VCAM-1 adhesion pathway defines contrasting mechanisms of lodgement of transplanted murine hemopoietic progenitors between bone marrow and spleen. Proc Natl Acad Sci U S A **92**:9647–51.

12. **Jacobsen K**, **Kravitz J**, **Kincade PW**, **Osmond DG**. 1996. Adhesion receptors on bone marrow stromal cells: in vivo expression of vascular cell adhesion molecule-1 by reticular cells and sinusoidal endothelium in normal and gamma-irradiated mice. Blood **87**:73–82.

13. **Stier S**, **Ko Y**, **Forkert R**, **Lutz C**, **Neuhaus T**, **Grünewald E**, **Cheng T**, **Dombkowski D**, **Calvi LM**, **Rittling SR**, **Scadden DT**. 2005. Osteopontin is a hematopoietic stem cell niche component that negatively regulates stem cell pool size. J Exp Med **201**:1781–91.

14. **Williams DA**, **Rios M**, **Stephens C**, **Patel VP**. 1991. Fibronectin and VLA-4 in haematopoietic stem cell-microenvironment interactions. Nature **352**:438–41.

15. **Thorén LA**, **Liuba K**, **Bryder D**, **Nygren JM**, **Jensen CT**, **Qian H**, **Antonchuk J**, **Jacobsen S-EW**. 2008. Kit regulates maintenance of quiescent hematopoietic stem cells. J Immunol **180**:2045–53.

16. **Orlic D**, **Fischer R**, **Nishikawa S**, **Nienhuis AW**, **Bodine DM**. 1993. Purification and characterization of heterogeneous pluripotent hematopoietic stem cell populations expressing high levels of c-kit receptor. Blood **82**:762–70.

17. **Driessen RL**, **Johnston HM**, **Nilsson SK**. 2003. Membrane-bound stem cell factor is a key regulator in the initial lodgment of stem cells within the endosteal marrow region. Exp Hematol **31**:1284–91.

18. **Kovach NL**, **Lin N**, **Yednock T**, **Harlan JM**, **Broudy VC**. 1995. Stem cell factor modulates avidity of alpha 4 beta 1 and alpha 5 beta 1 integrins expressed on hematopoietic cell lines. Blood **85**:159–67.

19. **Lorenz E**, **Uphoff D**, **Reid TR**, **Shelton E**. 1951. Modification of irradiation injury in mice and guinea pigs by bone marrow injections. J Natl Cancer Inst **12**:197–201.

20. **Till JE**, **McCulloch EA**. 1961. A direct measurement of the radiation sensitivity of normal mouse bone marrow cells. Radiat Res **14**:213–22.

21. **Becker AJ**, **McCulloch EA**, **Till JE**. 1963. Cytological demonstration of the clonal nature of spleen colonies derived from transplanted mouse marrow cells. Nature **197**:452–4.

22. **Paige CJ**, **Kincade PW**, **Shinefeld LA**, **Sato VL**. 1981. Precursors of murine B lymphocytes. Physical and functional characterization, and distinctions from myeloid stem cells. J Exp Med **153**:154–65.

23. **Paige CJ**, **Kincade PW**, **Moore MA**, **Lee G**. 1979. The fate of fetal and adult B-cell progenitors grafted into immunodeficient CBA/N mice. J Exp Med **150**:548–63.

24. **Hodgson GS**, **Bradley TR**. 1979. Properties of haematopoietic stem cells surviving 5-fluorouracil treatment: evidence for a pre-CFU-S cell? Nature **281**:381–2.

25. **Ploemacher RE**, **Brons RH**. 1989. Separation of CFU-S from primitive cells responsible for reconstitution of the bone marrow hemopoietic stem cell compartment following irradiation: evidence for a pre-CFU-S cell. Exp Hematol **17**:263–6.

26. **Bradley TR**, **Metcalf D**. 1966. The growth of mouse bone marrow cells in vitro. Aust J Exp Biol Med Sci **44**:287–99.

27. **Purton LE**, **Scadden DT**. 2007. Limiting Factors in Murine Hematopoietic Stem Cell Assays. Cell Stem Cell **1**:263–270.

28. **van Os R**, **Kamminga LM**, **de Haan G**. 2004. Stem cell assays: something old, something new, something borrowed. Stem Cells **22**:1181–90.

29. **Coulombel L**. 2004. Identification of hematopoietic stem/progenitor cells: strength and drawbacks of functional assays. Oncogene **23**:7210–7222.

30. **Dick JE**. 2008. Stem cell concepts renew cancer research. Blood **112**:4793–807.

31. **Okada S**, **Nakauchi H**, **Nagayoshi K**, **Nishikawa S**, **Miura Y**, **Suda T**. 1992. In vivo and in vitro stem cell function of c-kit- and Sca-1-positive murine hematopoietic cells. Blood **80**:3044–50.

32. **Kiel MJ**, **Yilmaz OH**, **Iwashita T**, **Yilmaz OH**, **Terhorst C**, **Morrison SJ**. 2005. SLAM family receptors distinguish hematopoietic stem and progenitor cells and reveal endothelial niches for stem cells. Cell **121**:1109–21.

33. **Murray L**, **Chen B**, **Galy A**, **Chen S**, **Tushinski R**, **Uchida N**, **Negrin R**, **Tricot G**, **Jagannath S**, **Vesole D**. 1995. Enrichment of human hematopoietic stem cell activity in the CD34+Thy-1+Lin- subpopulation from mobilized peripheral blood. Blood **85**:368–78.

34. **Bhatia M**, **Wang JC**, **Kapp U**, **Bonnet D**, **Dick JE**. 1997. Purification of primitive human hematopoietic cells capable of repopulating immune-deficient mice. Proc Natl Acad Sci U S A **94**:5320–5.

35. **Conneally E**, **Cashman J**, **Petzer A**, **Eaves C**. 1997. Expansion in vitro of transplantable human cord blood stem cells demonstrated using a quantitative assay of their lympho-myeloid repopulating activity in nonobese diabetic-scid/scid mice. Proc Natl Acad Sci U S A **94**:9836–41.

36. **Lansdorp PM**, **Sutherland HJ**, **Eaves CJ**. 1990. Selective expression of CD45 isoforms on functional subpopulations of CD34+ hemopoietic cells from human bone marrow. J Exp Med **172**:363–6.

37. **Coggle JE**, **Gordon MY**. 1975. Quantitative measurements on the haemopoietic systems of three strains of mice. Exp Hematol **3**:181–6.

38. **Abkowitz JL**, **Catlin SN**, **McCallie MT**, **Guttorp P**. 2002. Evidence that the number of hematopoietic stem cells per animal is conserved in mammals. Blood **100**:2665–7.

39. **Gordon MY**, **Lewis JL**, **Marley SB**. 2002. Of mice and men...and elephants. Blood **100**:4679–80.

40. **Bonig H**, **Papayannopoulou T**. 2013. Hematopoietic stem cell mobilization: updated

conceptual renditions. Leukemia **27**:24–31.

41. **Wright DE**, **Wagers AJ**, **Gulati AP**, **Johnson FL**, **Weissman IL**. 2001. Physiological migration of hematopoietic stem and progenitor cells. Science **294**:1933–6.

42. **Abkowitz JL**, **Robinson AE**, **Kale S**, **Long MW**, **Chen J**. 2003. Mobilization of hematopoietic stem cells during homeostasis and after cytokine exposure. Blood **102**:1249–53.

43. **Kiel MJ**, **Morrison SJ**. 2008. Uncertainty in the niches that maintain haematopoietic stem cells. Nat Rev Immunol **8**:290–301.

44. **Trumpp A**, **Essers M**, **Wilson A**. 2010. Awakening dormant haematopoietic stem cells. Nat Rev Immunol **10**:201–9.

45. **Whetton AD**, **Graham GJ**. 1999. Homing and mobilization in the stem cell niche. Trends Cell Biol **9**:233–8.

46. **Winkler IG**, **Sims NA**, **Pettit AR**, **Barbier V**, **Nowlan B**, **Helwani F**, **Poulton IJ**, **van Rooijen N**, **Alexander KA**, **Raggatt LJ**, **Lévesque J-P**. 2010. Bone marrow macrophages maintain hematopoietic stem cell (HSC) niches and their depletion mobilizes HSCs. Blood **116**:4815–28.

47. **Semerad CL**, **Liu F**, **Gregory AD**, **Stumpf K**, **Link DC**. 2002. G-CSF is an essential regulator of neutrophil trafficking from the bone marrow to the blood. Immunity **17**:413–423.

48. **Christopher MJ**, **Liu F**, **Hilton MJ**, **Long F**, **Link DC**. 2009. Suppression of CXCL12 production by bone marrow osteoblasts is a common and critical pathway for cytokine-induced mobilization. Blood **114**:1331–9.

49. **Christopherson KW**, **Cooper S**, **Hangoc G**, **Broxmeyer HE**. 2003. CD26 is essential for normal G-CSF-induced progenitor cell mobilization as determined by CD26-/- mice. Exp Hematol **31**:1126–34.

50. **Liu F**, **Poursine-Laurent J**, **Link DC**. 1997. The granulocyte colony-stimulating factor receptor is required for the mobilization of murine hematopoietic progenitors into peripheral blood by cyclophosphamide or interleukin-8 but not flt-3 ligand. Blood **90**:2522–8.

51. **Broxmeyer HE**, **Orschell CM**, **Clapp DW**, **Hangoc G**, **Cooper S**, **Plett PA**, **Liles WC**, **Li X**, **Graham-Evans B**, **Campbell TB**, **Calandra G**, **Bridger G**, **Dale DC**, **Srour EF**. 2005. Rapid mobilization of murine and human hematopoietic stem and progenitor cells with AMD3100, a CXCR4 antagonist. J Exp Med **201**:1307–18.

52. **Bonig H**, **Chudziak D**, **Priestley G**, **Papayannopoulou T**. 2009. Insights into the biology of mobilized hematopoietic stem/progenitor cells through innovative treatment schedules of the CXCR4 antagonist AMD3100. Exp Hematol **37**:402–15.e1.

53. **Flomenberg N**, **Devine SM**, **Dipersio JF**, **Liesveld JL**, **McCarty JM**, **Rowley SD**, **Vesole DH**, **Badel K**, **Calandra G**. 2005. The use of AMD3100 plus G-CSF for autologous hematopoietic progenitor cell mobilization is superior to G-CSF alone. Blood **106**:1867–74.

54. **Calandra G**, **McCarty J**, **McGuirk J**, **Tricot G**, **Crocker S-A**, **Badel K**, **Grove B**, **Dye A**, **Bridger G**. 2008. AMD3100 plus G-CSF can successfully mobilize CD34+ cells from non-Hodgkin's lymphoma, Hodgkin's disease and multiple myeloma patients previously failing mobilization with chemotherapy and/or cytokine treatment: compassionate use data. Bone Marrow Transplant **41**:331–8.

55. **Andrews RG**, **Bartelmez SH**, **Knitter GH**, **Myerson D**, **Bernstein ID**, **Appelbaum FR**, **Zsebo KM**. 1992. A c-kit ligand, recombinant human stem cell factor, mediates reversible expansion of multiple CD34+ colony-forming cell types in blood and marrow of baboons. Blood **80**:920–7.

56. **Andrews RG**, **Bensinger WI**, **Knitter GH**, **Bartelmez SH**, **Longin K**, **Bernstein ID**, **Appelbaum FR**, **Zsebo KM**. 1992. The ligand for c-kit, stem cell factor, stimulates the circulation of cells that engraft lethally irradiated baboons. Blood **80**:2715–20.

57. **Craddock CF**, **Nakamoto B**, **Andrews RG**, **Priestley G V**, **Papayannopoulou T**. 1997. Antibodies to VLA4 integrin mobilize long-term repopulating cells and augment cytokine-induced mobilization in primates and mice. Blood **90**:4779–88.

58. **Ramirez P**, **Rettig MP**, **Uy GL**, **Deych E**, **Holt MS**, **Ritchey JK**, **DiPersio JF**. 2009. BIO5192, a small molecule inhibitor of VLA-4, mobilizes hematopoietic stem and progenitor cells. Blood **114**:1340–3.

59. **Bonig H**, **Watts KL**, **Chang K-H**, **Kiem H-P**, **Papayannopoulou T**. 2009. Concurrent blockade of alpha4-integrin and CXCR4 in hematopoietic stem/progenitor cell mobilization. Stem Cells **27**:836–7.

60. **European Medicines Agency**. 2012. Reflection paper on classification of advanced therapy medicinal products (EMA/CAT/600280/2010).

61. **Ginn SL**, **Alexander IE**, **Edelstein ML**, **Abedi MR**, **Wixon J**. 2013. Gene therapy clinical trials worldwide to 2012 - an update. J Gene Med **15**:65–77.

62. **Wilson JM**. 2005. Gendicine: the first commercial gene therapy product. Hum Gene Ther **16**:1014–5.

63. **Peng Z**. 2005. Current status of gendicine in China: recombinant human Ad-p53 agent for treatment of cancers. Hum Gene Ther **16**:1016–27.

64. **Garber K**. 2006. China approves world's first oncolytic virus therapy for cancer treatment. J Natl Cancer Inst **98**:298–300.

65. **Wirth T**, **Parker N**, **Ylä-Herttuala S**. 2013. History of gene therapy. Gene **525**:162–9.

66. **Ylä-Herttuala S**. 2012. Endgame: glybera finally recommended for approval as the first gene therapy drug in the European union. Mol Ther **20**:1831–2.

67. **Wierzbicki AS**, **Viljoen A**. 2013. Alipogene tiparvovec: gene therapy for lipoprotein lipase deficiency. Expert Opin Biol Ther **13**:7–10.

68. **Morrison C**. 2015. $ 1-million price tag set for Glybera gene therapy. Nat Biotechnol **33**:217–218.

69. **Regalado A**. 2016. The World's Most Expensive Medicine Is a Bust. MIT Technol Rev.

70. **Jaski BE**, **Jessup ML**, **Mancini DM**, **Cappola TP**, **Pauly DF**, **Greenberg B**, **Borow K**, **Dittrich H**, **Zsebo KM**, **Hajjar RJ**, **Calcium Up-Regulation by Percutaneous Administration of Gene Therapy In Cardiac Disease (CUPID) Trial Investigators**. 2009. Calcium upregulation by percutaneous administration of gene therapy in cardiac disease (CUPID Trial), a first-in-human phase 1/2 clinical trial. J Card Fail **15**:171–81.

71. **Manno CS**, **Chew AJ**, **Hutchison S**, **Larson PJ**, **Herzog RW**, **Arruda VR**, **Tai SJ**, **Ragni M V**, **Thompson A**, **Ozelo M**, **Couto LB**, **Leonard DGB**, **Johnson FA**, **McClelland A**, **Scallan C**, **Skarsgard E**, **Flake AW**, **Kay MA**, **High KA**, **Glader B**. 2003. AAV-mediated factor IX gene transfer to skeletal muscle in patients with severe hemophilia B. Blood **101**:2963–72.

72. **Carpentier AC**, **Frisch F**, **Labbé SM**, **Gagnon R**, **de Wal J**, **Greentree S**, **Petry H**, **Twisk J**, **Brisson D**, **Gaudet D**. 2012. Effect of alipogene tiparvovec (AAV1-LPL(S447X)) on postprandial chylomicron metabolism in lipoprotein lipase-deficient patients. J Clin Endocrinol Metab **97**:1635–44.

73. **Nathwani AC**, **Tuddenham EGD**, **Rangarajan S**, **Rosales C**, **McIntosh J**, **Linch DC**, **Chowdary P**, **Riddell A**, **Pie AJ**, **Harrington C**, **O'Beirne J**, **Smith K**, **Pasi J**, **Glader B**, **Rustagi P**, **Ng CYC**, **Kay MA**, **Zhou J**, **Spence Y**, **Morton CL**, **Allay J**, **Coleman J**, **Sleep S**, **Cunningham JM**, **Srivastava D**, **Basner-Tschakarjan E**, **Mingozzi F**, **High KA**, **Gray JT**, **Reiss UM**, **Nienhuis AW**, **Davidoff AM**. 2011. Adenovirus-associated virus vector-mediated gene transfer in hemophilia B. N Engl J Med **365**:2357–65.

74. **Manno CS**, **Pierce GF**, **Arruda VR**, **Glader B**, **Ragni M**, **Rasko JJ**, **Rasko J**, **Ozelo MC**, **Hoots K**, **Blatt P**, **Konkle B**, **Dake M**, **Kaye R**, **Razavi M**, **Zajko A**, **Zehnder J**, **Rustagi PK**, **Nakai H**, **Chew A**, **Leonard D**, **Wright JF**, **Lessard RR**, **Sommer JM**, **Tigges M**, **Sabatino D**, **Luk A**, **Jiang H**, **Mingozzi F**, **Couto L**, **Ertl HC**, **High KA**, **Kay MA**. 2006. Successful transduction of liver in hemophilia by AAV-Factor IX and limitations imposed by the host immune response. Nat Med **12**:342–7.

75. **Bainbridge JWB**, **Smith AJ**, **Barker SS**, **Robbie S**, **Henderson R**, **Balaggan K**, **Viswanathan A**, **Holder GE**, **Stockman A**, **Tyler N**, **Petersen-Jones S**, **Bhattacharya SS**, **Thrasher AJ**, **Fitzke FW**, **Carter BJ**, **Rubin GS**, **Moore AT**, **Ali RR**. 2008. Effect of gene therapy on visual function in Leber's congenital amaurosis. N Engl J Med **358**:2231–9.

76. **Maguire AM**, **Simonelli F**, **Pierce EA**, **Pugh EN**, **Mingozzi F**, **Bennicelli J**, **Banfi S**, **Marshall KA**, **Testa F**, **Surace EM**, **Rossi S**, **Lyubarsky A**, **Arruda VR**, **Konkle B**, **Stone E**, **Sun J**, **Jacobs J**, **Dell'Osso L**, **Hertle R**, **Ma J**, **Redmond TM**, **Zhu X**, **Hauck B**, **Zelenaia O**, **Shindler KS**, **Maguire MG**, **Wright JF**, **Volpe NJ**, **McDonnell JW**, **Auricchio A**, **High KA**, **Bennett J**. 2008. Safety and efficacy of gene transfer for Leber's congenital amaurosis. N Engl J Med **358**:2240–8.

77. **Jacobson SG**, **Cideciyan A V**, **Ratnakaram R**, **Heon E**, **Schwartz SB**, **Roman AJ**, **Peden MC**, **Aleman TS**, **Boye SL**, **Sumaroka A**, **Conlon TJ**, **Calcedo R**, **Pang J-J**, **Erger KE**, **Olivares MB**, **Mullins CL**, **Swider M**, **Kaushal S**, **Feuer WJ**, **Iannaccone A**, **Fishman GA**, **Stone EM**, **Byrne BJ**, **Hauswirth WW**. 2012. Gene therapy for leber congenital amaurosis caused by RPE65 mutations: safety and efficacy in 15 children and adults followed up to 3 years. Arch Ophthalmol (Chicago, Ill 1960) **130**:9–24.

78. **Kaplitt MG**, **Feigin A**, **Tang C**, **Fitzsimons HL**, **Mattis P**, **Lawlor PA**, **Bland RJ**, **Young D**, **Strybing K**, **Eidelberg D**, **During MJ**. 2007. Safety and tolerability of gene therapy with an adeno-associated virus (AAV) borne GAD gene for Parkinson's disease: an open label, phase I trial. Lancet (London, England) **369**:2097–105.

79. **Leone P**, **Shera D**, **McPhee SWJ**, **Francis JS**, **Kolodny EH**, **Bilaniuk LT**, **Wang D-J**, **Assadi M**, **Goldfarb O**, **Goldman HW**, **Freese A**, **Young D**, **During MJ**, **Samulski RJ**, **Janson CG**. 2012. Long-term follow-up after gene therapy for canavan disease. Sci Transl Med **4**:165ra163.

80. **Aiuti A**, **Slavin S**, **Aker M**, **Ficara F**, **Deola S**, **Mortellaro A**, **Morecki S**, **Andolfi G**, **Tabucchi A**, **Carlucci F**, **Marinello E**, **Cattaneo F**, **Vai S**, **Servida P**, **Miniero R**, **Roncarolo MG**, **Bordignon C**. 2002. Correction of ADA-SCID by stem cell gene therapy combined with nonmyeloablative conditioning. Science **296**:2410–3.

81. **Cavazzana-Calvo M**, **Hacein-Bey S**, **de Saint Basile G**, **Gross F**, **Yvon E**, **Nusbaum P**, **Selz F**, **Hue C**, **Certain S**, **Casanova JL**, **Bousso P**, **Deist FL**, **Fischer A**. 2000. Gene therapy of human severe combined immunodeficiency (SCID)-X1 disease. Science **288**:669–72.

82. **Cavazzana-Calvo M**, **Payen E**, **Negre O**, **Wang G**, **Hehir K**, **Fusil F**, **Down J**, **Denaro M**, **Brady T**, **Westerman K**, **Cavallesco R**, **Gillet-Legrand B**, **Caccavelli L**, **Sgarra R**, **Maouche-Chrétien L**, **Bernaudin F**, **Girot R**, **Dorazio R**, **Mulder G-J**, **Polack A**, **Bank A**, **Soulier J**, **Larghero J**, **Kabbara N**, **Dalle B**, **Gourmel B**, **Socie G**, **Chrétien S**, **Cartier N**, **Aubourg P**, **Fischer A**, **Cornetta K**, **Galacteros F**, **Beuzard Y**, **Gluckman E**, **Bushman F**, **Hacein-Bey-Abina S**, **Leboulch P**. 2010. Transfusion independence and HMGA2 activation after gene therapy of human β-thalassaemia. Nature **467**:318–322.

83. **Blaese RM**, **Culver KW**, **Miller AD**, **Carter CS**, **Fleisher T**, **Clerici M**, **Shearer G**, **Chang L**, **Chiang Y**, **Tolstoshev P**, **Greenblatt JJ**, **Rosenberg SA**, **Klein H**, **Berger M**, **Mullen CA**, **Ramsey WJ**, **Muul L**, **Morgan RA**, **Anderson WF**. 1995. T lymphocyte-directed gene therapy for ADA- SCID: initial trial results after 4 years. Science **270**:475–80.

84. **Aiuti A**, **Cattaneo F**, **Galimberti S**, **Benninghoff U**, **Cassani B**, **Callegaro L**, **Scaramuzza S**, **Andolfi G**, **Mirolo M**, **Brigida I**, **Tabucchi A**, **Carlucci F**, **Eibl M**, **Aker M**, **Slavin S**, **Al-Mousa H**, **Al Ghonaium A**, **Ferster A**, **Duppenthaler A**, **Notarangelo L**, **Wintergerst U**, **Buckley RH**, **Bregni M**, **Marktel S**, **Valsecchi MG**, **Rossi P**, **Ciceri F**, **Miniero R**, **Bordignon C**, **Roncarolo M-G**. 2009. Gene therapy for immunodeficiency due to adenosine deaminase deficiency. N Engl J Med **360**:447–58.

85. **Candotti F**, **Shaw KL**, **Muul L**, **Carbonaro D**, **Sokolic R**, **Choi C**, **Schurman SH**, **Garabedian E**, **Kesserwan C**, **Jagadeesh GJ**, **Fu P-Y**, **Gschweng E**, **Cooper A**, **Tisdale JF**, **Weinberg KI**, **Crooks GM**, **Kapoor N**, **Shah A**, **Abdel-Azim H**, **Yu X-J**, **Smogorzewska M**, **Wayne AS**, **Rosenblatt HM**, **Davis CM**, **Hanson C**, **Rishi RG**, **Wang X**, **Gjertson D**, **Yang OO**, **Balamurugan A**, **Bauer G**, **Ireland JA**, **Engel BC**, **Podsakoff GM**, **Hershfield MS**, **Blaese RM**, **Parkman R**, **Kohn DB**. 2012. Gene therapy for adenosine deaminase-deficient severe combined immune deficiency: clinical comparison of retroviral vectors and treatment plans. Blood **120**:3635–46.

86. **Hacein-Bey-Abina S**, **Le Deist F**, **Carlier F**, **Bouneaud C**, **Hue C**, **De Villartay J-P**, **Thrasher AJ**, **Wulffraat N**, **Sorensen R**, **Dupuis-Girod S**, **Fischer A**, **Davies EG**, **Kuis W**, **Leiva L**, **Cavazzana-Calvo M**. 2002. Sustained correction of X-linked severe combined immunodeficiency by ex vivo gene therapy. N Engl J Med **346**:1185–93.

87. **Cartier N**, **Hacein-Bey-Abina S**, **Bartholomae CC**, **Veres G**, **Schmidt M**, **Kutschera I**, **Vidaud M**, **Abel U**, **Dal-Cortivo L**, **Caccavelli L**, **Mahlaoui N**, **Kiermer V**, **Mittelstaedt D**, **Bellesme C**, **Lahlou N**, **Lefrère F**, **Blanche S**, **Audit M**, **Payen E**, **Leboulch P**, **L'Homme B**, **Bougnères P**, **Von Kalle C**, **Fischer A**, **Cavazzana-Calvo M**, **Aubourg P**. 2009. Hematopoietic stem cell gene therapy with a lentiviral vector in X-linked adrenoleukodystrophy. Science **326**:818–23.

88. **Biffi A**, **Montini E**, **Lorioli L**, **Cesani M**, **Fumagalli F**, **Plati T**, **Baldoli C**, **Martino S**, **Calabria A**, **Canale S**, **Benedicenti F**, **Vallanti G**, **Biasco L**, **Leo S**, **Kabbara N**, **Zanetti G**, **Rizzo WB**, **Mehta NAL**, **Cicalese MP**, **Casiraghi M**, **Boelens JJ**, **Del Carro U**, **Dow DJ**, **Schmidt M**, **Assanelli A**, **Neduva V**, **Di Serio C**, **Stupka E**, **Gardner J**, **von Kalle C**, **Bordignon C**, **Ciceri F**, **Rovelli A**, **Roncarolo MG**, **Aiuti A**, **Sessa M**, **Naldini L**. 2013. Lentiviral hematopoietic stem cell gene therapy benefits metachromatic leukodystrophy. Science **341**:1233158.

89. **Hacein-Bey-Abina S**, **Garrigue A**, **Wang GP**, **Soulier J**, **Lim A**, **Morillon E**, **Clappier E**, **Caccavelli L**, **Delabesse E**, **Beldjord K**, **Asnafi V**, **MacIntyre E**, **Dal Cortivo L**, **Radford I**, **Brousse N**, **Sigaux F**, **Moshous D**, **Hauer J**, **Borkhardt A**, **Belohradsky BH**, **Wintergerst U**, **Velez MC**, **Leiva L**, **Sorensen R**, **Wulffraat N**, **Blanche S**, **Bushman FD**, **Fischer A**, **Cavazzana-Calvo M**. 2008. Insertional oncogenesis in 4 patients after retrovirus-mediated gene therapy of SCID-X1. J Clin Invest **118**:3132–3142.

90. **Howe SJ**, **Mansour MR**, **Schwarzwaelder K**, **Bartholomae C**, **Hubank M**, **Kempski H**, **Brugman MH**, **Pike-Overzet K**, **Chatters SJ**, **de Ridder D**, **Gilmour KC**, **Adams S**, **Thornhill SI**, **Parsley KL**, **Staal FJT**, **Gale RE**, **Linch DC**, **Bayford J**, **Brown L**, **Quaye M**, **Kinnon C**, **Ancliff P**, **Webb DK**, **Schmidt M**, **von Kalle C**, **Gaspar HB**, **Thrasher AJ**. 2008. Insertional mutagenesis combined with acquired somatic mutations causes leukemogenesis following gene therapy of SCID-X1 patients. J Clin Invest **118**:3143–50.

91. **Wang GP**, **Berry CC**, **Malani N**, **Leboulch P**, **Fischer A**, **Hacein-Bey-Abina S**, **Cavazzana-Calvo M**, **Bushman FD**. 2010. Dynamics of gene-modified progenitor cells analyzed by tracking retroviral integration sites in a human SCID-X1 gene therapy trial. Blood **115**:4356–4366.

92. **Ott MG**, **Schmidt M**, **Schwarzwaelder K**, **Stein S**, **Siler U**, **Koehl U**, **Glimm H**, **Kühlcke K**, **Schilz A**, **Kunkel H**, **Naundorf S**, **Brinkmann A**, **Deichmann A**, **Fischer M**, **Ball C**, **Pilz I**, **Dunbar C**, **Du Y**, **Jenkins NA**, **Copeland NG**, **Lüthi U**, **Hassan M**, **Thrasher AJ**, **Hoelzer D**, **von Kalle C**, **Seger R**, **Grez M**. 2006. Correction of X-linked chronic granulomatous disease by gene therapy, augmented by insertional activation of MDS1-EVI1, PRDM16 or SETBP1. Nat Med **12**:401–9.

93. **Stein S**, **Ott MG**, **Schultze-Strasser S**, **Jauch A**, **Burwinkel B**, **Kinner A**, **Schmidt M**, **Krämer A**, **Schwäble J**, **Glimm H**, **Koehl U**, **Preiss C**, **Ball C**, **Martin H**, **Göhring G**, **Schwarzwaelder K**, **Hofmann W-K**, **Karakaya K**, **Tchatchou S**, **Yang R**, **Reinecke P**, **Kühlcke K**, **Schlegelberger B**, **Thrasher AJ**, **Hoelzer D**, **Seger R**, **von Kalle C**, **Grez M**. 2010. Genomic instability and myelodysplasia with monosomy 7 consequent to EVI1 activation after gene therapy for chronic granulomatous disease. Nat Med **16**:198–204.

94. **Derse D**, **Crise B**, **Li Y**, **Princler G**, **Lum N**, **Stewart C**, **McGrath CF**, **Hughes SH**, **Munroe DJ**, **Wu X**. 2007. Human T-cell leukemia virus type 1 integration target sites in the human genome: comparison with those of other retroviruses. J Virol **81**:6731–41.

95. **Deichmann A**, **Hacein-Bey-Abina S**, **Schmidt M**, **Garrigue A**, **Brugman MH**, **Hu J**, **Glimm H**, **Gyapay G**, **Prum B**, **Fraser CC**, **Fischer N**, **Schwarzwaelder K**, **Siegler M**, **de Ridder D**, **Pike-Overzet K**, **Howe SJ**, **Thrasher AJ**, **Wagemaker G**, **Abel U**, **Staal FJT**, **Delabesse E**, **Villeval J**, **Aronow B**, **Hue C**, **Prinz C**, **Wissler M**, **Klanke C**, **Weissenbach J**, **Alexander I**, **Fischer A**, **von Kalle C**, **Cavazzana-Calvo M**. 2007. Vector integration is nonrandom and clustered and influences the fate of lymphopoiesis in SCID-X1 gene therapy. J Clin Invest **117**:2225–32.

96. **Mitchell RS**, **Beitzel BF**, **Schroder ARW**, **Shinn P**, **Chen H**, **Berry CC**, **Ecker JR**, **Bushman FD**. 2004. Retroviral DNA integration: ASLV, HIV, and MLV show distinct target site preferences. PLoS Biol **2**:E234.

97. **Cattoglio C**, **Facchini G**, **Sartori D**, **Antonelli A**, **Miccio A**, **Cassani B**, **Schmidt M**, **von Kalle C**, **Howe S**, **Thrasher AJ**, **Aiuti A**, **Ferrari G**, **Recchia A**, **Mavilio F**. 2007. Hot spots of retroviral integration in human CD34+ hematopoietic cells. Blood **110**:1770–8.

98. **Yu SF**, **von Rüden T**, **Kantoff PW**, **Garber C**, **Seiberg M**, **Rüther U**, **Anderson WF**, **Wagner EF**, **Gilboa E**. 1986. Self-inactivating retroviral vectors designed for transfer of whole genes into mammalian cells. Proc Natl Acad Sci U S A **83**:3194–8.

99. **Miyoshi H**, **Blömer U**, **Takahashi M**, **Gage FH**, **Verma IM**. 1998. Development of a self-inactivating lentivirus vector. J Virol **72**:8150–8157.

100. **Zufferey R**, **Dull T**, **Mandel RJ**, **Bukovsky A**, **Quiroz D**, **Naldini L**, **Trono D**. 1998. Self-inactivating lentivirus vector for safe and efficient in vivo gene delivery. J Virol **72**:9873–80.

101. **Modlich U**, **Navarro S**, **Zychlinski D**, **Maetzig T**, **Knoess S**, **Brugman MH**, **Schambach A**, **Charrier S**, **Galy A**, **Thrasher AJ**, **Bueren J**, **Baum C**. 2009. Insertional transformation of hematopoietic cells by self-inactivating lentiviral and gammaretroviral vectors. Mol Ther **17**:1919–28.

102. **Montini E**, **Cesana D**, **Schmidt M**, **Sanvito F**, **Ponzoni M**, **Bartholomae C**, **Sergi Sergi L**, **Benedicenti F**, **Ambrosi A**, **Di Serio C**, **Doglioni C**, **von Kalle C**, **Naldini L**. 2006. Hematopoietic stem cell gene transfer in a tumor-prone mouse model uncovers low genotoxicity of lentiviral vector integration. Nat Biotechnol **24**:687–696.

103. **Montini E**, **Cesana D**, **Schmidt M**, **Sanvito F**, **Bartholomae CC**, **Ranzani M**, **Benedicenti F**, **Sergi LS**, **Ambrosi A**, **Ponzoni M**, **Doglioni C**, **Di Serio C**, **von Kalle C**, **Naldini L**. 2009. The genotoxic potential of retroviral vectors is strongly modulated by vector design and integration site selection in a mouse model of HSC gene therapy. J Clin Invest **119**:964–75.

104. **Miller DG**, **Adam MA**, **Miller AD**. 1990. Gene transfer by retrovirus vectors occurs only in cells that are actively replicating at the time of infection. Mol Cell Biol **10**:4239–42.

105. **Roe T**, **Reynolds TC**, **Yu G**, **Brown PO**. 1993. Integration of murine leukemia virus DNA depends on mitosis. EMBO J **12**:2099–108.

106. **Lewis PF**, **Emerman M**. 1994. Passage through mitosis is required for oncoretroviruses but not for the human immunodeficiency virus. J Virol **68**:510–6.

107. **Naldini L**, **Blömer U**, **Gallay P**, **Ory D**, **Mulligan R**, **Gage FH**, **Verma IM**, **Trono D**. 1996. In vivo gene delivery and stable transduction of nondividing cells by a lentiviral vector. Science **272**:263–7.

108. **Naldini L**, **Blömer U**, **Gage FH**, **Trono D**, **Verma IM**. 1996. Efficient transfer, integration, and sustained long-term expression of the transgene in adult rat brains injected with a lentiviral vector. Proc Natl Acad Sci U S A **93**:11382–8.

109. **Lewis P**, **Hensel M**, **Emerman M**. 1992. Human immunodeficiency virus infection of cells arrested in the cell cycle. EMBO J **11**:3053–8.

110. **Watts KL**, **Adair J**, **Kiem H-P**. 2011. Hematopoietic stem cell expansion and gene therapy. Cytotherapy **13**:1164–71.

111. **Modrow S**, **Falke D**, **Truyen U**, **Schätzl H**. 2010. Molekulare Virologie, 3rd edition. Spektrum Akademischer Verlag, Heidelberg.

112. **Jones MS**, **Harrach B**, **Ganac RD**, **Gozum MM a**, **Dela Cruz WP**, **Riedel B**, **Pan C**, **Delwart EL**, **Schnurr DP**. 2007. New adenovirus species found in a patient presenting with gastroenteritis. J Virol **81**:5978–84.

113. **Al Qurashi YMA**, **Alkhalaf MA**, **Lim L**, **Guiver M**, **Cooper RJ**. 2012. Sequencing and phylogenetic analysis of the hexon, fiber, and penton regions of adenoviruses isolated from AIDS patients. J Med Virol **84**:1157–65.

114. **Wang H**, **Li Z-Y**, **Liu Y**, **Persson J**, **Beyer I**, **Möller T**, **Koyuncu D**, **Drescher MR**, **Strauss R**, **Zhang X-B**, **Wahl JK**, **Urban N**, **Drescher C**, **Hemminki A**, **Fender P**, **Lieber A**. 2011. Desmoglein 2 is a receptor for adenovirus serotypes 3, 7, 11 and 14. Nat Med **17**:96–104.

115. **Gaggar A**, **Shayakhmetov DM**, **Lieber A**. 2003. CD46 is a cellular receptor for group B adenoviruses. Nat Med **9**:1408–1412.

116. **Nilsson EC**, **Storm RJ**, **Bauer J**, **Johansson SMC**, **Lookene A**, **Ångström J**, **Hedenström M**, **Eriksson TL**, **Frängsmyr L**, **Rinaldi S**, **Willison HJ**, **Pedrosa Domellöf F**, **Stehle T**, **Arnberg N**. 2011. The GD1a glycan is a cellular receptor for adenoviruses causing epidemic keratoconjunctivitis. Nat Med **17**:105–109.

117. **Roelvink PW**, **Lizonova A**, **Lee JG**, **Li Y**, **Bergelson JM**, **Finberg RW**, **Brough DE**, **Kovesdi I**, **Wickham TJ**. 1998. The coxsackievirus-adenovirus receptor protein can function as a cellular attachment protein for adenovirus serotypes from subgroups A, C, D, E, and F. J Virol **72**:7909–15.

118. **Knipe DM**, **Howley PM**. 2013. Fields Virology, 6th edition, 6thed. Wolters Kluwer Health/Lippincott Williams & Wilkins, Philadelphia.

119. **Matsushima Y**, **Shimizu H**, **Phan TG**, **Ushijima H**. 2011. Genomic characterization of a novel human adenovirus type 31 recombinant in the hexon gene. J Gen Virol **92**:2770–5.

120. **Dehghan S**, **Liu EB**, **Seto J**, **Torres SF**, **Hudson NR**, **Kajon AE**, **Metzgar D**, **Dyer DW**, **Chodosh J**, **Jones MS**, **Seto D**. 2012. Five genome sequences of subspecies B1 human adenoviruses associated with acute respiratory disease. J Virol **86**:635–6.

121. HAdV Working Group. http://hadvwg.gmu.edu/ accessed on 5/9/16.

122. **Walsh MP**, **Seto J**, **Jones MS**, **Chodosh J**, **Xu W**, **Seto D**. 2010. Computational analysis identifies human adenovirus type 55 as a re-emergent acute respiratory disease pathogen. J Clin Microbiol **48**:991–3.

123. **Walsh MP**, **Seto J**, **Liu EB**, **Dehghan S**, **Hudson NR**, **Lukashev AN**, **Ivanova O**, **Chodosh J**, **Dyer DW**, **Jones MS**, **Seto D**. 2011. Computational analysis of two species C human adenoviruses provides evidence of a novel virus. J Clin Microbiol **49**:3482–90.

124. **Robinson CM**, **Singh G**, **Henquell C**, **Walsh MP**, **Peigue-Lafeuille H**, **Seto D**, **Jones MS**, **Dyer DW**, **Chodosh J**. 2011. Computational analysis and identification of an emergent human adenovirus pathogen implicated in a respiratory fatality. Virology **409**:141–7.

125. **Liu EB**, **Ferreyra L**, **Fischer SL**, **Pavan J V**, **Nates S V**, **Hudson NR**, **Tirado D**, **Dyer DW**, **Chodosh J**, **Seto D**, **Jones MS**. 2011. Genetic analysis of a novel human adenovirus with a serologically unique hexon and a recombinant fiber gene. PLoS One **6**:e24491.

126. **Liu EB**, **Wadford DA**, **Seto J**, **Vu M**, **Hudson NR**, **Thrasher L**, **Torres S**, **Dyer DW**, **Chodosh J**, **Seto D**, **Jones MS**. 2012. Computational and serologic analysis of novel and known viruses in species human adenovirus D in which serology and genomics do not correlate. PLoS One **7**:e33212.

127. **Robinson CM**, **Zhou X**, **Rajaiya J**, **Yousuf MA**, **Singh G**, **DeSerres JJ**, **Walsh MP**, **Wong S**, **Seto D**, **Dyer DW**, **Chodosh J**, **Jones MS**. 2013. Predicting the next eye pathogen: analysis of a novel adenovirus. MBio **4**:e00595-12.

128. **Matsushima Y**, **Shimizu H**, **Kano A**, **Nakajima E**, **Ishimaru Y**, **Dey SK**, **Watanabe Y**, **Adachi F**, **Suzuki K**, **Mitani K**, **Fujimoto T**, **Phan TG**, **Ushijima H**. 2012. Novel human adenovirus strain, Bangladesh. Emerg Infect Dis **18**:846–8.

129. **Alissa Alkhalaf M**, **Al Qurashi YMA**, **Guiver M**, **Cooper RJ**. 2014. Genome sequences of three species d adenoviruses isolated from AIDS patients. Genome Announc **2**.

130. **Singh G**, **Robinson CM**, **Dehghan S**, **Schmidt T**, **Seto D**, **Jones MS**, **Dyer DW**, **Chodosh J**. 2012. Overreliance on the hexon gene, leading to misclassification of human adenoviruses. J Virol **86**:4693–5.

131. **Zhou X**, **Robinson CM**, **Rajaiya J**, **Dehghan S**, **Seto D**, **Jones MS**, **Dyer DW**, **Chodosh J**. 2012. Analysis of human adenovirus type 19 associated with epidemic keratoconjunctivitis and its reclassification as adenovirus type 64. Invest Ophthalmol Vis Sci **53**:2804–11.

132. **Matsushima Y**, **Shimizu H**, **Kano A**, **Nakajima E**, **Ishimaru Y**, **Dey SK**, **Watanabe Y**, **Adachi F**, **Mitani K**, **Fujimoto T**, **Phan TG**, **Ushijima H**. 2013. Genome sequence of a novel virus of the species human adenovirus d associated with acute gastroenteritis. Genome Announc **1**.

133. **Singh G**, **Zhou X**, **Lee JY**, **Yousuf MA**, **Ramke M**, **Ismail AM**, **Lee JS**, **Robinson CM**, **Seto D**, **Dyer DW**, **Jones MS**, **Rajaiya J**, **Chodosh J**. 2015. Recombination of the epsilon determinant and corneal tropism: Human adenovirus species D types 15, 29, 56, and 69. Virology **485**:452–9.

134. **Hage E**, **Gerd Liebert U**, **Bergs S**, **Ganzenmueller T**, **Heim A**. 2015. Human mastadenovirus type 70: a novel, multiple recombinant species D mastadenovirus isolated from diarrhoeal faeces of a haematopoietic stem cell transplantation recipient. J Gen Virol **96**:2734–42.

135. **Greber UF**, **Willetts M**, **Webster P**, **Helenius A**. 1993. Stepwise dismantling of adenovirus 2 during entry into cells. Cell **75**:477–86.

136. **Clarke MF**, **Apel IJ**, **Benedict MA**, **Eipers PG**, **Sumantran V**, **González-García M**, **Doedens M**, **Fukunaga N**, **Davidson B**, **Dick JE**, **Minn AJ**, **Boise LH**, **Thompson CB**, **Wicha M**, **Núñez G**. 1995. A recombinant bcl-x s adenovirus selectively induces apoptosis in cancer cells but not in normal bone marrow cells. Proc Natl Acad Sci U S A **92**:11024–8.

137. **Seth P**, **Brinkmann U**, **Schwartz GN**, **Katayose D**, **Gress R**, **Pastan Ira**, **Cowan K**. 1996. Adenovirus-mediated gene transfer to human breast tumor cells: an approach for cancer gene therapy and bone marrow purging. Cancer Res **56**:1346–51.

138. **Frey BM**, **Hackett NR**, **Bergelson JM**, **Finberg R**, **Crystal RG**, **Moore MA**, **Rafii S**. 1998. High-efficiency gene transfer into ex vivo expanded human hematopoietic progenitors and precursor cells by adenovirus vectors. Blood **91**:2781–92.

139. **Ahmed T**, **Lutton JD**, **Feldman E**, **Tani K**, **Asano S**, **Abraham NG**. 1998. Gene transfer of alpha interferon into hematopoietic stem cells. Leuk Res **22**:119–24.

140. **Watanabe T**, **Kelsey L**, **Ageitos A**, **Kuszynski C**, **Ino K**, **Heimann DG**, **Varney MT**, **Shepard HM**, **Vaillancourt MT**, **Maneval DC**, **Talmadge JE**. 1998. Enhancement of adenovirus-mediated gene transfer to human bone marrow cells. Leuk Lymphoma **29**:439–51.

141. **Watanabe T**, **Kuszynski C**, **Ino K**, **Heimann DG**, **Shepard HM**, **Yasui Y**, **Maneval DC**, **Talmadge JE**. 1996. Gene transfer into human bone marrow hematopoietic cells mediated by adenovirus vectors. Blood **87**:5032–9.

142. **Neering SJ**, **Hardy SF**, **Minamoto D**, **Spratt SK**, **Jordan CT**. 1996. Transduction of primitive human hematopoietic cells with recombinant adenovirus vectors. Blood **88**:1147–55.

143. **Chen L**, **Pulsipher M**, **Chen D**, **Sieff C**, **Elias A**, **Fine HA**, **Kufe DW**. 1996. Selective transgene expression for detection and elimination of contaminating carcinoma cells in hematopoietic stem cell sources. J Clin Invest **98**:2539–48.

144. **MacKenzie KL**, **Hackett NR**, **Crystal RG**, **Moore MA**. 2000. Adenoviral vector-mediated gene transfer to primitive human hematopoietic progenitor cells: assessment of transduction and toxicity in long-term culture. Blood **96**:100–8.

145. **Fan X**, **Brun A**, **Segren S**, **Jacobsen SE**, **Karlsson S**. 2000. Efficient adenoviral vector transduction of human hematopoietic SCID-repopulating and long-term culture-initiating cells. Hum Gene Ther **11**:1313–1327.

146. **Knaän-Shanzer S**, **Van Der Velde I**, **Havenga MJ**, **Lemckert AA**, **De Vries AA**, **Valerio D**. 2001. Highly efficient targeted transduction of undifferentiated human hematopoietic cells by adenoviral vectors displaying fiber knobs of subgroup B. Hum Gene Ther **12**:1989–2005.

147. **Nathwani AC**, **Persons DA**, **Stevenson SC**, **Frare P**, **McClelland A**, **Nienhuis AW**, **Vanin EF**. 1999. Adenovirus-mediated expresssion of the murine ecotropic receptor facilitates transduction of human hematopoietic cells with an ecotropic retroviral vector. Gene Ther **6**:1456–68.

148. **Shayakhmetov DM**, **Papayannopoulou T**, **Stamatoyannopoulos G**, **Lieber A**. 2000. Efficient gene transfer into human CD34(+) cells by a retargeted adenovirus vector. J Virol **74**:2567–83.

149. **Sakurai F**, **Mizuguchi H**, **Hayakawa T**. 2003. Efficient gene transfer into human CD34+ cells by an adenovirus type 35 vector. Gene Ther **10**:1041–1048.

150. **Yotnda P**, **Onishi H**, **Heslop HE**, **Shayakhmetov D**, **Lieber A**, **Brenner M**, **Davis A**. 2001. Efficient infection of primitive hematopoietic stem cells by modified adenovirus. Gene Ther **8**:930–937.

151. **Byk T**, **Haddada H**, **Vainchenker W**, **Louache F**. 1998. Lipofectamine and related cationic lipids strongly improve adenoviral infection efficiency of primitive human hematopoietic cells. Hum Gene Ther **9**:2493–502.

152. **Asada-Mikami R**, **Heike Y**, **Kanai S**, **Azuma M**, **Shirakawa K**, **Takaue Y**, **Krasnykh V**, **Curiel DT**, **Terada M**, **Abe T**, **Wakasugi H**. 2001. Efficient gene transduction by RGD-fiber modified recombinant adenovirus into dendritic cells. Jpn J Cancer Res **92**:321–7.

153. **Wickham TJ**, **Carrion ME**, **Kovesdi I**. 1995. Targeting of adenovirus penton base to new receptors through replacement of its RGD motif with other receptor-specific peptide motifs. Gene Ther **2**:750–6.

154. **Graham FL**, **Smiley J**, **Russell WC**, **Nairn R**. 1977. Characteristics of a human cell line transformed by DNA from human adenovirus type 5. J Gen Virol **36**:59–74.

155. **Fallaux FJ**, **Bout A**, **van der Velde I**, **van den Wollenberg DJ**, **Hehir KM**, **Keegan J**, **Auger C**, **Cramer SJ**, **van Ormondt H**, **van der Eb AJ**, **Valerio D**, **Hoeben RC**. 1998. New helper cells and matched early region 1-deleted adenovirus vectors prevent generation of replication-competent adenoviruses. Hum Gene Ther **9**:1909–17.

156. **Fallaux FJ**, **Kranenburg O**, **Cramer SJ**, **Houweling A**, **Van Ormondt H**, **Hoeben RC**, **Van Der Eb AJ**. 1996. Characterization of 911: a new helper cell line for the titration and propagation of early region 1-deleted adenoviral vectors. Hum Gene Ther **7**:215–22.

157. **Gilgenkrantz H**, **Duboc D**, **Juillard V**, **Couton D**, **Pavirani A**, **Guillet JG**, **Briand P**, **Kahn A**. 1995. Transient expression of genes transferred in vivo into heart using first-generation adenoviral vectors: role of the immune response. Hum Gene Ther **6**:1265–74.

158. **Yang Y**, **Su Q**, **Wilson JM**. 1996. Role of viral antigens in destructive cellular immune responses to adenovirus vector-transduced cells in mouse lungs. J Virol **70**:7209–12.

159. **Amalfitano A**, **Hauser MA**, **Hu H**, **Serra D**, **Begy CR**, **Chamberlain JS**. 1998. Production and characterization of improved adenovirus vectors with the E1, E2b, and E3 genes deleted. J Virol **72**:926–33.

160. **Armentano D**, **Zabner J**, **Sacks C**, **Sookdeo CC**, **Smith MP**, **St George JA**, **Wadsworth SC**, **Smith AE**, **Gregory RJ**. 1997. Effect of the E4 region on the persistence of transgene expression from adenovirus vectors. J Virol **71**:2408–16.

161. **Kochanek S**, **Clemens PR**, **Mitani K**, **Chen HH**, **Chan S**, **Caskey CT**. 1996. A new adenoviral vector: Replacement of all viral coding sequences with 28 kb of DNA independently expressing both full-length dystrophin and beta-galactosidase. Proc Natl Acad Sci U S A **93**:5731–6.

162. **Parks RJ**, **Chen L**, **Anton M**, **Sankar U**, **Rudnicki MA**, **Graham FL**. 1996. A helper-dependent adenovirus vector system: removal of helper virus by Cre-mediated excision of the viral packaging signal. Proc Natl Acad Sci U S A **93**:13565–70.

163. **Balamotis MA**, **Huang K**, **Mitani K**. 2004. Efficient delivery and stable gene expression in a hematopoietic cell line using a chimeric serotype 35 fiber pseudotyped helper-dependent adenoviral vector. Virology **324**:229–237.

164. **Saydaminova K**, **Ye X**, **Wang H**, **Richter M**, **Ho M**, **Chen H**, **Xu N**, **Kim J-S**, **Papapetrou E**, **Holmes MC**, **Gregory PD**, **Palmer D**, **Ng P**, **Ehrhardt A**, **Lieber A**. 2015. Efficient genome editing in hematopoietic stem cells with helper-dependent Ad5/35 vectors expressing site-specific endonucleases under microRNA regulation. Mol Ther — Methods Clin Dev **1**:14057.

165. **Gaj T**, **Gersbach CA**, **Barbas CF**. 2013. ZFN, TALEN, and CRISPR/Cas-based methods for genome engineering. Trends Biotechnol **31**:397–405.

166. **Pruett-Miller SM**, **Reading DW**, **Porter SN**, **Porteus MH**. 2009. Attenuation of Zinc Finger Nuclease Toxicity by Small-Molecule Regulation of Protein Levels. PLoS Genet **5**:e1000376.

167. **Li L**, **Krymskaya L**, **Wang J**, **Henley J**, **Rao A**, **Cao L**, **Tran C**, **Torres-Coronado M**, **Gardner A**, **Gonzalez N**, **Kim K**, **Liu P-Q**, **Hofer U**, **Lopez E**, **Gregory PD**, **Liu Q**, **Holmes MC**, **Cannon PM**, **Zaia JA**, **DiGiusto DL**. 2013. Genomic editing of the HIV-1 coreceptor CCR5 in adult hematopoietic stem and progenitor cells using zinc finger nucleases. Mol Ther **21**:1259–69.

168. **Holkers M**, **Maggio I**, **Henriques SFD**, **Janssen JM**, **Cathomen T**, **Gonçalves MAF V**. 2014. Adenoviral vector DNA for accurate genome editing with engineered nucleases. Nat Methods **11**:1051–7.

169. **Moehle EA**, **Rock JM**, **Lee Y-L**, **Jouvenot Y**, **DeKelver RC**, **Gregory PD**, **Urnov FD**, **Holmes MC**. 2007. Targeted gene addition into a specified location in the human genome using designed zinc finger nucleases. Proc Natl Acad Sci **104**:3055–3060.

170. **Lieber A**, **Steinwaerder DS**, **Carlson CA**, **Kay MA**. 1999. Integrating adenovirus-adeno-associated virus hybrid vectors devoid of all viral genes. J Virol **73**:9314–24.

171. **Nakai H**, **Montini E**, **Fuess S**, **Storm TA**, **Grompe M**, **Kay MA**. 2003. AAV serotype 2 vectors preferentially integrate into active genes in mice. Nat Genet **34**:297–302.

172. **Recchia A**, **Parks RJ**, **Lamartina S**, **Toniatti C**, **Pieroni L**, **Palombo F**, **Ciliberto G**, **Graham FL**, **Cortese R**, **La Monica N**, **Colloca S**. 1999. Site-specific integration mediated by a hybrid adenovirus/adeno-associated virus vector. Proc Natl Acad Sci U S A **96**:2615–20.

173. **Lombardo A**, **Cesana D**, **Genovese P**, **Di Stefano B**, **Provasi E**, **Colombo DF**, **Neri M**, **Magnani Z**, **Cantore A**, **Lo Riso P**, **Damo M**, **Pello OM**, **Holmes MC**, **Gregory PD**, **Gritti A**, **Broccoli V**, **Bonini C**, **Naldini L**. 2011. Site-specific integration and tailoring of cassette design for sustainable gene transfer. Nat Methods **8**:861–869.

174. **Ivics Z**, **Hackett PB**, **Plasterk RH**, **Izsvák Z**. 1997. Molecular reconstruction of Sleeping Beauty, a Tc1-like transposon from fish, and its transposition in human cells. Cell **91**:501–10.

175. **Zhang W**, **Muck-Hausl M**, **Wang J**, **Sun C**, **Gebbing M**, **Miskey C**, **Ivics Z**, **Izsvak Z**, **Ehrhardt A**. 2013. Integration profile and safety of an adenovirus hybrid-vector utilizing hyperactive sleeping beauty transposase for somatic integration. PLoS One **8**:e75344.

176. **Ivics Z**, **Katzer A**, **Stüwe EE**, **Fiedler D**, **Knespel S**, **Izsvák Z**. 2007. Targeted Sleeping Beauty transposition in human cells. Mol Ther **15**:1137–1144.

177. **Geurts AM**, **Yang Y**, **Clark KJ**, **Liu G**, **Cui Z**, **Dupuy AJ**, **Bell JB**, **Largaespada DA**, **Hackett PB**. 2003. Gene transfer into genomes of human cells by the sleeping beauty transposon system. Mol Ther **8**:108–17.

178. **Mátés L**, **Chuah MKL**, **Belay E**, **Jerchow B**, **Manoj N**, **Acosta-Sanchez A**, **Grzela DP**, **Schmitt A**, **Becker K**, **Matrai J**, **Ma L**, **Samara-Kuko E**, **Gysemans C**, **Pryputniewicz D**, **Miskey C**, **Fletcher B**, **VandenDriessche T**, **Ivics Z**, **Izsvák Z**. 2009. Molecular evolution of a novel hyperactive Sleeping Beauty transposase enables robust stable gene transfer in vertebrates. Nat Genet **41**:753–61.

179. **Yant SR**, **Ehrhardt A**, **Mikkelsen JG**, **Meuse L**, **Pham T**, **Kay M a**. 2002. Transposition from a gutless adeno-transposon vector stabilizes transgene expression in vivo. Nat Biotechnol **20**:999–1005.

180. **Izsvák Z**, **Ivics Z**, **Plasterk RH**. 2000. Sleeping Beauty, a wide host-range transposon vector for genetic transformation in vertebrates. J Mol Biol **302**:93–102.

181. **Hausl MA**, **Zhang W**, **Müther N**, **Rauschhuber C**, **Franck HG**, **Merricks EP**, **Nichols TC**, **Kay M a**, **Ehrhardt A**. 2010. Hyperactive sleeping beauty transposase enables persistent phenotypic correction in mice and a canine model for hemophilia B. Mol Ther **18**:1896–906.

182. **Holers VM**, **Kinoshita T**, **Molina H**. 1992. The evolution of mouse and human complement C3-binding proteins: divergence of form but conservation of function. Immunol Today **13**:231–6.

183. **Mrkic B**, **Pavlovic J**, **Rülicke T**, **Volpe P**, **Buchholz CJ**, **Hourcade D**, **Atkinson JP**, **Aguzzi A**, **Cattaneo R**. 1998. Measles virus spread and pathogenesis in genetically modified mice. J Virol **72**:7420–7427.

184. **Kemper C**, **Leung M**, **Stephensen CB**, **Pinkert C a.**, **Liszewski MK**, **Cattaneo R**, **Atkinson JP**. 2001. Membrane cofactor protein (MCP; CD46) expression in transgenic mice. Clin Exp Immunol **124**:180–189.

185. **Lai L**, **Alaverdi N**, **Maltais L**, **Morse HC**. 1998. Mouse cell surface antigens: nomenclature and immunophenotyping. J Immunol **160**:3861–8.

186. **Manchester M**, **Smith KA**, **Eto DS**, **Perkin HB**, **Torbett BE**. 2002. Targeting and hematopoietic suppression of human CD34+ cells by measles virus. J Virol **76**:6636–42.

187. **Marini FC**, **Shayakhmetov D**, **Gharwan H**, **Lieber A**, **Andreeff M**. 2002. Advances in gene transfer into haematopoietic stem cells by adenoviral vectors. Expert Opin Biol Ther **2**:847–856.

188. **DiPersio JF**, **Micallef IN**, **Stiff PJ**, **Bolwell BJ**, **Maziarz RT**, **Jacobsen E**, **Nademanee A**, **McCarty J**, **Bridger G**, **Calandra G**, **3101 Investigators**. 2009. Phase III prospective randomized double-blind placebo-controlled trial of plerixafor plus granulocyte colony-stimulating factor compared with placebo plus granulocyte colony-stimulating factor for autologous stem-cell mobilization and transplantation for . J Clin Oncol **27**:4767–73.

189. **DiPersio JF**, **Stadtmauer E a**, **Nademanee A**, **Micallef INM**, **Stiff PJ**, **Kaufman JL**, **Maziarz RT**, **Hosing C**, **Früehauf S**, **Horwitz M**, **Cooper D**, **Bridger G**, **Calandra G**, **3102 Investigators**. 2009. Plerixafor and G-CSF versus placebo and G-CSF to mobilize hematopoietic stem cells for autologous stem cell transplantation in patients with multiple myeloma. Blood **113**:5720–6.

190. **Yang Y**, **Nunes F a**, **Berencsi K**, **Furth EE**, **Gönczöl E**, **Wilson JM**. 1994. Cellular immunity to viral antigens limits E1-deleted adenoviruses for gene therapy. Proc Natl Acad Sci U S A **91**:4407–11.

191. **Ross J**, **Li L**. 2009. HSC mobilization: new incites and insights. Blood **114**:1283–4.

192. **Morral N**, **Parks RJ**, **Zhou H**, **Langston C**, **Schiedner G**, **Quinones J**, **Graham FL**, **Kochanek S**, **Beaudet AL**. 1998. High doses of a helper-dependent adenoviral vector yield supraphysiological levels of alpha1-antitrypsin with negligible toxicity. Hum Gene Ther **9**:2709–16.

193. **Knudsen E**, **Iversen PO**, **Bøyum A**, **Seierstad T**, **Nicolaysen G**, **Benestad HB**. 2011. G-CSF enhances the proliferation and mobilization, but not the maturation rate, of murine myeloid cells. Eur J Haematol **87**:302–11.

194. **Morrison SJ**, **Wright DE**, **Weissman IL**. 1997. Cyclophosphamide/granulocyte colony-stimulating factor induces hematopoietic stem cells to proliferate prior to mobilization. Proc Natl Acad Sci U S A **94**:1908–13.

195. **Harui A**, **Suzuki S**, **Kochanek S**, **Mitani K**. 1999. Frequency and stability of chromosomal integration of adenovirus vectors. J Virol **73**:6141–6.

196. **Buchholz F**, **Angrand PO**, **Stewart AF**. 1998. Improved properties of FLP recombinase evolved by cycling mutagenesis. Nat Biotechnol **16**:657–62.

197. **Wang H**, **Lieber A**. 2006. A helper-dependent capsid-modified adenovirus vector expressing adeno-associated virus rep78 mediates site-specific integration of a 27-kilobase transgene cassette. J Virol **80**:11699–709.

198. **Furze RC**, **Rankin SM**. 2008. Neutrophil mobilization and clearance in the bone marrow. Immunology **125**:281–288.

199. **Bradford GB**, **Williams B**, **Rossi R**, **Bertoncello I**. 1997. Quiescence, cycling, and turnover in the primitive hematopoietic stem cell compartment. Exp Hematol **25**:445–53.

200. **Morrison SJ**, **Weissman IL**. 1994. The long-term repopulating subset of hematopoietic stem cells is deterministic and isolatable by phenotype. Immunity **1**:661–73.

201. **Balaguer H**, **Galmes A**, **Ventayol G**, **Bargay J**, **Besalduch J**. 2004. Splenic rupture after granulocyte-colony-stimulating factor mobilization in a peripheral blood progenitor cell donor. Transfusion **44**:1260–1.

202. **Dincer AP**, **Gottschall J**, **Margolis DA**. 2004. Splenic rupture in a parental donor undergoing peripheral blood progenitor cell mobilization. J Pediatr Hematol Oncol **26**:761–3.

203. **Falzetti F**, **Aversa F**, **Minelli O**, **Tabilio A**. 1999. Spontaneous rupture of spleen during peripheral blood stem-cell mobilisation in a healthy donor. Lancet (London, England) **353**:555.

204. **Yue F**, **Cheng Y**, **Breschi A**, **Vierstra J**, **Wu W**, **Ryba T**, **Sandstrom R**, **Ma Z**, **Davis C**, **Pope BD**, **Shen Y**, **Pervouchine DD**, **Djebali S**, **Thurman RE**, **Kaul R**, **Rynes E**, **Kirilusha A**, **Marinov GK**, **Williams BA**, **Trout D**, **Amrhein H**, **Fisher-Aylor K**, **Antoshechkin I**, **DeSalvo G**, **See LH**, **Fastuca M**, **Drenkow J**, **Zaleski C**, **Dobin A**, **Prieto P**, **Lagarde J**, **Bussotti G**, **Tanzer A**, **Denas O**, **Li K**, **Bender MA**, **Zhang M**, **Byron R**, **Groudine MT**, **McCleary D**, **Pham L**, **Ye Z**, **Kuan S**, **Edsall L**, **Wu YC**, **Rasmussen MD**, **Bansal MS**, **Kellis M**, **Keller CA**, **Morrissey CS**, **Mishra T**, **Jain D**, **Dogan N**, **Harris RS**, **Cayting P**, **Kawli T**, **Boyle AP**, **Euskirchen G**, **Kundaje A**, **Lin S**, **Lin Y**, **Jansen C**, **Malladi VS**, **Cline MS**, **Erickson DT**, **Kirkup VM**, **Learned K**, **Sloan CA**, **Rosenbloom KR**, **Lacerda de Sousa B**, **Beal K**, **Pignatelli M**, **Flicek P**, **Lian J**, **Kahveci T**, **Lee D**, **Kent WJ**, **Ramalho Santos M**, **Herrero J**, **Notredame C**, **Johnson A**, **Vong S**, **Lee K**, **Bates D**, **Neri F**, **Diegel M**, **Canfield T**, **Sabo PJ**, **Wilken MS**, **Reh TA**, **Giste E**, **Shafer A**, **Kutyavin T**, **Haugen E**, **Dunn D**, **Reynolds AP**, **Neph S**, **Humbert R**, **Hansen RS**, **De Bruijn M**, **Selleri L**, **Rudensky A**, **Josefowicz S**, **Samstein R**, **Eichler EE**, **Orkin SH**, **Levasseur D**, **Papayannopoulou T**, **Chang KH**, **Skoultchi A**, **Gosh S**, **Disteche C**, **Treuting P**, **Wang Y**, **Weiss MJ**, **Blobel GA**, **Cao X**, **Zhong S**, **Wang T**, **Good PJ**, **Lowdon RF**, **Adams LB**, **Zhou XQ**, **Pazin MJ**, **Feingold EA**, **Wold B**, **Taylor J**, **Mortazavi A**, **Weissman SM**, **Stamatoyannopoulos JA**, **Snyder MP**, **Guigo R**, **Gingeras TR**, **Gilbert DM**, **Hardison**

RC, **Beer MA**, **Ren B**, **Mouse EC**. 2014. A comparative encyclopedia of DNA elements in the mouse genome. Nature **515**:355–364.

205. **Kanehisa M**, **Goto S**. 2000. KEGG: kyoto encyclopedia of genes and genomes. Nucleic Acids Res **28**:27–30.

206. **Manz MG**, **Boettcher S**. 2014. Emergency granulopoiesis. Nat Rev Immunol **14**:302–14.

207. **Ueda Y**, **Kondo M**, **Kelsoe G**. 2005. Inflammation and the reciprocal production of granulocytes and lymphocytes in bone marrow. J Exp Med **201**:1771–80.

208. **Day RB**, **Bhattacharya D**, **Nagasawa T**, **Link DC**. 2015. Granulocyte colony-stimulating factor reprograms bone marrow stromal cells to actively suppress B lymphopoiesis in mice. Blood **125**:pii: blood-2015-02-629444.

209. **Winkler IG**, **Bendall LJ**, **Forristal CE**, **Helwani F**, **Nowlan B**, **Barbier V**, **Shen Y**, **Cisterne A**, **Sedger LM**, **Levesque JP**. 2013. B-lymphopoiesis is stopped by mobilizing doses of G-CSF and is rescued by overexpression of the anti-apoptotic protein Bcl2. Haematologica **98**:325–333.

210. **Di Paolo NC**, **Shayakhmetov DM**. 2009. Adenovirus de-targeting from the liver. Curr Opin Mol Ther **11**:523–531.

211. **Stone D**, **Liu Y**, **Li Z-Y**, **Tuve S**, **Strauss R**, **Lieber A**. 2007. Comparison of adenoviruses from species B, C, E, and F after intravenous delivery. Mol Ther **15**:2146–53.

212. **Ganesh S**, **Gonzalez-Edick M**, **Gibbons D**, **Waugh J**, **Van Roey M**, **Jooss K**. 2009. Evaluation of biodistribution of a fiber-chimeric, conditionally replication-competent (oncolytic) adenovirus in CD46 receptor transgenic mice. Hum Gene Ther **20**:1201–13.

213. **Ni S**, **Bernt K**, **Gaggar A**, **Li Z-Y**, **Kiem H-P**, **Lieber A**. 2005. Evaluation of biodistribution and safety of adenovirus vectors containing group B fibers after intravenous injection into baboons. Hum Gene Ther **16**:664–77.

214. **DiPaolo N**, **Ni S**, **Gaggar A**, **Strauss R**, **Tuve S**, **Li ZY**, **Stone D**, **Shayakhmetov D**, **Kiviat N**, **Touré P**, **Sow S**, **Horvat B**, **Lieber AA**, **Tour?? P**, **Sow S**, **Horvat B**, **Lieber AA**. 2006. Evaluation of adenovirus vectors containing serotype 35 fibers for vaccination. Mol Ther **13**:756–65.

215. **Ni S**, **Gaggar A**, **Di Paolo N**, **Li ZY**, **Liu Y**, **Strauss R**, **Sova P**, **Morihara J**, **Feng Q**, **Kiviat N**, **Touré P**, **Sow PS**, **Lieber A**. 2006. Evaluation of adenovirus vectors containing serotype 35 fibers for tumor targeting. Cancer Gene Ther **13**:1072–81.

216. **Seregin SS**, **Appledorn DM**, **McBride AJ**, **Schuldt NJ**, **Aldhamen Y a**, **Voss T**, **Wei J**, **Bujold M**, **Nance W**, **Godbehere S**, **Amalfitano A**. 2009. Transient pretreatment with glucocorticoid ablates innate toxicity of systemically delivered adenoviral vectors without reducing efficacy. Mol Ther **17**:685–96.

217. **Parker AL**, **Waddington SN**, **Nicol CG**, **Shayakhmetov DM**, **Buckley SM**, **Denby L**, **Kemball-Cook G**, **Ni S**, **Lieber A**, **McVey JH**, **Nicklin S a**, **Baker AH**. 2006. Multiple vitamin K-dependent coagulation zymogens promote adenovirus-mediated gene delivery to hepatocytes. Blood **108**:2554–2561.

218. **Alba R**, **Bradshaw AC**, **Parker AL**, **Bhella D**, **Waddington SN**, **Nicklin SA**, **van Rooijen N**, **Custers J**, **Goudsmit J**, **Barouch DH**, **McVey JH**, **Baker AH**. 2009. Identification of coagulation factor (F)X binding sites on the adenovirus serotype 5 hexon: effect of mutagenesis on FX interactions and gene transfer. Blood **114**:965–71.

219. **Kalyuzhniy O**, **Di Paolo NC**, **Silvestry M**, **Hofherr SE**, **Barry M a**, **Stewart PL**, **Shayakhmetov DM**. 2008. Adenovirus serotype 5 hexon is critical for virus infection of hepatocytes in vivo. Proc Natl Acad Sci U S A **105**:5483–8.

220. **Waddington SN**, **McVey JH**, **Bhella D**, **Parker AL**, **Barker K**, **Atoda H**, **Pink R**, **Buckley SMK**, **Greig JA**, **Denby L**, **Custers J**, **Morita T**, **Francischetti IMB**, **Monteiro RQ**, **Barouch DH**, **van Rooijen N**, **Napoli C**, **Havenga MJE**, **Nicklin SA**, **Baker AH**. 2008. Adenovirus serotype 5 hexon mediates liver gene transfer. Cell **132**:397–409.

221. **Shayakhmetov DM**, **Li Z-Y**, **Ni S**, **Lieber A**. 2004. Analysis of adenovirus sequestration in the liver, transduction of hepatic cells, and innate toxicity after injection of fiber-modified vectors. J Virol **78**:5368–5381.

222. **Koizumi N**, **Mizuguchi H**, **Sakurai F**, **Yamaguchi T**, **Watanabe Y**, **Hayakawa T**. 2003. Reduction of natural adenovirus tropism to mouse liver by fiber-shaft exchange in combination with both CAR- and alphav integrin-binding ablation. J Virol **77**:13062–72.

223. **Ito M**, **Hiramatsu H**, **Kobayashi K**, **Suzue K**, **Kawahata M**, **Hioki K**, **Ueyama Y**, **Koyanagi Y**, **Sugamura K**, **Tsuji K**, **Heike T**, **Nakahata T**. 2002. NOD/SCID/gamma(c)(null) mouse: an excellent recipient mouse model for engraftment of human cells. Blood **100**:3175–82.

224. **van der Loo JC**, **Hanenberg H**, **Cooper RJ**, **Luo FY**, **Lazaridis EN**, **Williams DA**. 1998. Nonobese diabetic/severe combined immunodeficiency (NOD/SCID) mouse as a model system to study the engraftment and mobilization of human peripheral blood stem cells. Blood **92**:2556–70.

225. **Rongvaux A**, **Willinger T**, **Takizawa H**, **Rathinam C**, **Auerbach W**, **Murphy AJ**, **Valenzuela DM**, **Yancopoulos GD**, **Eynon EE**, **Stevens S**, **Manz MG**, **Flavell RA**. 2011. Human thrombopoietin knockin mice efficiently support human hematopoiesis in vivo. Proc Natl Acad Sci U S A **108**:2378–83.

226. **Bradfute SB**, **Goodell MA**. 2003. Adenoviral transduction of mouse hematopoietic stem cells. Mol Ther **7**:334–340.

227. **Lozier JN**, **Csako G**, **Mondoro TH**, **Krizek DM**, **Metzger ME**, **Costello R**, **Vostal JG**, **Rick ME**, **Donahue RE**, **Morgan R a**. 2002. Toxicity of a first-generation adenoviral vector in rhesus macaques. Hum Gene Ther **13**:113–24.

228. **Brunetti-Pierri N**, **Palmer DJ**, **Beaudet AL**, **Carey KD**, **Finegold M**, **Ng P**. 2004. Acute toxicity after high-dose systemic injection of helper-dependent adenoviral vectors into nonhuman primates. Hum Gene Ther **15**:35–46.

229. **Stroncek DF**, **Dittmar K**, **Shawker T**, **Heatherman A**, **Leitman SF**. 2004. Transient spleen enlargement in peripheral blood progenitor cell donors given G-CSF. J Transl Med **2**:25.

230. **Stroncek D**, **Shawker T**, **Follmann D**, **Leitman SF**. 2003. G-CSF-induced spleen size changes in peripheral blood progenitor cell donors. Transfusion **43**:609–13.

231. **Tak T**, **Tesselaar K**, **Pillay J**, **Borghans J a M**, **Koenderman L**. 2013. What's your age again? Determination of human neutrophil half-lives revisited. J Leukoc Biol **94**:595–601.

232. **Tripathy SK**, **Black HB**, **Goldwasser E**, **Leiden JM**. 1996. Immune responses to transgene–encoded proteins limit the stability of gene expression after injection of replication–defective adenovirus vectors. Nat Med **2**:545–550.

233. **Muruve DA**, **Cotter MJ**, **Zaiss AK**, **White LR**, **Liu Q**, **Chan T**, **Clark SA**, **Ross PJ**, **Meulenbroek RA**, **Maelandsmo GM**, **Parks RJ**. 2004. Helper-dependent adenovirus vectors elicit intact innate but attenuated adaptive host immune responses in vivo. J Virol **78**:5966–5972.

234. **Sun J**, **Ramos A**, **Chapman B**, **Johnnidis JB**, **Le L**, **Ho Y-J**, **Klein A**, **Hofmann O**, **Camargo FD**. 2014. Clonal dynamics of native haematopoiesis. Nature **514**:322–327.

235. **Sumiyoshi T**, **Holt NG**, **Hollis RP**, **Ge S**, **Cannon PM**, **Crooks GM**, **Kohn DB**. 2009. Stable transgene expression in primitive human CD34+ hematopoietic stem/progenitor cells, using the Sleeping Beauty transposon system. Hum Gene Ther **20**:1607–26.

236. **Xue X**, **Huang X**, **Nodland SE**, **Mátés L**, **Ma L**, **Izsvák Z**, **Ivics Z**, **LeBien TW**, **McIvor RS**, **Wagner JE**, **Zhou X**. 2009. Stable gene transfer and expression in cord blood-derived CD34+ hematopoietic stem and progenitor cells by a hyperactive Sleeping Beauty transposon system. Blood **114**:1319–30.

237. **Huang X**, **Guo H**, **Tammana S**, **Jung Y-C**, **Mellgren E**, **Bassi P**, **Cao Q**, **Tu ZJ**, **Kim YC**, **Ekker SC**, **Wu X**, **Wang SM**, **Zhou X**. 2010. Gene transfer efficiency and genome-wide integration profiling of Sleeping Beauty, Tol2, and piggyBac transposons in human primary T cells. Mol Ther **18**:1803–1813.

238. **Ding S**, **Wu X**, **Li G**, **Han M**, **Zhuang Y**, **Xu T**. 2005. Efficient transposition of the piggyBac (PB) transposon in mammalian cells and mice. Cell **122**:473–83.

239. **Urasaki A**, **Morvan G**, **Kawakami K**. 2006. Functional dissection of the Tol2 transposable element identified the minimal cis-sequence and a highly repetitive sequence in the subterminal region essential for transposition. Genetics **174**:639–49.

240. **Agudo J**, **Ruzo A**, **Kitur K**, **Sachidanandam R**, **Blander JM**, **Brown BD**. 2012. A TLR and Non-TLR Mediated Innate Response to Lentiviruses Restricts Hepatocyte Entry and Can be Ameliorated by Pharmacological Blockade. Mol Ther **20**:2257–2267.

241. **Shayakhmetov DM**, **Gaggar A**, **Ni S**, **Li ZY**, **Lieber A**. 2005. Adenovirus binding to blood factors results in liver cell infection and hepatotoxicity. J Virol **79**:7478–7491.

242. **Morsy MA**, **Gu M**, **Motzel S**, **Zhao J**, **Lin J**, **Su Q**, **Allen H**, **Franlin L**, **Parks RJ**, **Graham FL**, **Kochanek S**, **Bett AJ**, **Caskey ACT**, **Caskey CT**. 1998. An adenoviral vector deleted for all viral coding sequences results in enhanced safety and extended expression of a leptin transgene. Appl Biol Sci **95**:7866–7871.

243. **Aiuti A**, **Cassani B**, **Andolfi G**, **Mirolo M**, **Biasco L**, **Recchia A**, **Urbinati F**, **Valacca C**, **Scaramuzza S**, **Aker M**, **Slavin S**, **Cazzola M**, **Sartori D**, **Ambrosi A**, **Di Serio C**, **Roncarolo MG**, **Mavilio F**, **Bordignon C**. 2007. Multilineage hematopoietic reconstitution without clonal selection in ADA-SCID patients treated with stem cell gene therapy. J Clin Invest **117**:2233–40.

244. **Carlson CM**, **Dupuy AJ**, **Fritz S**, **Roberg-Perez KJ**, **Fletcher CF**, **Largaespada DA**. 2003. Transposon mutagenesis of the mouse germline. Genetics **165**:243–256.

245. **Luo G**, **Ivics Z**, **Izsvák Z**, **Bradley A**. 1998. Chromosomal transposition of a Tc1/mariner-like element in mouse embryonic stem cells. Proc Natl Acad Sci U S A **95**:10769–73.

246. **Raper SE**, **Chirmule N**, **Lee FS**, **Wivel NA**, **Bagg A**, **Gao GP**, **Wilson JM**, **Batshaw ML**. 2003. Fatal systemic inflammatory response syndrome in a ornithine transcarbamylase deficient patient following adenoviral gene transfer. Mol Genet Metab **80**:148–158.

247. **Zielske SP**, **Gerson SL**. 2002. Lentiviral transduction of P140K MGMT into human CD34(+) hematopoietic progenitors at low multiplicity of infection confers significant resistance to BG/BCNU and allows selection in vitro. Mol Ther **5**:381–387.

248. **Gerson SL**, **Phillips W**, **Kastan M**, **Dumenco LL**, **Donovan C**. 1996. Human CD34+ hematopoietic progenitors have low, cytokine-unresponsive O6-alkylguanine-DNA alkyltransferase and are sensitive to O6-benzylguanine plus BCNU. Blood **88**:1649–55.

249. **Xu-Welliver M**, **Kanugula S**, **Pegg AE**. 1998. Isolation of human O6-alkylguanine-DNA alkyltransferase mutants highly resistant to inactivation by O6-benzylguanine. Cancer Res **58**:1936–45.

250. **Neff T**, **Horn PA**, **Peterson LJ**, **Thomasson BM**, **Thompson J**, **Williams DA**, **Schmidt M**, **Georges GE**, **Kalle C Von**, **Kiem H**. 2003. Methylguanine methyltransferase – mediated in vivo selection and chemoprotection of allogeneic stem cells in a large-animal model. J Clin Invest **112**:1581–1588.

251. **Sheu J**, **Beltzer J**, **Fury B**, **Wilczek K**, **Tobin S**, **Falconer D**, **Nolta J**, **Bauer G**. 2015. Large-scale production of lentiviral vector in a closed system hollow fiber bioreactor. Mol Ther Methods Clin Dev **2**:15020.

252. **Wang H**, **Liu Y**, **Li Z**, **Tuve S**, **Stone D**, **Kalyushniy O**, **Shayakhmetov D**, **Verlinde CLM**, **Stehle T**, **McVey J**, **Baker A**, **Peng K-W**, **Roffler S**, **Lieber A**. 2008. In vitro and in vivo properties of adenovirus vectors with increased affinity to CD46. J Virol **82**:10567–79.

253. **Maizel J V**, **White DO**, **Scharff MD**. 1968. The polypeptides of adenovirus. I. Evidence for multiple protein components in the virion and a comparison of types 2, 7A, and 12. Virology **36**:115–25.

254. **Martin M**, **Solanki M**, **Zhang W**, **Ruzsics Z**, **Ehrhardt A**. 2015. Ad 2 . 0 : a novel recombineering platform for high-throughput generation of tailored adenoviruses **43**:e50.

255. **Warming S**, **Costantino N**, **Court DL**, **Jenkins NA**, **Copeland NG**. 2005. Simple and highly efficient BAC recombineering using galK selection. Nucleic Acids Res **33**:e36.

256. **Palmer D**, **Ng P**. 2003. Improved system for helper-dependent adenoviral vector production. Mol Ther **8**:846–52.

257. **Jungblut M**, **Oeltze K**, **Zehnter I**, **Hasselmann D**, **Bosio A**. 2009. Standardized preparation of single-cell suspensions from mouse lung tissue using the gentleMACS Dissociator. J Vis Exp 1–4.

258. **Moldt B**, **Miskey C**, **Staunstrup NH**, **Gogol-Döring A**, **Bak RO**, **Sharma N**, **Mátés L**, **Izsvák Z**, **Chen W**, **Ivics Z**, **Mikkelsen JG**. 2011. Comparative genomic integration profiling of Sleeping Beauty transposons mobilized with high efficacy from integrase-defective lentiviral vectors in primary human cells. Mol Ther **19**:1499–510.

259. **Langmead B**, **Trapnell C**, **Pop M**, **Salzberg SL**. 2009. Ultrafast and memory-efficient alignment of short DNA sequences to the human genome. Genome Biol **10**:R25.

7 Acknowledgments

First of all, I would like to thank my supervisor André Lieber for the opportunity to work on this project, for his constant support even when the going was tough, and for creating a frutitious work environment.

Further, I would like to thank Wolfgang Uckert for his supervision, his constructive feedback and his support in this endeavour.

I am deeply grateful to all former and current members of the Lieber lab, for the countless times that their assitance and input helped to push this project forward and to not loose faith. Special thanks to Roma Yumul, Kamola Saydaminova and Hongjie Wang, without whom this project would not have been possible. Additional thanks to Donna Prunkard of the UW Flow Cytometry Core and the animal technicians and veterinarians of the K-Wing SPF facility.

Moreover, I would like to thank our collaborators in the groups of Thalia Papayannopoulou, Anja Ehrhardt, Hans-Peter Kiem and Zsuzsanna Izsvak for their tireless efforts and help in all stages of this work.

Further, a big “Dankeschön” to my parents, for their unconditional love and support throughout my life and for the trust they invested in me.

Lastly, I want to thank my wife Sarah, without whom I would not be where I am today, who supported me in this endeavor, helped me to push on when times were challenging, and who proofread every draft and poster even though they were incomprehensible to her.

8 Publications

Choi I-K, Strauss R, Richter M, Yun C-O, Lieber A. 2013. Strategies to increase drug penetration in solid tumors. **Front Oncol** 3:193.

Wang H, Yumul R, Cao H, Ran L, Fan X, Richter M, Epstein F, Gralow J, Zubieta C, Fender P, Lieber A. 2013. Structural and functional studies on the interaction of adenovirus fiber knobs and desmoglein 2. **J Virol** 87:11346–62.

Richter M, Yumul R, Wang H, Saydaminova K, Ho M, May D, Baldessari A, Gough M, Drescher C, Urban N, Roffler S, Zubieta C, Carter D, Fender P, Lieber A. 2015. Preclinical safety and efficacy studies with an affinity-enhanced epithelial junction opener and PEGylated liposomal doxorubicin. **Mol Ther Methods Clin Dev** 2:15005.

Wang H, Ducournau C, Saydaminova K, Richter M, Yumul R, Ho M, Carter D, Zubieta C, Fender P, Lieber A. 2015. Intracellular Signaling and Desmoglein 2 Shedding Triggered by Human Adenoviruses Ad3, Ad14, and Ad14P1. **J Virol** 89:10841–59.

Saydaminova K, Ye X, Wang H, Richter M, Ho M, Chen H, Xu N, Kim J-S, Papapetrou E, Holmes MC, Gregory PD, Palmer D, Ng P, Ehrhardt A, Lieber A. 2015. Efficient genome editing in hematopoietic stem cells with helper-dependent Ad5/35 vectors expressing site-specific endonucleases under microRNA regulation. **Mol Ther Methods Clin Dev** 1:14057.

Richter M, Saydaminova K, Yumul R, Krishnan R, Liu J, Nagy E-E, Singh M, Izsvák Z, Cattaneo R, Uckert W, Palmer D, Ng P, Haworth KG, Kiem H-P, Ehrhardt A, Papayannopoulou T, Lieber A. 2016. In vivo transduction of primitive hematopoietic stem cells after mobilization and intravenous injection of integrating adenovirus vectors. **Blood** 128:2206–2218.

Saydaminova K, Strauss R, Xie M, Bartek J, Richter M, van Rensburg R, Drescher C, Ehrhardt A, Ding S, Lieber A. 2016. Sensitizing ovarian cancer cells to chemotherapy by interfering with pathways that are involved in the formation of cancer stem cells. **Cancer Biol Ther** 17:1079–1088.

Yumul R, Richter M, Lu Z-Z, Saydaminova K, Wang H, Wang C-HK, Carter D, Lieber A. 2016. Epithelial Junction Opener Improves Oncolytic Adenovirus Therapy in Mouse Tumor Models. **Hum Gene Ther** 27:325–37.

Richter M, Yumul R, Saydaminova K, Wang H, Gough M, Baldessari A, Cattaneo R, Lee F, Wang C-HK, Jang H, Astier A, Gopal A, Carter D, Lieber A. 2016. Preclinical safety, pharmacokinetics, pharmacodynamics, and biodistribution studies with Ad35K++ protein: a novel rituximab cotherapeutic. **Mol Ther Methods Clin Dev** 5:16013

9 Eidesstattliche Erklärung

Hiermit versichere ich, die vorliegende Dissertation selbständig und nur unter Verwendung der im Text angegebenen Hilfen und Hilfsmittel angefertigt zu haben und dass hierbei keine Zusammenarbeit mit einem gewerblichen Promotionsberater stattfand. Ein Promotionsverfahren zu einem früheren Zeitpunkt, an einer anderen Hochschule oder bei einem anderen Fachbereich wurde nicht beantragt. Mir ist die dem angestrebten Verfahren zugrunde liegende Promotionsordnung der Lebenswissenschaftlichen Fakultät der Humboldt-Universität zu Berlin vom 27. Juni 2012 bekannt.

Datum ....